Macroscopic observation of hydrodynamics and pseudomonas aeruginosa bioflim processes in a porous media reactor
by Feisal Abedeen

A thesis submitted in partial fulfillment of the requirements for the degree of Master of Science in Environmental Engineering
Montana State University

Abstract:
Microorganisms in the subsurface microenvironment can be made to play an active role in the solution of several industrial problems. A prior knowledge of the fundamental processes regarding cause and effect relationships is however essential in order to exploit these microorganisms effectively and safely. In order to study this, a simulation of the naturally occurring processes in the subsurface was attempted using porous media. Biofilm accumulation, mass transport of fluid and nutrients, biotransformation and reactor dynamics were studied inside thin rectangular glass reactors. Pseudomonas aeruginosa was made to adsorb and grow inside these reactors on packing media of varying dimensions. The substrate feed consisted of glucose, oxygen and micronutrient salts in distilled water, provided at a constant pressure drop across the system. Analytical techniques were invented or improvised for in situ measurement of spatial and temporal variations of the above variables. The experimental analysis yielded hydrodynamic and biochemical data, which was then integrated. Results indicated that these variables are highly inter-linked through mass balances over the respective compartments and phases.

MACROSCOPIC OBSERVATION OF HYDRODYNAMICS AND *PSEUDOMONAS AERUGINOSA* BIOFILM PROCESSES IN A POROUS MEDIA REACTOR

by

Feisal Abedeen

A thesis submitted in partial fulfillment
of the requirements for the degree

of

Master of Science

in

Environmental Engineering

MONTANA STATE UNIVERSITY
Bozeman, Montana

November 1990

APPROVAL

of a thesis submitted by

Feisal Abedeen

This thesis has been read by each member of the thesis committee and has been found to be satisfactory regarding content, English usage, format, citations, bibliographic style, and consistency, and is ready for submission to the College of Graduate Studies.

7 December 1990
Date

Chairperson, Graduate Committee

Approved for the Major Department

12 Dec 1990
Date

Head, Major Department

Approved for the College of Graduate Studies

Dec. 14, 1990
Date

Graduate Dean

STATEMENT OF PERMISSION TO USE

In presenting this thesis in partial fulfillment of the requirements for a Masters degree at Montana State University, I agree that the Library shall make it available to borrowers under rules of the Library. Brief quotations from this thesis are allowable without special permission, provided that accurate acknowledgement of source is made.

Requests for permission for extended quotation from or reproduction of this thesis in whole or in parts may be granted by the copyright holder.

Signature Faisal Abedeen

Date 12/17/90

ACKNOWLEDGEMENTS

I wish to express my gratitude to the following persons in making my M.S. program at Montana State University enjoyable and fruitful:

Bill Characklis, my academic advisor, who provided me with personal guidance and motivation, my research supervisor Al Cunningham for his care and patience in supervising my research, Warren Jones who helped me with the preparation of this thesis, and, Paul Stoodley who was always an asset in the laboratory.

Acknowledgement is also made to the office staff of National Science Foundation Engineering Research Center (or I.P.A.), Department of Civil Engineering and Media Services. I am grateful to USGS and EPA for being my financial sponsors.

Thanks to Brent Peyton, Ewout van Der Wende, Gabi Walser, Robert Mueller, Bill Drury, Satoshi Okabe, Linda Anderson, Ernie, Susie and Joel Leadbetter, Craig Bjorgensen, Dave Davies, Whonchee Lee, Randy Boyce, Anne Camper and Tammy Hartpence (all from Bozeman) for being great friends.

TABLE OF CONTENTS

TABLE OF CONTENTS (contd.)

LIST OF TABLES

LIST OF TABLES (contd.)

LIST OF FIGURES

LIST OF FIGURES (Contd.)

LIST OF FIGURES (contd.)

ABSTRACT

Microorganisms in the subsurface microenvironment can be made to play an active role in the solution of several industrial problems. A prior knowledge of the fundamental processes regarding cause and effect relationships is however essential in order to exploit these microorganisms effectively and safely. In order to study this, a simulation of the naturally occurring processes in the subsurface was attempted using porous media. Biofilm accumulation, mass transport of fluid and nutrients, biotransformation and reactor dynamics were studied inside thin rectangular glass reactors. *Pseudomonas aeruginosa* was made to adsorb and grow inside these reactors on packing media of varying dimensions. The substrate feed consisted of glucose, oxygen and micronutrient salts in distilled water, provided at a constant pressure drop across the system. Analytical techniques were invented or improvised for *in situ* measurement of spatial and temporal variations of the above variables. The experimental analysis yielded hydrodynamic and biochemical data, which was then integrated. Results indicated that these variables are highly inter-linked through mass balances over the respective compartments and phases.

INTRODUCTION

Background

A literature review shows that a number of similar studies have been made in packed beds or simulated porous media reactors. Microorganisms attached or adhering to solid surfaces have a tremendous advantage over suspended cells as they are assured of a continuous supply of nutrients and perhaps a more stable niche in which to proliferate. It also provides for a higher interaction between varied microbial communities. For instance, in a natural mixed culture system, the species found at the substrata are obligate anaerobes, followed by facultative aerobes and the surface population is likely to be an aerobic heterotroph species. Therefore, there is a strong driving force for microorganisms, especially those that occur in nature, to evolve as a biofilm species in preference to suspended cells.

Biofilms have been known to be useful in many situations while proving to be a nuisance in others. For instance, biofilms occurring on ship hulls and other submersed surfaces provide a significant loss of momentum by increasing the fluid energy loss at the surface. Inside pipes, tubes, on metal surfaces and on any electro-chemically suited surface such as the mammalian tooth, they cause a corrosion of the substrata leading to a deterioration and ultimate loss of the surface. They also provide significant heat transfer losses on surfaces that conduct heat in cooling or heating equipment. On the other hand, biofilms have been used for many decades to treat waste water as in trickling filters, for selective adsorption of toxic chemicals on activated surfaces in filtration-adsorption columns, as the final stage in small and medium scale water treatment plants with the biofilm growing naturally in the subsurface cores, and, for enzyme immobilization techniques. In general, they have existed for almost as long as man has existed. Recently, however, the active use of microorganisms for environmental applications is being viewed as a viable alternative to conventional chemical or mechanical

treatment methods. The Environmental Protection Agency has evolved its own program known as the Superfund Innovative Technology Evaluation Program (SITE, 1989) which is now in its fifth year. The program deals with evaluating treatment technologies necessary to implement new federal and state cleanup standards aimed at permanent remedies rather than short term solutions. Technologies undergoing review are listed in Table 1.

Table 1 Comparison of treatment technologies considered for remediation of hazardous compounds in the groundwater by the USEPA.

	Method of treatment	percentage
1.	Biological	11.3
2.	Fixed biofilm	3.8
3.	Physical/chemical	53.1
4.	Solidification/stabilization	18.9
5.	Thermal	17.0

Of relevance in the above table is the deceptively small number of treatment methodologies based on biofilms grown on surfaces. The main difference between this and other treatment methods is the absence of any secondary problems associated with or a consequence of the method.

A number of physical, chemical and biological processes occur on any surface which contains microorganisms, in the presence of adequate amount of energy and microenvironmental conditions (Figure 1). The transfer, transport and transformation rates are unique to every microorganism and many of the kinetic and stoichiometric coefficients remain constant under similar influencing factors (such as pH, temperature, pressure and concentration).

A general macroscopic material balance for a single component is,

E1..NET RATE OF ACCUMULATION = NET RATE OF TRANSFER OR TRANSPORT + NET RATE OF TRANSFORMATION

In order to construct the balance, the first two terms may be experimentally measured while the last (function of an intensive property - changing only with factors that describe the environment) is calculated. It is relatively difficult to directly measure transformation processes.

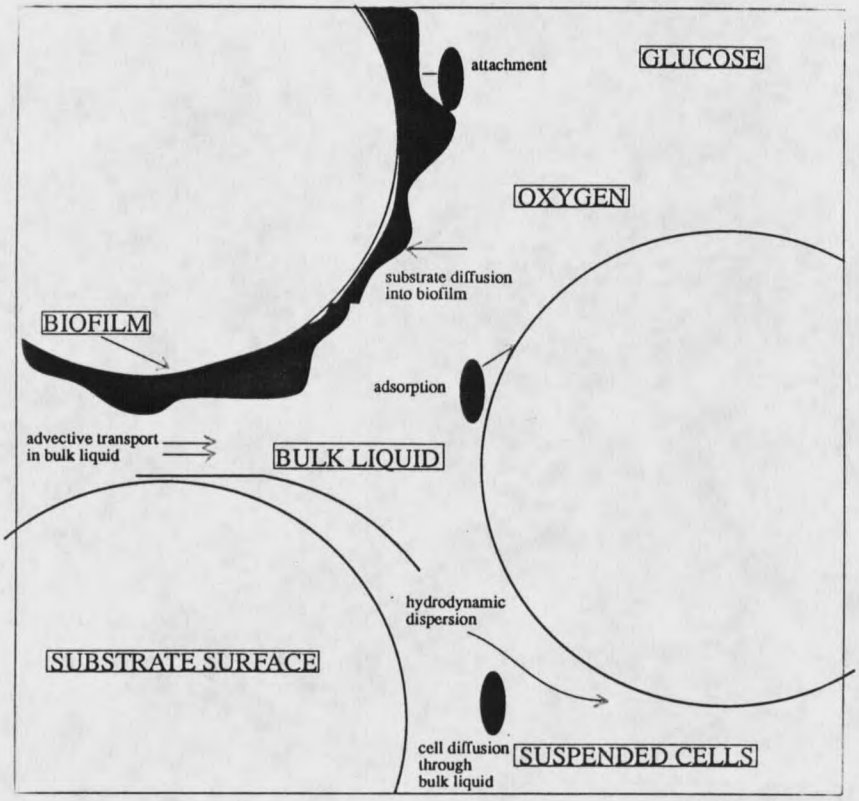

Figure 1. Biofilm accumulation patterns observed in the subsurface are caused by transport, interfacial transfer and transformation processes, including filtration, exclusively seen in porous media.

Biofilm Dynamics

Biofilms influence heat, mass and momentum transfer losses on surfaces when accumulated to a sufficient thickness. They also cause a metal loss when involved in corrosion. Advantages of immobilized cell systems include: ability to maintain a high reactor cell concentration at a range of residence times, and, an insignificant loss of biomass due to washout or hydraulic upsets caused by unexpectedly high dilution rates. Several investigators have observed that an initially adsorbed organic biofilm will sufficiently modify the inert surface so as to enhance bacterial adsorption. Cell transport to a surface is probably dominated by

molecular or eddy diffusion and is gravity assisted in preference to motility or chemotaxis.

Bacterial cellular sticking efficiency has been found to be proportional to shear stress (Characklis et al., 1984). Also, the maximum number of adherent cells were observed to be much less than the total surface monolayer coverage (about 1 - 3 % under non-growth conditions.)

As the fundamentals of biofilm technology were established, the development of fixed film waste water treatment and fermentation processes brought about the need for a model to describe substrate utilization and biomass concentration.

Recently there has been a large amount of research on extra cellular polymeric substances (EPS). Theories vary about EPS production as being a process to attach cells onto a surface, to being a mechanism for transport away from unfavorable nutrient conditions. On the other hand, there is strong evidence to suggest that EPS production is higher in viable cells as compared to starved cells. Research also suggests that EPS has highly dynamic physical and chemical characteristics which are dependent on the environmental conditions, and is supervised by the cell.

Bryers and Characklis (1982) have found that a reduction in suspended biomass concentration results in a decrease of measured deposition rate. This also indicates that rate of suspended biomass deposition is limited by the rate of bacterial particle transport to the surface rather than the rate of cell adhesion at the surface. Sometimes the overall deposition rates may decrease with increasing Reynolds number because of decreasing cell adhesion rate (sticking efficiency) even though the particle transport rate is increasing. Biofilm production due to cell growth and EPS production was found to be the major contributor to net biofilm accumulation. Also, the biofilm decay rate for thin biofilms had a negligible influence on net biofilm accumulation. Biofilm detachment rate due to shear forces was the major negative factor contributing to net biofilm accumulation. When biofilm thickness was greater than the viscous

sublayer in a flow system, the frictional resistance undergoes a large increase.

Reactor Theory

In an ideal Plug Flow Reactor (PFR), A) mixing is lateral and not axial and is incomplete, B) the residence time is high and there are no statistical fluctuations, and, C) there are changes with respect to time, and, axial and radial distance for nutrients and biomass. Many of these characteristics are in direct contrast to those found in a well mixed reactor such as a CSTR. Further, unlike a pipe flow regime where molecular diffusion, created by concentration gradients, dominates; in porous media there are pressure or velocity gradients creating hydrodynamic dispersion. This dispersion is several times in magnitude compared to molecular diffusion. The material balance mentioned earlier may be written for each component:

Substrate Balance

$$E2.. \quad \frac{dS}{dt} = D_s \frac{d^2S}{dZ^2} - v \frac{dS}{dZ} + R$$

SUBSTRATE ACCUMULATION DIFFUSION ADVECTION SUBSTRATE CONSUMPTION

where S is the bulk liquid substrate concentration, t the reactor operation time, v the axial velocity, D_s the effective dispersivity for transfer of substrate from bulk liquid into biofilm and R the net rate of substrate metabolism as given by the mass balance shown below. This is the equation for axial substrate plug flow neglecting advective and diffusive flow in x and y directions. D_s includes lateral, transverse and molecular diffusion and accounts for the higher dispersion in porous media. Assuming that the EPS non growth-associated transformation rate is negligible and that growth is limited by concentration of a single substrate S, the transformation or consumption term may be separated into terms for the cells and EPS. The term R includes both biomass in suspension and suspended material.

$$E3.. \quad R = -\mu_{max} X \frac{S}{(K_s + S)} - \mu_{max} X K_g \frac{S}{(K_s + S)} Y_{X/S}$$

SUBSTRATE CONSUMPTION RATE = CELLULAR CONSUMPTION + EXTRA-CELLULAR CONSUMPTION

μ_{max} is the maximum specific growth rate of the species, X the total concentration of cells in bulk liquid and biofilm, K_s the Monod half-saturation constant for the growth limiting substrate, K_g the EPS growth associated coefficient and $Y_{X/S}$ the growth yield of the biomass.

Biomass Balance for Suspended Cells

$$E4.. \frac{dX_s}{dt} + v \frac{dX_s}{dZ} = D \frac{d^2X_s}{dZ^2} + \mu_{max} X_s \frac{S}{(K_s + S)} + R_d$$

ACCUMULATION ADVECTION DIFFUSION NET GROWTH NET DETACHMENT

where R_d is the net detachment rate of cells from biofilm into bulk liquid and X_s the concentration of planktonic cells.

Biomass balance for Biofilm Cells

$$E5.. \frac{dX_b}{dt} = \mu_{max} X_b \frac{S_b}{(K_s + S_b)} + \mu_{max} X_b K_g \frac{S_b}{(K_s + S_b)} + R_d + R_{ad}$$

BIOFILM ACC. CELL. BIOFILM GROWTH EXTRA-CELL. BIOFILM GROWTH DETACHMENT ADSORPTION

where X_b is the concentration of biofilm cells, S_b the substrate concentration in the biofilm and R_{ad} the net rate of adsorption of suspended cells from bulk liquid to the substratum. The other assumptions are made that growth is single substrate limited and the net decay rate is negligible compared to the net growth rate. The EPS growth term is omitted from the biomass balance for suspended cells as it is traditionally associated with biofilm formation on substrata. In reality, this might not hold true.

Energy (Momentum Transfer) Balance

The above balances are mass balances. The system is assumed to be at steady-state with respect to temperature and thus there is no need for a heat balance. The energy loss across the reactor system (due to pressure drop) is the result of viscous and inertial forces, given by the equation of the form:

$$E6.. \quad \frac{P_1 - P_2}{L} = a \frac{\Omega v}{g_c} + b \frac{\sigma v^2}{g_c}$$

where P is the pressure at points 1 and 2 (influent and effluent respectively), L is the reactor length, a the viscous resistance coefficient (inverse hydraulic permeability), b the inertial resistance coefficient, Ω the absolute viscosity of the bulk fluid, σ the absolute density, v the superficial velocity and g_c the Newtons law proportionality constant. a and b may be determined experimentally for different kinds of porous media. If pure viscous flow is assumed, the above energy equation converts into the Darcy equation.

The Darcian approach is limited to Reynolds numbers less than 10. Hence, considering the relative importance of the suspended cells and/or the impaction of substrate medium on the particles, it is likely that the Darcian approach is limited in that it completely neglects inertial forces. These could play an important role in increasing biofilm accumulation rates in the porous media reactors.

Significance of Research

Petroleum Formation Plugging

This is an area in which biofilms are a definite menace. Oil is recovered from the subsurface through producing wells by providing sufficient pressure into injection wells. These wells are strategically located at varying distances from each other for the most hydraulically and economically efficient recovery of crude oil. Either fresh water or sea-water may be used for the purpose and often a part of this is recycled

after a preliminary treatment. Even though the injected water is pre-treated, inorganic salts are present in the soil and the hydrocarbons in the crude oil provide the carbon source. Microorganisms are introduced into the system either through injected water or they may exist *in situ*. These cultures begin to grow and adhere to the soil surface. Depending upon the porosity of the aquifer, they may penetrate the saturated zone along with transport of water and hydrocarbons. Eventually, they block the pores of the aquifer and prevent efficient hydrocarbon removal by bringing about high pressure drops and low flow rates.

Kolbel and Hush (1989) found that when a natural system was analyzed, biofilm cells were mostly gram positive pigmented fermentative glucose degraders while the suspended cells were mostly gram negative non-pigmented anaerobic rods. Regardless, it must be remembered that the diversity of soil microorganisms is very great. A large variety of bacteria and fungi exist in any soil sample due the abundant availability of nutrient and microenvironmental conditions. This microbial diversity has been extensively studied and a number of resulting microbial community interactions have been observed (Ward et al., 1987).

At the field site, the soil types are also very varied in terms of size, structure and nutrient content. This soil heterogeneity enhances the complexity. These two factors (microorganism diversity and soil heterogeneity) make the characterization of any soil sample a challenging task. In addition, there is an absence of a standard technique for characterization of a mixed cultures enrichment. Most enrichment methods are biased - you usually find the microbe that you look for.

Understandably, the predictive modelling of a field site, with respect to bioremediation, is no mean task and is always subject to a question of interpretation. For initial success of a theoretical prediction, the methodology for writing the model is more critical than the accuracy obtained for one field situation.

Crude oil may be present in a wetted porous rock in the form of oil

droplets. In order to decrease interfacial surface tension, surfactant is either introduced into the reservoir or produced *in situ* by enhancing bacterial activity, the latter being utilized to enhance oil recovery. Soil microorganisms themselves help in oil recovery by reducing viscosity and through the process of selective plugging. Recovery of oil was found to increase from 20 % OIP (oil in place) to 40 % OIP when bacteria were introduced into cores. Thus the results demonstrate the surfactant effect of bacterial cultures. Bubela (1984) found that for cores having similar porosities and permeabilities, the extent of plugging is decided by the nature of pore size distribution i.e. the concentration of suspended cells decides whether plugging occurs or not. Therefore the authors claim that pore size distribution is more important than the average pore size. Additionally, when a low concentration of bacterial cells was introduced into a porous medium, the permeability did not significantly decrease, thus providing the concept of 'limiting bacterial concentration'.

Adhesion and Filtration of Bacterial Cells

Loosedrecht et al., (1987) attempt to measure adhesion as a function of the contact angle of water using a micro-filter grown biofilm. The contact angle is related to hydrophobicity, which increases with decreasing surface energy. In the same study, hydrophobicity of a *Pseudomonas aeruginosa* biofilm was measured by two other methods (contact angle was found to be about 25.7 degrees), and compared to the affinity of cells to the hydrocarbon phase. The other methods were based on adhesion of cells to polystyrene and the distribution of cells between a Dextran/PEG phase respectively.

In another study, the same authors relate electrophoretic mobility to adhesion. Solid and bacterial surfaces are commonly negatively charged and these are counterbalanced by opposite charges. Between like charges, electrostatic repulsion is compensated by van der Waals attraction. In chemostat experiments it was observed that bacteria became more

hydrophobic during the exponential growth phase (high μ_{max}). These results may explain the mechanism of flocculation in suspension and adhesion to surfaces in reactors with high growth rates.

Bouwer (1987) has measured the deposition efficiency of small particles in a packed bed. For 1 mm size particles in a 0.5 mm bed, the removal is effected primarily by means of interception (transport caused by velocity gradients), giving a collection or removal efficiency of 0 to 0.1. The rate of effective particle capture, R_p may be defined:

E8.. $R_p = \alpha K_d c$

where α is the sticking efficiency ranging from 0.1 to 0.001, K_d is the overall particle transfer coefficient, and, c is the bulk liquid particle concentration.

The rate of effective particle transfer is the ratio between rate of particle sticking to packed bed element to rate of particle approaching the same. Sticking efficiency is defined as the ratio between the number of contacts between particle and biofilm leading to successful attachment and removal, to the total number of contacts.

Filtration has also been known to enhance plugging. When biocide is introduced into the aquifer in order to control souring, microorganisms are either killed or inhibited. As a consequence, sloughing may occur at the biofilm-substrata interface causing large pieces of biofilm or aggregates of cells to break away. These may be embedded in the pores of the formation at a distance from the point of biocide addition. Also, at a large enough distance, the biocide residual may approach zero and microorganisms may begin to grow and form a dense biofilm, creating formation plugging problems anew. Filtration might also be mechanically caused as a consequence of souring, by the precipitation of iron sulfides in pores.

Both detachment and attachment of bacteria to surfaces may be

beneficial during starvation. For instance, in the soil environment, detachment would cause transport of the cell and attachment to small particles would also increase the velocity of transport.

Shaw, Bramhill et al. (1985) studied the significance of the polysaccharide glycocalyx. In the past, studies on plugging of rock cores dealt mostly with dead bacteria and the importance of the exopolysaccharide glycocalyx (EPS) was underestimated. Recently, it has been shown that surface colonization of live bacterial populations in cores leads to the production of large quantities of EPS, which can cause a decrease in permeability as high as 99 %. This EPS is the result of an auto-mechanism of bacteria to adapt to low nutrient environments. It contains a hydrated matrix of mostly anionic polymers, which form chemical bonds with organic and inorganic nutrients through ion-exchange processes.

The authors observed that the slowest rate of plugging occurred in media that contained dead bacterial cells and inert silicon carbide particles, while the fastest rate of plugging occurred in media that contained both live bacteria and inert particles. In the former case a final permeability was reached when the filter cake formed its own pores and inherent permeability.

The other interesting observation was made by injecting biocide into cores that had been previously plugged with bacterial cultures. Biocide addition of a type which kills bacterial cells did not increase permeability as rapidly as an oxidant, which kills bacteria and also dissolves EPS. The authors conclude that biofilm formation is an ecologically predictable reaction of cells in order to restrict flow and entrap nutrients for use by the population.

Reservoir or Product Souring

When sulfate is present as a nutrient, sulfate reducing bacteria metabolize it to organic sulfur which causes souring. Souring has been defined as "The formation by bacterial activity of sufficient hydrogen

sulfide in the reservoir (reservoir souring) or product (product souring) to materially affect the properties of the reservoir or product fluid (e.g. oil, gas or water)" (W. Subcasky, Chevron - personal communication). Even if sulfate and short chain hydrocarbons are not initially present in the system, there may be microorganisms such as general fermentative heterotrophs (GAB) that can metabolize the nutrients into those that may be useful for SRBs. The oil industry has determined that at some time period after the initial breakthrough, souring will occur, regardless of the reservoir conditions and little can be done to prevent it entirely. The important requirements are a liquid phase and a reducing environment - conditions that are almost always prevalent in most oil recovery operation environments. The situation is far worse for sea-water flood systems as the fluids are rich in sulfates and assimilable organic carbon. Sulfur must be mechanically or chemically removed or separated from the hydrocarbons to meet crude standards. The hydrogen sulfide or sulfur di oxide gases, formed mainly in formations and injection/production wells as a result of bio-chemical or chemical reactions must be continuously disposed. Souring is therefore expensive to control especially since EPA imposes stringent air and effluent discharge quality standards.

Bioremediation

This is a field wherein the positive influence of microorganisms may be utilized. For instance, at contaminant spill sites, chemical/mechanical treatment strategies are adopted for the saturated zone where transport of fluids is easy and the contaminating hydrocarbons may be pumped out, treated and pumped back to the fluid stream. However, when microscale levels of contaminant concentrations (decided by regulatory agencies) are desired, these methods may no longer be cost effective. At very low concentrations, the process may be replaced by microbial degradation.

Bouwer and Cobb (1987) show how a biofilm model may be useful in predicting the most likely electron acceptor and donor (or most likely

metabolic pathway) in a heterogenous environment. Since specific microorganisms biodegrade a specific micro-pollutant the model may help in two ways: A) it could predict which nutrient needs to be added into the subsurface for enhancing biodegradation (or predict the micronutrient most likely to be biodegraded) or, B) it could predict which microorganism species needs to be introduced into the soil. Either of the methods eliminate guesswork in designing expensive injection/extraction wells and pumping systems.

In their model, the basic modelling equation is derived by simultaneously solving equations for the following: A) flux of substrate across fluid boundary layer (Ficks first law), calculated as a function of axial distance, B) steady-state substrate utilization by Monod kinetics and diffusive transport within the biofilm, and, C) steady-state biofilm thickness formation related to maintenance energy of biomass by Monod kinetics.

A similar theory applies to the vadose zone where most of the contamination problems occur. Since there is not much transport in this zone, treatment becomes difficult and there is a stagnation of contaminants. Land farming has been conventionally practiced as an effective treatment method.

In one study (Raymond et al., 1976), several kinds of oils were introduced into soils under optimum conditions for biodegradation. The average reduction in concentration varied between 49 and 90 % depending on oil and soil types. The average rate of degradation of oil was found to be 2.4 $m^3/4 \times 10^3$ m^2 per month.

Selective Plugging

Like the above microbially enhanced solution options above, this method for improving recovery of hydrocarbons from formations is in its research stage. Often, during oil recovery operations in injection/production well systems, the pressure drop created by the

injected water is lost due to losses in the recovery zones. If these zones are "selectively plugged", the hydrocarbon loss will be lower and the required pressure drop would be sustained. Introduction of chemicals into these loss zones has been successfully used to form precipitates and block the pores. However, microorganisms form a suitable alternative with the advantage of naturally selecting for the larger pore size first.

McLeod et al. (1988) found that the percent plugging of cores is a function of pore volumes of injected bacteria and is of greater importance for viable cells as compared to dead or starved cells. The starvation of *Klebsiella pneumonae* was observed to cause a reduction in the glycocalyx content of the biofilm. A reduction in EPS content theoretically implies

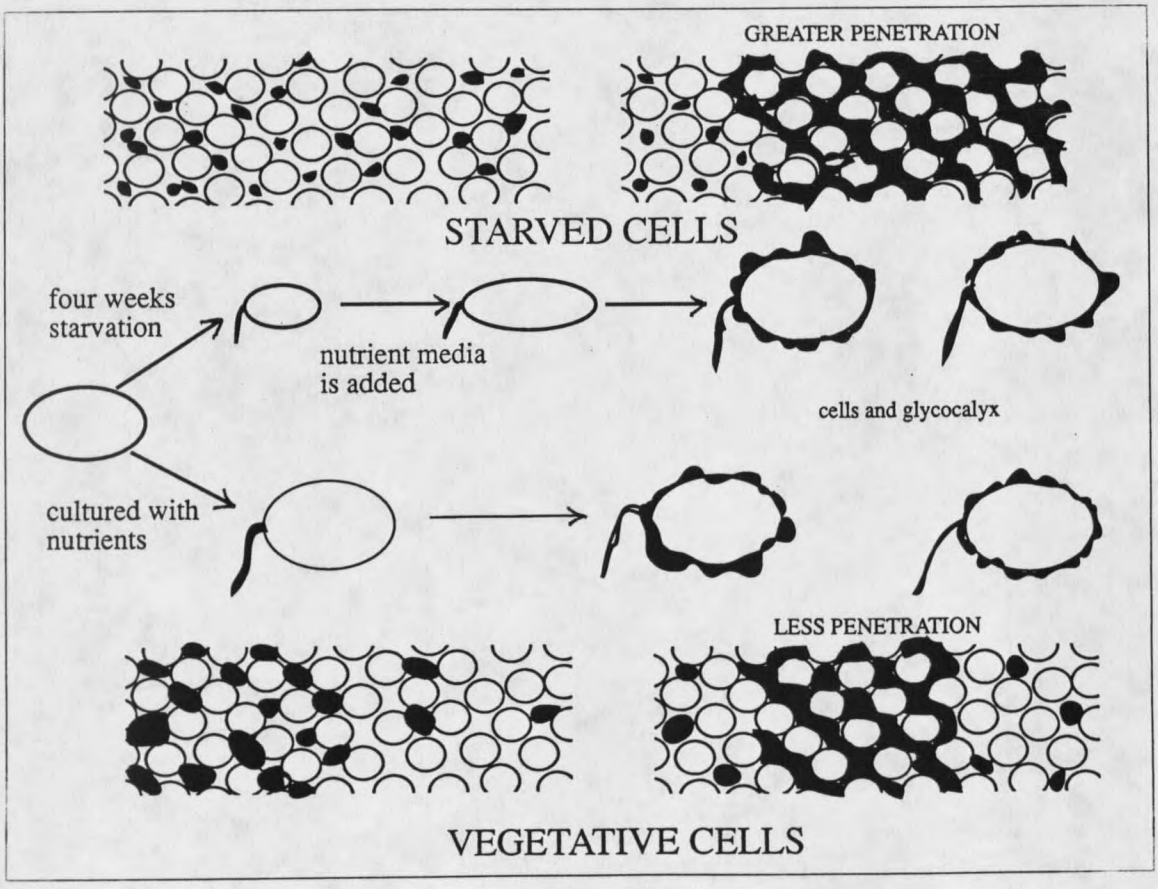

Figure 2. Studies have shown that starved cell cultures contain submicron sized bacterial cells, which when stimulated with nutrients, gradually attain normal size and growth. Lappin-Scott et al., 1988 measured deeper penetration into cores when starved cell suspensions were injected.

a reduction of bacterial adhesion and core plugging. Another observation was that respiration per vegetative cell was highest in the middle section of the core. It is stipulated that the biomass, aggregated at the inlet end, may have limited either substrate.

Lappin-Scott et al. (1988) use similar theory with sandstone cores in place of glass media. Their results show that when starved *Klebsiella pneumonia* were injected along with nutrients, the cell size and shape changed from small cocci to larger rods. The authors used 200 - 400 mDarcy for permeability, which is representative of oil well formation data. The injection of finely dispersed solids in oil or water, or *in situ* chemical reactions leading to insoluble precipitates are methods that are currently in use for plugging. This study indicates that bacteria offer a feasible alternative owing to deeper penetration and selective plugging of permeability zones.

Starved cells penetrate deeper into cores and form a better resistance to fluid flow (Figure 2). If these cell cultures were injected at selected locations, they would be first transported into the larger pores. With the provision of nutrients they would block the pores. The present study has shown that the larger the particle diameter (or pore size), the higher the biofilm accumulation (due to higher substrate flux).

Research Purpose

Goal

Develop a fundamental understanding of processes which control transport, attachment, growth and activity of microorganisms in porous media.

Objective 1:

Develop experimental methods for monitoring temporal and spatial distribution of biofilm and related variables.

Objective 2:

Conduct a process analysis including all relevant biochemical and hydrodynamic variables.

Experimental Tasks

Preliminary work was accomplished by Crawford (1987). One of first objectives was to confirm the consistency of the previous experimental procedures. A confirmatory method, using dye tracer study, was also developed for measurement of biofilm thickness *in situ*. The analytical techniques were standardized to avoid misinterpretation of experimental data in the future.

Six sets of experiments were run in an orderly manner shown (Figure 3), each with a specific objective. The progression of these experiments was such that a preceding experiment formed a basis for designing the succeeding one. The modelling work was not completed and is thus not mentioned in the thesis.

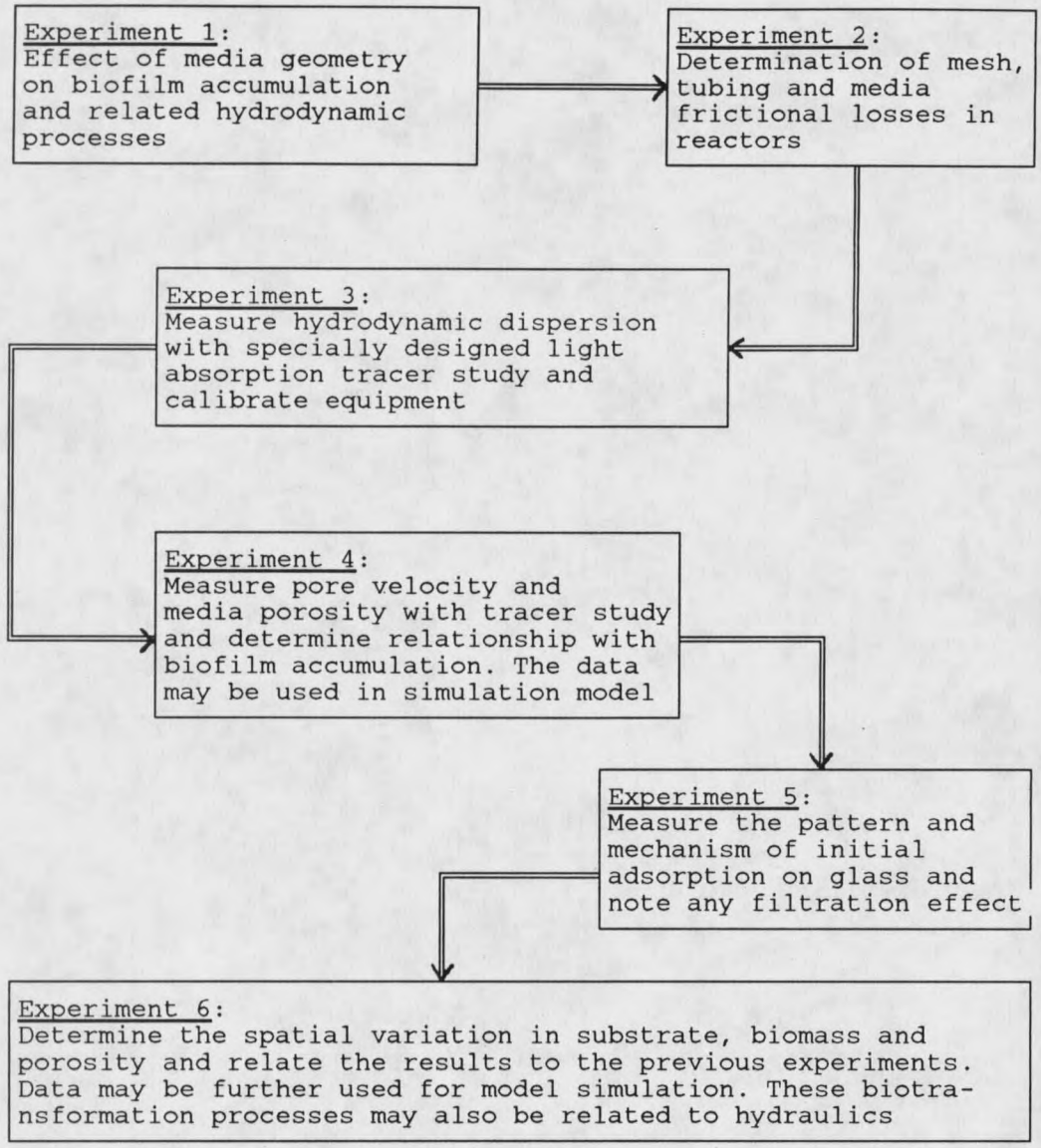

Figure 3. Schematic of sequential order of tasks for the six sets of experiments.

EXPERIMENTAL METHODS

Description of Experimental Systems

System 1 was used for experiments 1 to 5 and System 2 for experiment 6 (Figure 4 and 5 respectively). The systems utilized a constant head reservoir which was connected by rubber tubing to glass tube reactors arranged in parallel to provide a continuous supply of nutrient media. A pipette was provided at the effluent end to measure volumetric flow rate. System 2 used continuous inoculation from a chemostat and had no recycle stream while System 1 was batch inoculated (via syringe) and used recycle flow. Improvements were incorporated into System 2 because A) the micropore filter (0.2 micron Capsule filter, Gelman Sciences, Inc.)

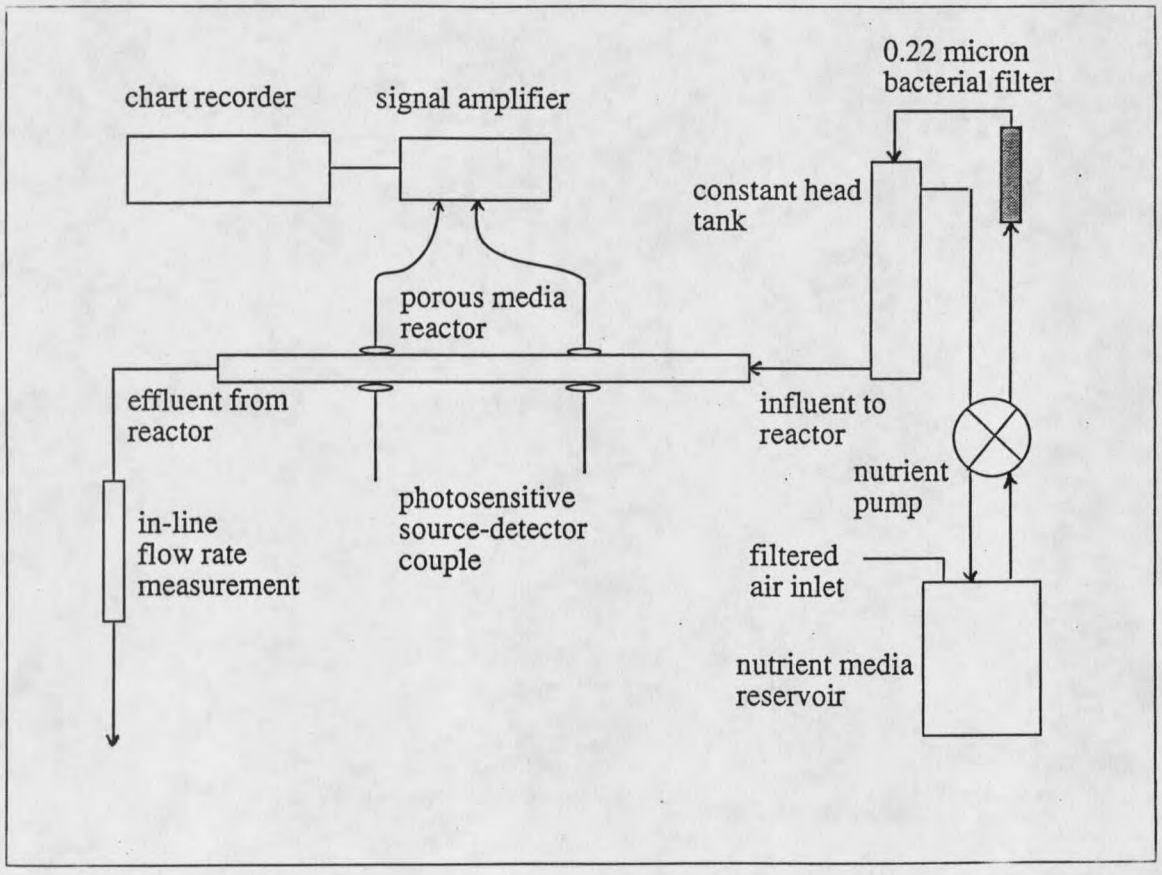

Figure 4 Experimental apparatus used in the experiments 1 through 5. A similar scheme was used for the residence time distri-bution study in the simulated porous media.

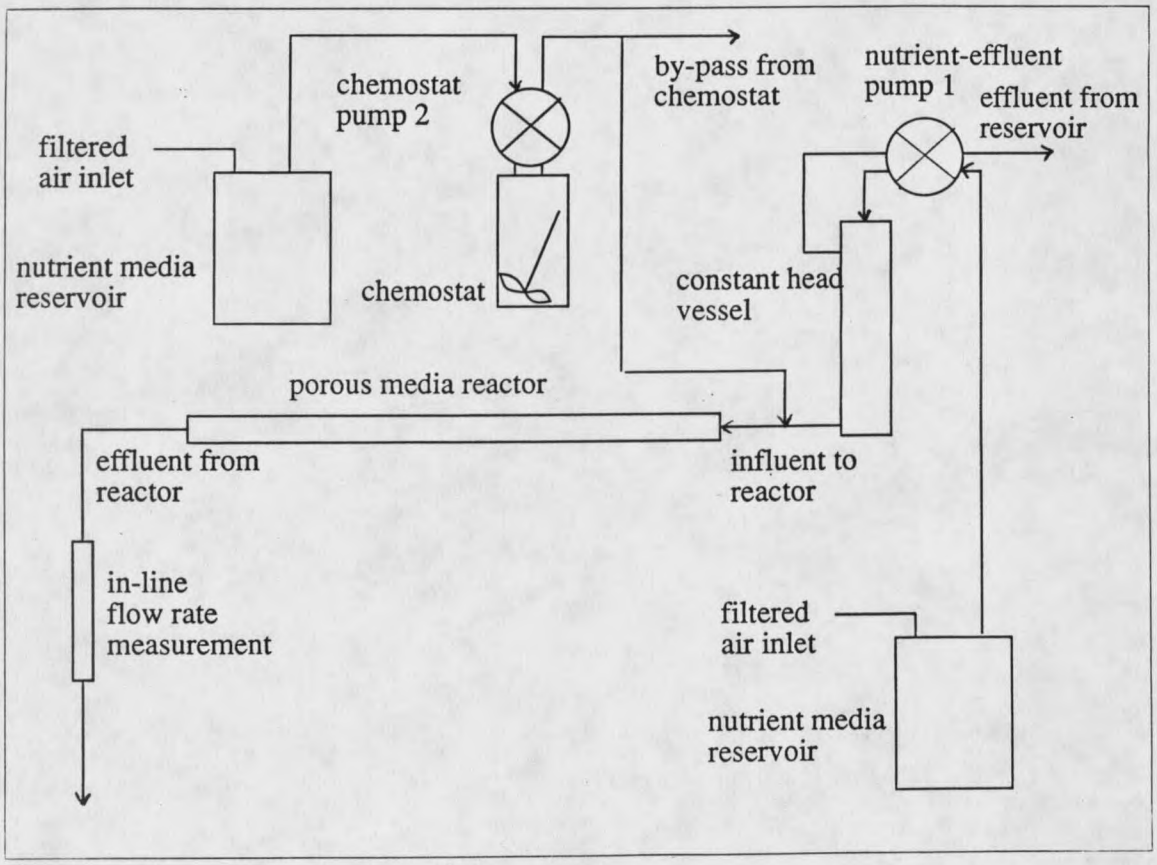

Figure 5 Schematic of experimental apparatus used for experiment 6. Note the absence of recycle, the different method used for inoculum and absence of micro-filter.

had bacterial growth though the recycle feed was sterile, B) a larger volume of inoculum was needed for experiment 6, and, C) air bubbles, which sometimes provided significant pressure drop across the system, could be easily removed.

The assembled equipment was autoclaved at 18 psi and 120°C. The tubing was silicone (Masterflex size 14 ID 1.6 mm, size 15 ID 4.8 mm or size 17 ID 6.4 mm depending on need) rubber and the pumps were 100 or 600 RPM (Peristaltic Masterflex). Only the tubing used in the segmented reactor was made of oxygen impermeable material (Masterflex Neoprene size 17). At several locations along the system, cotton plugged air inlets (with negligible resistance) were placed to prevent pressure build-up. All

the effluent streams had back-flow prevention devices which additionally helped prevent or delay contamination.

Construction of Reactor

The reactor and glass spheres (Ferro, Cataphote Division, Jackson, Miss.) were constructed of plain borosilicate glass and had a tolerance of 5 micrometer. In order to keep the glass beads in their packed form, a steel wire mesh of high porosity was used. This material did not show any sign of corrosion and when examined for cells did not behave as a filter (Crawford, 1987). The wire mesh was cut into pieces which had the same area as the glass reactors and were glued either at the entrance, or 1 cm inside the reactor for the larger reactors. In the former case, silicone tubing along with silicone glue held the mesh in place and each time the tubing was removed, the mesh came apart. In the second case, the enclosed mesh enabled a change of tubing without disturbing reactor contents. In either case, the tubing was merely slipped over the glass reactor and glued down (Figure 6). It was presumed that the closest possible packing was achieved. The reactors were manually packed with media until no more could be added. When sand was used as the media, it was sieved using

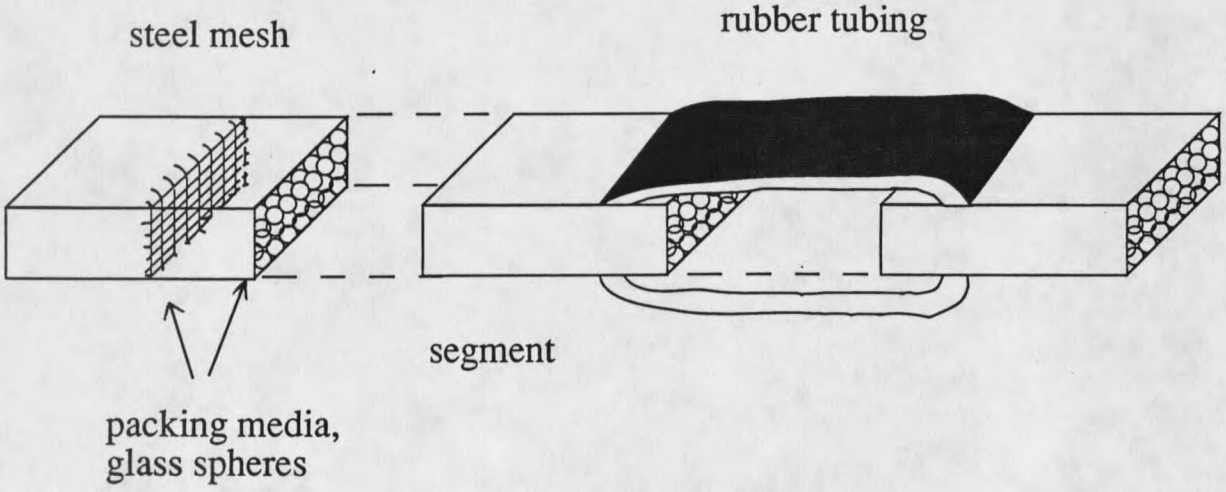

Figure 6 An exaggerated cross-sectional view of a porous media reactor as constructed. Note that the design called for a handicraft skill with glass and other materials.

Table 2. Description of the porous media reactors

Exp. no.	D_{pe} (cm)	Initial Porosity	V_r (cm^3)	L (cm)	r_H (cm)
Exp 1					
Reac. 1	0.0396	0.4577	0.60	5.0	0.00557
2	0.0500	0.4075	0.60	5.0	0.00566
3	0.0465	0.4602	0.60	5.0	0.00656
4	0.0085	0.3859	0.60	5.0	0.00089
5	0.0110	0.4598	0.60	5.0	0.00157
6	0.0396	0.4547	1.02	8.5	0.00554
7	0.0110	0.4598	1.08	9.0	0.00158
8	0.0500	0.4075	1.08	8.5	0.00572
Exp 2					
Reac. 1	0.10	0.4298	8.18	30.3	0.017
2	0.10	0.4298	4.16	15.4	0.017
3	0.10	0.4298	8.18	30.3	0.017
Exp 3					
Reac. 1	0.10	0.4298	8.18	30.3	0.017
Exp 4					
Reac. 1	0.10	0.4298	1.35	5.0	0.017
2	0.10	0.4298	1.35	5.0	0.017
Exp 5					
Reac. 1	0.10	0.4298	9.72	36.0	0.017
Exp 6					
Reac. 1	0.10	0.4298	15.12	56.0	0.017
2	0.10	0.4298	15.12	56.0	0.017

where D_{pe} is the equivalent initial diameter of spheres, V_r is the volume of reactor (cross sectional area x length), r_H is the average media pore size and L is the length of the reactor.

standard sieving techniques, and the average diameter was calculated from the weight fraction of material retained or passing through.

System Operation

Any extraction or inoculation of material from the reactor system was accompanied by a 70 % ethanol spray and dry heat scorching if the surface in question was heat resistant. The head loss was varied for different experiments and similar substrate loading rates were maintained. However, during the experiment, head loss was unchanged. In System 1 nutrient was pumped from the nutrient media reservoir to the constant head reservoir, the excess (overflow) being recycled back to the substrate reservoir. The flow rate of recycle stream was kept higher than that of the influent stream by using larger diameter tubing. System 2 simply discarded excess media from the constant head reservoir.

The temperature fluctuated between 27 - 32°C. Needles used in sampling/inoculation were gage 26s or 27 stainless steel. (size 26s ID 115 microns OD 470 microns; size 27 ID 200 microns OD 400 microns). The rubber tubing was thick enough to provide sufficient sealing ability when pierced. Dow Corning silicone glue was exclusively used wherever needed.

Nutrient Media

Concentrated solutions of various compatible nutrients were made up and filter sterilized. Each time the required amount was pipetted to make up 11 liter of substrate with distilled water. After the pH was adjusted to 6.8 with dilute sodium hydroxide or hydrochloric acid it was autoclaved for 45 minutes at 18 psi and 120°C. The exceptions to this procedure were glucose and calcium chloride, which were separately autoclaved in 100 ml conical shake flasks for 15 minutes. These were then cooled and added aseptically to the cool bulk substrate and well mixed by shaking the substrate reservoir. Prepared substrate was discarded after two days in order to avoid contamination and precipitation of phosphates, and

substituted by a fresh batch.

Calcium concentration in the substrate media has an effect on biofilm density, maximum film thickness, biofilm rates and EPS production. In previous studies (Turakhia, 1986), better initial adsorption was achieved with a higher concentration of free calcium. Keeping this in mind, the concentration of calcium maintained was limited only by the solubility product of calcium phosphate, the most insoluble species.

Table 3. Substrate nutrient composition (Siebel, 1987)

Nutrient	mg L^{-1}
Glucose	25.6
Nutrient solution	
Ammonium chloride	7.2
Magnesium sulfate. 7 H2O	2.0
Calcium chloride	1.0
Micronutrient:	
Zinc sulfate. 7 H_2O	0.100
Manganese sulfate. H_2O	0.008
Copper sulfate. 5 H_2O	0.002
Sodium borate. 10 H_2O	0.001
Other nutrients	
Iron sulfate. 7 H_2O	0.112
Aceto nitrilic acid	0.400
Buffer	
Sodium phosphate, Na_2HPO_4	213.0
Potassium phosphate, KH_2PO_4	204.0

Table 4. Characterization of distilled water

pH	5.1 (winter) to 6.4 (summer)
TOC	0.2 mg L^{-1}
Viable cell count,R2A agar	usually < 100 CFU/ml
Conductivity	39 microMho

Bacterial Culture and Inoculation

A pure culture was used for the experiments for the following reasons: A) a uniform biofilm resulted B) modeling a single species was

easier, and, C) kinetic and stoichiometric coefficients for *Pseudomonas aeruginosa* were widely available.

A stock culture was prepared, identified by the Rapid NFT technique (Trademark of API System, S.A.) and then frozen in vials at -7.0°C. Small quantities were withdrawn from these vials whenever needed and cultured. This process acclimatized the bacteria to the expected reactor nutrient conditions. A test (described below) indicated that the procedure was effective. The growth rate and viable concentration of cells was enhanced several times with each additional 'acclimatization'.

Table 5. Characterization of *Pseudomonas aeruginosa* (Brock, 1988)

Heterotrophic aerobic bacteria belonging to Pseudomonads. Opportunistic pathogen associated with infections of the urinary and respiratory tracts in humans. Especially harmful to immuno-compromised individuals. Primarily a soil microorganism. Produce water-soluble yellow-green fluorescent pigment but do not form poly-beta-hydroxy butyrate. Highly studied organism.
Metabolism
Can utilize sugars, fatty acids, di- and tri- carboxylic acids, alcohols, aromatic compounds, amino acids, and amines and many more compounds. May produce small amounts of acid from aerobic glucose metabolism. May use nitrate for denitrification as an alternate electron acceptor (other than oxygen). Produce pyocyanin, live in neutral environments at temperatures to 43°C.
Physical characteristics
Size : 0.5 - 1.0 micron by 1.5 - 4.0 micron. Gram negative, non-spore forming, slightly curved rods Motile by means of single polar flagella.
Identification
No photosynthetic pigments. No gas formation from glucose. Positive to oxidase test.

In system 1, a bacterial cell suspension of 3 - 4 times the void reactor volume was injected into the influent of the reactor. The nutrient media flow was stopped for 8 - 10 hours, i.e. reactor contents were

quiescent, to promote adsorption to the surfaces in the reactor.

For system 2, a chemostat was operated in a semi-batch mode. It was initially run as a batch reactor for 24 hours until sufficient cell numbers could be plated (appearance of turbidity). The reactor was now maintained with sterile nutrient media dilution. Whenever reactor inoculation was needed, effluent from the chemostat was used. However, a batch dilution was needed such that all visible turbidity disappeared. This additional step was felt necessary in order to eliminate the occurrence of filtration processes. The viability of the inoculum was quantified by a plate count. The inoculation was continued for 5 - 10 hours at a flow rate which was a fraction of the initial reactor flow rate. The reactor was then plugged off for about 4 hours. Some experiments required a second inoculum for initiation of adsorption and growth.

Analytical Procedures

Hydraulic Conductivity and Flow Rate

Flow rate was a convenient parameter for monitoring the progress of the experiment as biofilm thickness effects the pore size. Flow conditions are better expressed in terms of hydraulic conductivity or intrinsic permeability, both of which are functions of the hydraulic gradient. Intrinsic permeability accounts for the properties of the fluid (density and viscosity). Darcys relation has been derived based on the assumption that the flow is laminar and the Reynolds number never exceeds 10.

E9.. $Q = - A K dh/dL$

where Q is the volumetric flow rate, A the cross sectional area of channel, dh/dL the hydraulic gradient and K the hydraulic conductivity (LT^{-1}). Intrinsic permeability is defined from this relation

E10.. $K = C d^2 \sigma/\Omega$

where C is a constant characteristic of the porous media, and d is the

grain size. The term C x d^2 is a constant for the porous media, known as the intrinsic permeability k (L^2).

Biofilm Thickness Measurement

The reactors were narrow enough to be inserted under the eyepiece of a compound microscope (Bausch and Lomb, Inc.). As light enters the glass and water, refraction occurs at the surfaces and an apparent image is created. Refraction would occur thrice at the air-glass, glass-biofilm and biofilm-bulk liquid interfaces (Figure 7). In order to reduce errors in measurement caused by refraction, a calibration was performed for the micrometer with a standard scale.

Looking through the eyepiece of the microscope, a cross section of the biofilm is seen in concurrence with the micrometer divisions. Thus a biofilm growing on the glass beads can easily be quantified in terms of biofilm thickness. In order to measure film thickness on reactor walls, the eyepiece was focused first on the glass surface and then on the biofilm surface and the difference in the vertical displacement of the microscope microscale divisions was noted. The latter procedure is subject to an error because of the difficulty in optically locating the irregular surface of the biofilm.

Micrometer calibration:

(Full scale = 100 divisions, Zoom setting = 1.0)
Total magnification = objective x eyepiece (= 10)

35 x = 30.3 microns per division
100 x = 10.3 "
430 x = 2.35 "

Viable Aerobic Heterotrophic Cell Count

Culture plates were prepared by sterilizing a 24 mg L^{-1} solution of R_2A agar nutrient media, for 20 minutes at 21 psi and 120°C. The melting temperature of the resulting solution was 70°C and the solidifying temperature 40°C. 15 ml each was poured into sterile plates and allowed to solidify unperturbed. Dilution water tubes were prepared by making up 9 ml of buffer solution per test tube. The buffer solution contained the same

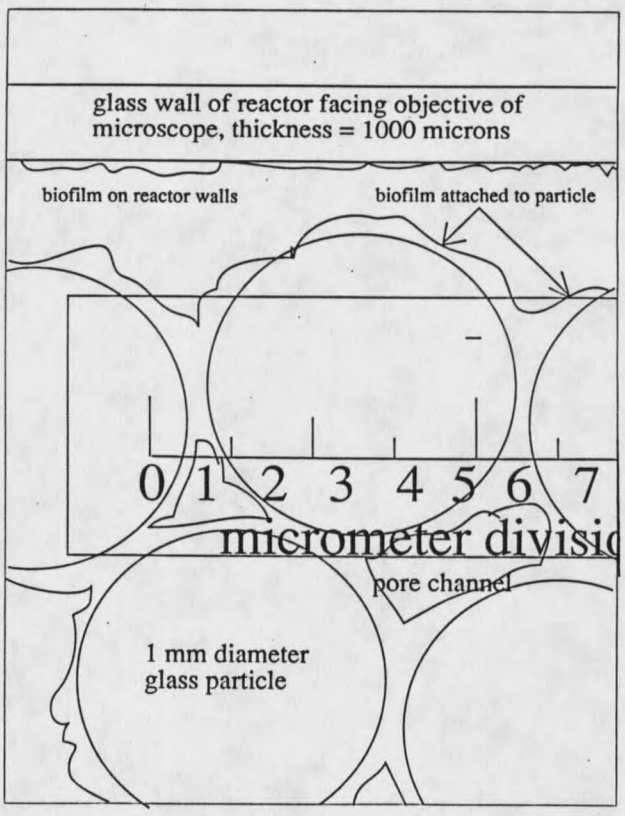

Figure 7 The flat glass reactor when viewed through the eyepiece of a microscope. The objective lens of the microscope would be on the viewers side (above figure). Figure not drawn to scale.

concentration of phosphates as the substrate. Following sterilization of these dilution water tubes, serial dilutions were performed for the sample containing viable cells as follows. 1 ml sample was added to the first 9 ml dilution water. After vortexing, 1 ml of the resulting solution was then added to the next dilution water tube. This created a 1/10 dilution factor. 0.1 ml of diluted sample was then plated on sterile agar plates. It was spread out evenly over the agar with a bent glass rod and the plate was incubated a day at room temperature. The number of serial dilutions was preplanned in order to obtain plates with the adequate number of colonies (30 - 300 per plate). When colonies were clearly visible on the

agar plates, they were counted and the numbers reported as Colony Forming Units (CFU) per plate. These were converted to CFU ml^{-1} by accounting for the total dilution of the original sample.

Total Organic Carbon

A small volume of sample was injected into the semi-permeable membrane port of a carbon analyzer (Dohrman DC 80 Automated Laboratory Total Organic Carbon Analyzer, Santa Barbara, CA). Ultra violet light and strong oxidant (persulfate) was provided in an acid solution to effectively oxidize all organic carbon. The procedure for calibration and analysis was taken from the operation manual (Dohrman DC 80 Systems Manual, Santa Barbara, CA). Whenever concentration of soluble (dissolved) organic carbon (SOC) was desired, the sample was passed through a 25 mm glass microfiber filter before analysis. The glass microfiber filters (Gelman Sciences, 1 micron) were placed into a muffle furnace at 500°C for 45 minutes to remove traces of carbon. This filtration method was found inadequate at concentrations less than 5 mg-C/l and for original sample size of less than 2 ml.

All glassware was washed carefully with dilute chromic acid and then rinsed with excess carbon free water. Before injecting a sample, concentrated phosphoric acid was added to it to ensure a pH of 2 - 3 for better oxidation and to remove carbonates and bi-carbonates. The sample was also oxygen purged to remove dissolved carbon di oxide. Before beginning an analysis, the instrument was calibrated with a previously prepared standard solution.

Glucose Analysis

The enzymatic method (Sigma Diagnostics, Procedure #10, Sigma Chemical Co.) was used. The test is based on the catalytic oxidation of glucose (glucose oxidase) into gluconic acid followed by a second catalytic (peroxidase) oxidation into ortho-dianisidine. The final product

has a brown coloration which may be measured with a spectrophotometer.

The direct method as applicable to serum or plasma was used since the sample was not markedly turbid. For a detailed description refer procedure manual. The volume ratio of sample to Combined enzyme reagent was maintained at 0.5 to 5. i.e. 0.5 ml of sample for 5 ml of enzyme for a glucose concentration of 25 mg L^{-1}. A spectrophotometer (DMS 90 UV - Visible light Spectrophotometer, Varian Techtron, Mulgrave, Australia) was used for determination of light absorption with a wavelength of 475 nm. The results were recorded with the help of software (INTERFACE CHECK1, Software for DMS 90/Plus Single Component, Varian Techtron). Each time a new analysis was commenced, the solutions and instruments were recalibrated.

Tracer Techniques

Mean Reactor Media Porosity: Porosity was approximated as a function of pore velocity and specific discharge. In porous media, two types of velocities may be defined. Specific discharge (or superficial velocity) is a function of volumetric flow rate and empty reactor cross section area. Pore velocity (or Darcy velocity) is the velocity of bulk liquid within the pore. For the latter porous media is presumed to be approximated by a bundle of fine capillaries. In reality, the flow paths are not linear and tortuosity must be considered an important phenomena. Bouwer (1978) has related these variables in porous media assuming that the effects of tortuosity are negligible:

$$\text{E11.. Effective media porosity} = \frac{\text{Specific discharge}}{\text{pore velocity}}$$

Pore velocity was measured with dye tracer studies in which two Cadmium sulfide light sensitive detectors were placed in parallel with two visible light emitting diodes with the reactor in-between them (Figure 4). Both the sets of source/detector cells were placed inside a block of

opaque polycarbonate specially designed for the purpose. These LEDs were wired to a 12 volt DC current source. The detector cells were wired via an amplifier to a voltmeter, whose output was recorded on a chart recorder (Model SRLG, Sergeant Co.). The blocks were designed to be light tight when placed together with the reactor. The distance between each source/detector set could be varied but was set at 4.7 cm for this experiment. The qualities desired for the dye were: A) least amount of adsorption and diffusion into cells, B) negligible deleterious effect on viability of cells, and, C) good light absorption characteristics, even in the presence of biofilm.

Biomass causes diffusion and adsorption of tracer. The extent of dye adsorption on packing media and biofilm depends on the diffusion characteristics of the dye. Jimenez et al. (1988) have shown that the rate of diffusion of a chemical is inversely related to its molecular weight. However, at lower flow velocities, and in small reactor channels, dyes with higher molecular weights, such as Dextran blue, will diffuse very slowly into the packing media and biofilm. This increases the possibility of flow channelling of flow during dye addition, leading to unrealistic results. Thus, a compromise was made between diffusive properties and flow through the media at low velocity. After assessing a number of available dyes, bromothymol blue was chosen.

Table 6. Characterization of bromothymol blue (Conn, 1953)

Chemical name Dibromothymolsulfonphthalein. Molecular weight 624.4 Molecular formula C27H2805SBr2 Dissociation constant, pK = 7.0
Color indication was as follows: acid.....pH 6.0.....yellow neutral.....pH 7.0.....green alkaline.....pH 7.6.....blue

It was used as a biological stain and an indicator in culture media. Preliminary tests with the dye (described below) showed that it was harmless to *Pseudomonas aeruginosa*.

Technique of Pulse dye Injection: A 50 ml saturated solution of bromothymol blue was made up with distilled water, the pH was adjusted to 6.8 with acid/base, and it was autoclaved for 15 minutes. On cooling it was transferred into sterile 10 ml rubber-capped tubes. Whenever needed, a hypodermic syringe was used to extract the sterile solution of dye. For a single pulse input, 0.2 ml of dye was injected into the influent stream within a few seconds at 5.0 cm distance from the entrance to the reactor. Once in the reactor the tracer dispersed through the bulk liquid and biofilm and a chart recorder registered the amount of light transmitted (or absorbed) through the reactor continuously. From the resulting concentration-time curves, the (center of mass) distance between the curves was calculated (method 3). This was the time taken for the center of the pulse to move the distance between the light sensors. The pore velocity was used to calculate media porosity. The procedure was repeated after 364 hours of biofilm growth. Porosity may also be theoretically calculated from mean biofilm thickness (method 1) or analytically determined for sterile media (method 3).

Method 1 Theoretical calculation (assuming uniform biofilm thickness)

1 : Calculate volume/particle V_p assuming spherical shape of particle with diameter D_{p_i} with shape factor Q_s.

E12.. $$V_p = \frac{4}{3} \pi \frac{(Q_s D_{p_i})^3}{8} = 0.524 D_{pe}^3$$

where D_{pi} is the average diameter of sterile media

2 : Calculate the volume of solids V_t present in reactor of volume V_r, based on initial porosity E.

E13.. $$\text{Initial porosity} = \frac{\text{total reactor vol - total solid vol}}{\text{total reactor vol}} = \frac{V_r - V_t}{V_t}$$

3 : Calculate total number of particles in reactor, N_p

E14.. $$N_p = \frac{V_t}{V_p}$$

4 : Calculate effective porosity E' for any given biofilm thickness L_f using equivalent diameter Dpe.

E15.. $$E' = \frac{V_r - V_t - (\pi\ Dpe^2\ N_p\ L_f)}{V_r}$$

Using this method, the porosities as shown in Table 2 were obtained.

Method 2 Analytical determination of media porosity for sterile media

$$E16..\ \text{Porosity of reactor} = \frac{(\text{vol of empty dry reactor} - \text{dry particle vol})}{\text{vol of empty dry reactor}}$$

$$E17..\ \text{particle volume} = \frac{(W1 - W2)}{\sigma}$$

where W1 is the weight of crucible and particles, W2 is the weight of empty dry crucible and σ is the specific gravity of the particles which is determined as shown below.

$$E18..\ \sigma = \frac{(w4 - w1)}{\{(w2 - w1) - (w3 - w4)\}}$$

where σ is the specific gravity of the media, w1 is the weight of empty dry sp. gravity bottle, w2 is the weight of bottle and 25 cm3 water, w3 that of bottle and particles with water (made up to 25 cm3) and w4 is the empty dry weight of bottle and particles.

Using this method, the following specific gravities were obtained:

Borosilicate glass : 2.469 to 2.540
Sand : 2.676 to 2.805

Hydrodynamic Dispersion: From the resulting input and output concentration-time curves, the mean residence time and mean variance was calculated for the initial and final reactor conditions ie. clean media and media with biofilm growth. By comparing the two, change in dispersion due to the biofilm was estimated. The Dispersion Model for a plug flow system was found to be suitable for analysis. Expecting a large dispersion, the "large deviation from plug flow, or D/UL > 0.01" was used. Also, the influent/effluent streams to the reactor were assumed to be plug flow, making the vessel one with 'closed' boundary conditions, or a closed vessel (plug flow conditions outside vessel up to the boundaries). The dye injection was presumed to be a pulse input. In practice, however, the mean and variance of the reactor residence time is the difference between the respective influent and effluent values. The Dispersion number, D/UL, was first estimated by approximation. The Mean Residence Time was calculated using both the methods shown below, but only the tracer method was used in calculations. This was necessary for consistency, as the porosity of the

media changed with biofilm growth and hence was a function of axial distance. The second method, using flow rate, yielded a space average value as the changing volume of reactor was not measured.

Method 3 Mean media porosity determined from tracer study

1 : Plot the concentration-time curves

The following variables were then determined for each curve:

E19.. Analytical Mean Residence Time = $\frac{\text{Reactor volume}}{\text{Flow rate}}$ (for sterile media only)

E20.. Mean residence time, MRT = $\Sigma\ Cit_i/\Sigma\ C_i$

E21.. Mean variance, VAR = $\Sigma\ C_i t_i^2/\Sigma\ C_i$

E22.. Dimensionless mean variance = $\frac{(VAR)}{(MRT)^2}$

where C_i is the concentration of dye at time t_i and $\delta\ t_i$ is the constant time interval.

2 : Find the difference in mean and variance between input and output.

Delta Mean residence time (DMRT) for the reactor = $MRT_{out} - MRT_{in}$
Delta Mean variance (DVAR) for reactor = $VAR_{out} - VAR_{in}$

3 : Find the Dispersion number, D/UL.

(First approximation) Delta Dimensionless Mean Variance = $2(D/UL) = DVAR/(DMRT)^2$

E23.. Dimensionless Delta Mean Variance (DDMR) = $2\ (D/UL) - 2(D/UL)^2\ [1 - e^{-UL/D}]$

4 : Find the effective dispersivity D.

D/UL is known and D may be evaluated for each set of curves i.e. for sterile media and for biofilm media since U and L are known.

(Theory adapted from Octave and Levenspiel, 1984.)

where VAR is the mean variance (minutes^2), MRT is the mean residence time of the reactors from dye study in minutes, D is the effective dispersivity in cm^2/sec, U is the pore velocity as described earlier in cm/sec and L is the length of the section over which dispersion is being evaluated (23 cm). The Dispersion number for the reactor is a product of the following:

E24.. D/UL = D/Ud * d/L

where D/Ud is a function of Schmidt number and Reynold number. If the flow was solely by diffusive transport, the reciprocal quantity, Ud/D, would be the Bodenstein number and D would approach the molecular diffusion (rather than the hydrodynamic axial dispersion). In the above theory, the 'tailing' phenomena has not been taken into consideration primarily because the recovery of dye was about 90 %. No correction for the "tailing" phenomena was felt necessary at this stage.

Dissolved Oxygen

The reactor size permitted the removal of only small volumes of sample, (0.5 to 1.5 ml). Therefore a microelectrode (tip diameter 50 microns, Diamond General Development Corp., Ann Arbor, Michigan) was found necessary. The membrane for the microelectrode tip was provided and placed in the laboratory. The open end of the syringe was glued to a glass tube of 2 ml capacity, which acted as a reservoir for drawn sample. Liquid from the reactor flowed into the reservoir by the pressure gradient existing across the reactor. A 6 cm long 27 gage steel needle was pierced into the oxygen impermeable rubber tubing (Figure 8). The oxygen and reference microelectrodes were positioned into the reservoir and held steady by means of a clamp. The purpose of the fine capillary needle was to accommodate the extraction of sample at a rate which did not perturb the hydrodynamic conditions existing in the reactor. This extraction rate was maintained at 10 % or less of the total reactor flow rate.

The microelectrode and reference electrode were coupled to an amplifier which read the current in picoamperes, which in turn was wired to a chart recorder that plotted the current continuously. Before use, the system was calibrated by saturating a solution, similar to the reactor contents, with oxygen and nitrogen alternately and plotting the resulting curves. Ten such saturation cycles needed to be performed before stability was achieved. Using the calibration, picoamperes were converted to units

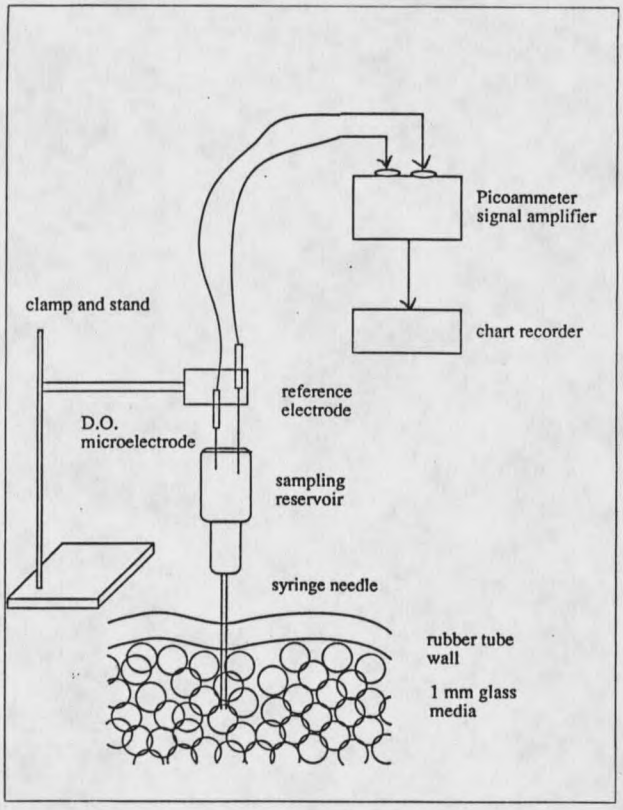

Figure 8 Schematic outline for the sampling/extraction method employed for determination of substrate glucose, organic carbon and oxygen.

of concentration in mg L^{-1} of oxygen. Although the oxygen analysis was performed within 5 minutes, re-dissolution of oxygen into the sample from the atmosphere was possible. Experiment 6 indicated that a maximum of 1.5 mg L^{-1} of oxygen could possibly have re-dissolved into the reservoir sample during analysis. This analytical error spells the need for an improved procedure for determination of dissolved oxygen *in situ*.

Mesh and Tubing Losses

The purpose of the experiment was A) to determine and compare the hydraulic resistance due to mesh, tubing and packing media, and, B) to verify the accuracy of the frictional resistance measurement techniques. Mesh, tubing and media losses were determined for two identical 30.3 cm reactors of cross sectional area 0.27 cm^2 one of which was packed with 1 mm glass spheres and a third 15.4 cm reactor of similar dimensions also filled with the same media (Figure 9). Sterile water was pumped through the reactors at varying flow rates and pressures. The pressure difference across each reactor was measured with liquid U-level manometers.

Experimental plots of friction factor as a function of Reynolds number correlate reasonably well with those calculated from Kozeney-Carman (Figure 10) but not with Fahien and Leva relations. The experiment

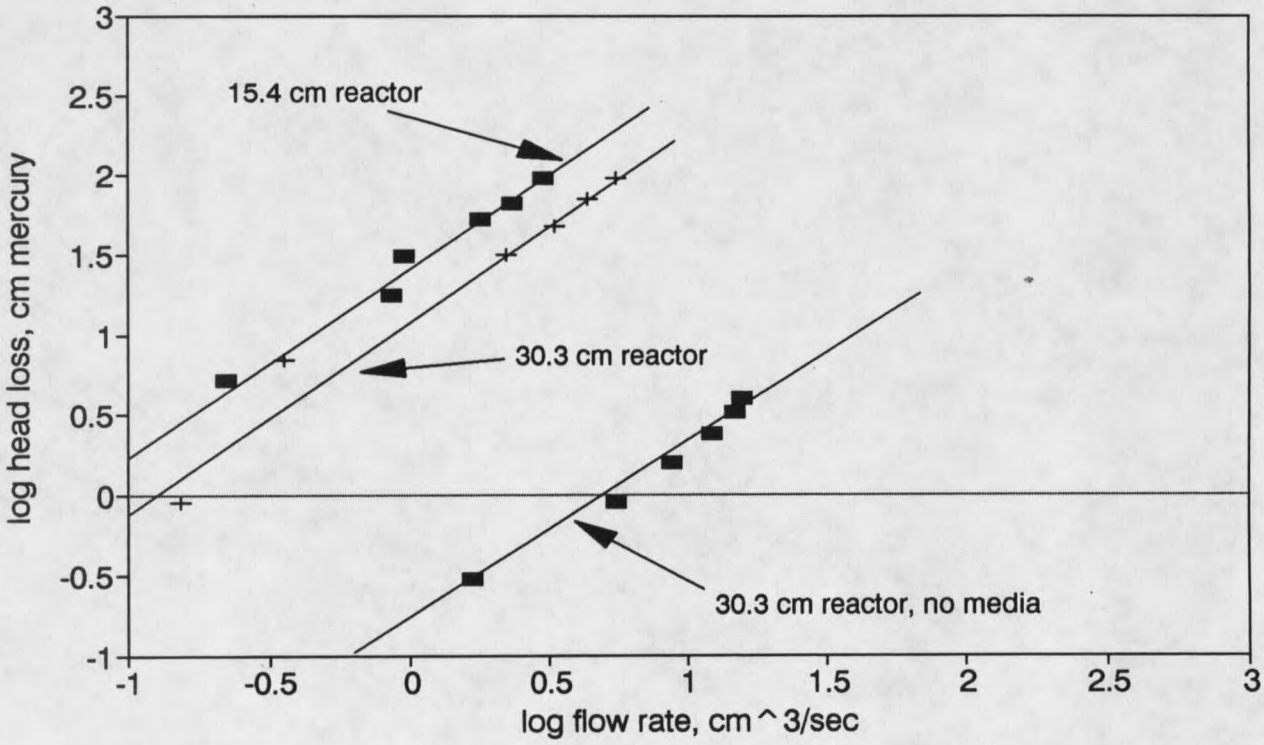

Figure 9 Pressure loss caused by mesh and tubing for different reactors. (Media, whenever used, was 1 mm glass spheres and cross sectional area of reactor 0.27 cm^2).

concludes that frictional losses due to the steel mesh and reactor surfaces are negligible when compared to losses due to tortuous flow paths in the packing media.

Aseptic Sampling Techniques

Extraction or introduction of sample from or into the system was accomplished by means of a sterile hypodermic syringe needle. The thick walls of the rubber tubing promoted a self-sealing ability of the pierced area. The area to be affected (external to the reactor system) was sprayed with 70% ethanol and/or wiped clean with iso-propyl alcohol with sterile cotton swabs. The area surrounding the equipment was kept aseptic by wiping all exposed surfaces with a 700 ppm solution of Roccal (a commercial biocide) before sampling. A flame was used for heat-scorching

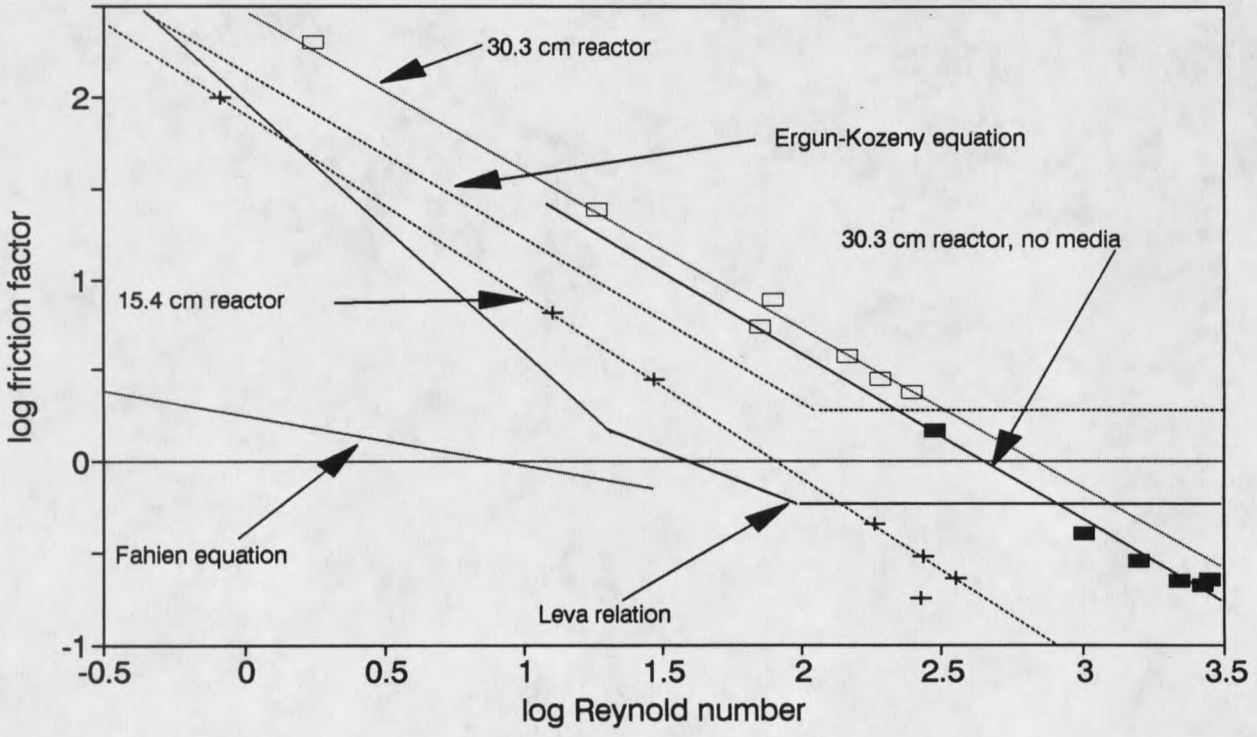

Figure 10 Comparison of experimental data obtained from the previous reactors, with the Ergun-Kozeny (Ergun, 1952) Fahien (Fahien and Schriver, 1961) and Leva (Leva, 1959) relations.

any heat resistant surfaces. For example, when replacing consumed nutrient media jugs, the glass connectors were placed in the flame and sprayed with ethanol on cooling. At varying stages of the experiment, a viable plate count was made and the colonies were visually observed. Whenever contamination was detected, the experiment was repeated. For example, the contamination in experiment 6 was detected after about 200 hours of experimental time. It was probably caused by the substrate sampling technique used for the determination of SOC, TOC, glucose and oxygen.

Destructive Analyses

Whenever an analysis of the reactor contents was required, the flow of nutrients was first terminated and then the rubber tubing was cut off from both ends of the reactor. For segmented reactors it was additionally cut off between each segment. Only sterile equipment was used in the analysis. The packing media was poured into a beaker and a measured quantity of sterile water was used (in addition to scraping) to wash down any cells sticking to the inner walls of the reactor. In order to detach cells from the glass beads, the beaker containing the spheres and biomass was placed into an ultrasonic sonicator for 15 minutes. This was re-sonicated and stirred immediately before sampling. All analyses were performed within a short period of time, however TOC samples were frozen for later analysis as a matter of convenience.

Test for Acclimatization of *Pseudomonas aeruginosa*

This test was performed in order to quantify the increase in the viability of cells caused by "acclimatization". Note that virtually all experiments used a similar 'adsorption-acclimatization' step during the initial stages of the experiment. 0.2 ml of culture from the frozen stock was placed into 75 ml of substrate solution (Table 3) in a 100 ml conical flask. The flask was stoppered by a foam stopper and then placed on a shaking table. When there was no more visible change in turbidity, (24

hours at 37°C) the batch culture in the flask underwent a viable heterotrophic plate count. 0.5 ml from this flask was then placed into another fresh batch of 50 ml substrate and treated identically. The results showed (Table 7), for the same time period, there was a 2.5 fold increase in cell concentration with the first acclimatization step and a 30 fold increase with the second step.

Table 7 Increase in cell viability caused by "acclimatization"

First acclimatization step

Initial:
Concentration of cells = 10^{11} x 0.2 / 75 = 2.7 x 10^{8} CFU ml^{-1}

After 24 hours:

S.no.	Dilution factor	Plate count	CFU ml^{-1}
1.	1.21 x 10^{-6}	TNTC	-
2.	1.21 x 10^{-7}	117	9.7 x 10^{8}
3.	1.21 x 10^{-8}	11	9.1 x 10^{8}

Average = 9.4 x 10^{8} CFU ml^{-1} = final concentration of cells
Percentage increase in CFU ml^{-1} = 248.1 %

Second acclimatization step

Initial:
Concentration of cells = final concentration from previous step
= 9.4 x 10^{8} x 0.5 / 50
= 9.4 x 10^{6} CFU ml^{-1}

After 24 hours:

S.no.	Dilution factor	Plate count	CFU ml^{-1}
1.	1.0 x 10^{-5}	TNTC	-
2.	1.0 x 10^{-6}	316	3.2 x 10^{8}
3.	1.0 x 10^{-7}	32	3.2 x 10^{8}

Average = 3.2 x 10^{8} CFU ml^{-1} = final concentration of cells
Percentage increase in CFU ml^{-1} = 3304.2 %

Toxicity of Bromothymol blue to *Pseudomonas aeruginosa*

The experiment was designed to detect any deleterious effect of the dye on a pure culture of *Pseudomonas aeruginosa*. Conditions similar to those inside the reactor (time of exposure, concentration of dye and cell concentration) were simulated in test tubes.

Calculation of dye concentration needed to simulate reactor conditions:

Approximate typical flow rate from experiments = 0.027cm^3/sec
Approximate rate of tracer flow = 0.0015 cm^3/sec
Volume of cell culture per unit volume tracer = 0.027/0.0015
= 18.3 ml

18.3 ml of a pure culture of *Pseudomonas aeruginosa* from a batch reactor containing 10^8 CFU ml^{-1} after a 48 hour acclimatization step in substrate media, as previously explained, was placed into sterile 20 ml test tubes. 1 ml of a saturated solution of bromothymol blue was introduced into these test tubes and serial dilutions were made. After a five minute exposure to the dye, the solutions in the dilution tubes underwent a viable heterotrophic plate count with R_2A agar. The control experiment consisted of dye-free test tubes that were treated identically. The results, as shown below indicate a negligible effect of bromothymol blue on the bacterial viability. On the contrary, the dye behaved as a carbon source for *Pseudomonas aeruginosa*.

S.no.	Dilution factor	Plate count without dye	with dye
1.	10^{-3}	-	TNTC
2.	10^{-4}	_	TNTC
3.	10^{-5}	230	TNTC
4.	10^{-6}	21	171
5.	10^{-7}	14	9
6.	10^{-8} (not used in calculation)	0	0

Average viable cell concentration without dye = 1.9 x 10^7 CFU ml^{-1}

Average viable cell concentration with dye = 1.3 x 10^8 CFU ml^{-1}

TNTC - "too numerous to count" or much greater than 300 CFU/plate.

RESULTS

Comparison of Short Reactor Behavior

The extent of biofilm accumulation was found to be proportional to the particle size, for the same pressure drop. In experiment 1, eight reactors differing in media size and geometry were connected and operated in parallel, so that they had a constant pressure drop of 16 cm of water across the influent and effluent ends. They were provided the same nutrient media and inoculated with *Pseudomonas aeruginosa* (see Methods). Pure culture conditions were maintained with aseptic techniques. Biofilm thickness and volumetric flow rate were recorded at periodic intervals of time and the experiment was allowed to progress until a relatively constant flow rate and film thickness was obtained. The biofilm thickness was found to be uniform axially as well as radially, with respect to reactor length though there was some standard deviation at different locations. The flat glass reactor internal walls also supported biofilm growth whose thickness was comparable to that accumulating on the media. Table 8 summarizes the characteristics of the reactors and their flow dynamics. The biofilm thickness measurements (Figure 11) displayed higher standard deviation on sand than on the uniform glass beads. "Entrained" biomass could also be visually observed in sand, probably on account of it being more angular than glass beads. Friction factor in a porous media bioreactor increased steeply after a "critical biofilm thickness" was obtained. The friction factor for sand media was twice that for glass media and the Reynolds number half that for glass. A linear relationship was observed between permeability and biofilm thickness, when plotted dimensionless on a logarithmic scale. These aspects are discussed in the following chapter.

The steady-state film thickness was higher with glass as media when compared to sand at similar substrate loading rates. In general, the permeability stabilized in 2 - 2.5 days to a minimum value while biofilm

Table 8 Summarization of porous media reactors and flow dynamics.

Experiment #	k_i x E-06cm^2	percent reduction of k	MRT (minutes)	maximum L_f x E-06 m	τ_i gm/cm-sec^2	dh (cm)	$NRe_{,i}$	Glucose loading rate gm/cm^2-hr
Exp 1								
Reac. 1	1.91	95.4	0.1	38.5	4.71		2.38	0.0324
2	1.78	95.1	0.1	38.5	4.84		2.79	0.0302
3	2.66	96.7	0.05	15.4	5.52		3.88	0.045
4	1.01	91.3	0.1	0.8	18.4		0.27	0.0171
5	0.56	98.5	0.22	7.7	4.9	16.0	0.19	0.0096
6	1.81	95.8	0.19	46.2	2.64		1.32	0.018
7	1.07	92.5	0.37	15.4	5.11		0.20	0.010
8	2.27	96.5	0.15	53.9	3.39		1.98	0.021
Exp 2								
Reac. 1								
2	varied	-	varied	-	varied	varied	varied	-
3								
Exp 3								
Reac. 1	2.94	79.4	3.5	25.0	0.169	6.5	0.62	0.0033
2	2.94	71.5	3.5	25.0	0.169	6.5	0.62	0.0033
Exp 4								
Reac. 1	6.99	41.3	0.52	41.0	0.188	0.5	0.68	0.0037
2	5.99	42.7	0.61	36.0	0.161	0.5	0.59	0.0032
Exp 5								
Reac. 1	10.3	-	3.2	negligible	0.22	-	0.80	0.0044
Exp 6								
Reac. 1	10.3	77.3	4.92	120	0.22	4.5	0.81	0.0051
2	10.3	81.8	4.92	120	0.22	4.5	0.81	0.0051

where K_i is the initial intrinsic permeability, MRT is the mean residence time of the bulk liquid, L_f is the biofilm thickness, τ_i the initial shear stress at the biofilm-bulk liquid interface, dh the head loss across the reactor and $NRe_{,i}$ the initial Reynolds number.

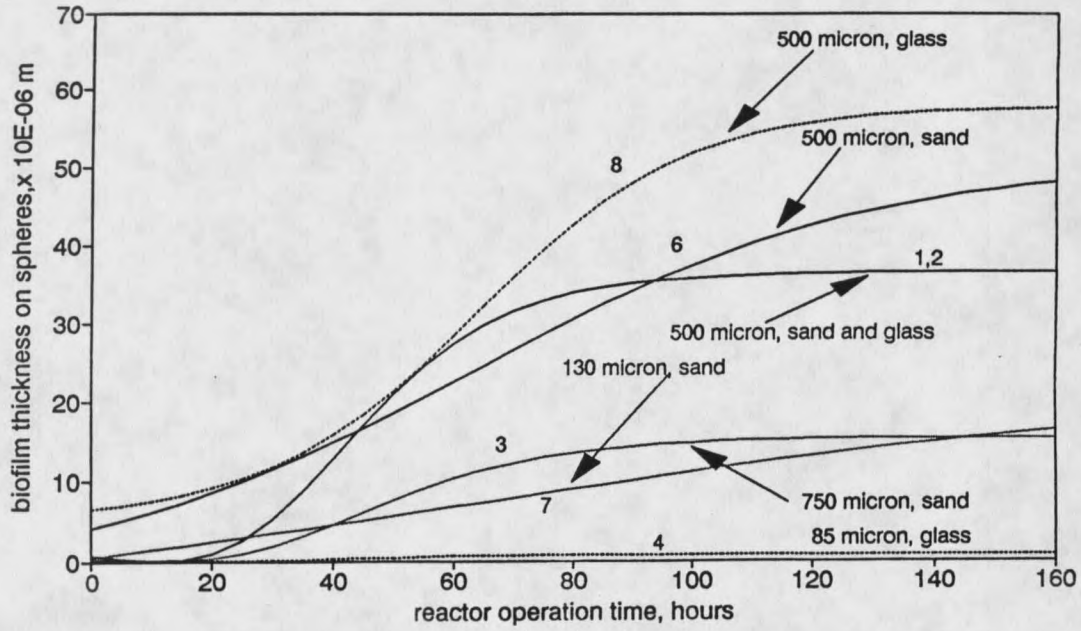

Figure 11 Biofilm accumulation for different media geometry as a function of reactor operation time. The glucose loading rate was between 96 and 450 gm m^{-2} hr^{-1}. (Numbers correspond to the reactors Table 8, Experiment 1).

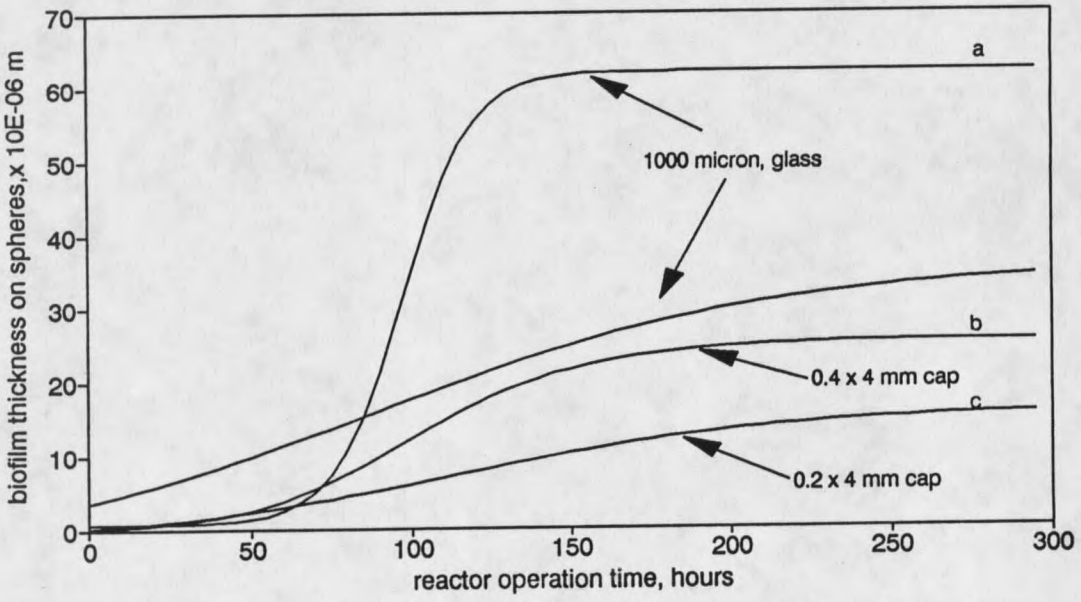

Figure 12 Biofilm thickness data obtained from previous (Crawford, 1987 shown as a,b,c) capillary and porous media reactors as a function of time.

thickness required 4 - 4.5 days to attain a maximum value. All reactors therefore encountered a 1.5 day lag between attainment of steady-state permeability and biofilm thickness. In experiment 1, the average reduction in permeability at steady-state was 95 %.

Tracer Study

Hydrodynamic Dispersion

The light source/sensor couples were placed 23 cm apart. Bromothymol blue was then injected into the influent and the concentration-time curves (Figures 13, 14) obtained for influent and effluent (as described in Methods). This was then converted to hydrodynamic dispersion for both conditions (sterile and with steady-state biofilm growth). The pressure drop across the system was kept constant at 6.5 cm. Recovery of dye was calculated by summing up and comparing the area below the input and output concentration-time curves. It was determined to be about 90 - 95 % by mass, of the input quantity of dye.

Table 9. Calculation of effective dispersivity (Experiment 3)

Condition	Mean residence time (MRT, minutes)	Mean variance (VAR, $mins^2$)
Initial (sterile reactor)		
Influent	0.77	0.142
Effluent	2.29	0.71
After 364 hours of growth		
Influent	6.43	18.43
Effluent	11.31	30.17

Condition	DMRT (mins)	$(DMRT)^2$ $(mins)^2$	DVAR $(mins)^2$	DDMR (dimensionless)
Sterile	1.52	2.31	0.568	0.246
With biofilm	4.88	23.81	11.74	0.493

These results (Table 9) were used to compute axial dispersion, discussed in greater detail further in this thesis.

Mean Reactor Media Porosity

Theoretically calculated porosity (from assumption of uniform biofilm thickness) and that from dye tracer study were found to be identical only when the surface area coverage of biofilm was considered. This area was found to be in the range of 40 to 50 %. The basic experimental system for porosity measurement (experiment 4) was identical to that used for dispersion study (experiment 3). Measurements were made over short distances (less than 5 cm). Reactor porosity could not be determined with conventional techniques when biomass was present on media. Biofilm contains about 90 % water and this must be taken into account in any measurement of porosity. Porosity was quantified by three methods: A) theoretically, assuming uniform film thickness, B) experimentally from dye tracer studies (Table 10), and, C) analytically, using the conventional technique for sterile media. Since there was no significant observed change in biofilm thickness across the length of the short reactors, film thickness could be related to porosity or pore velocity, as a function of time. Replicates were run in parallel for comparison. The experiment began sterile and was then inoculated with *Pseudomonas aeruginosa*, the same variables being measured each time. Pressure drop across the reactors was maintained constant at 0.5 cm. The light source/sensor couples were spaced 4.7 cm apart.

Table 10 Calculation of media porosity from dye study

Time (Hrs)	Tracer time t (secs)	V_p (cm/sec)	Flow rate (cm^3/sec)	v (cm/sec)	Mean porosity
Initial	210	0.1095	0.016	0.044	0.4018
364	954	0.0241	0.0033	0.00917	0.3805

where v is the specific discharge or superficial velocity, Q the volumetric flow rate in cm^3/sec, A is the empty reactor cross sectional area (0.27 cm^2), V_p the pore velocity and t the tracer time in seconds.

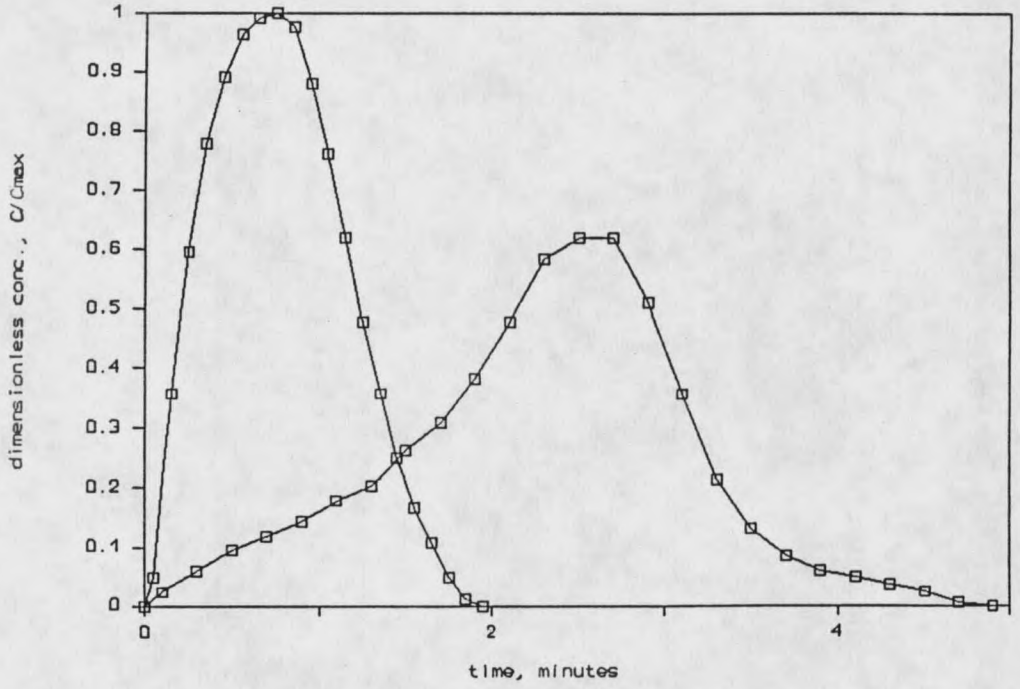

Figure 13 Influent tracer curves with sterile packing media. Higher peaks correspond to influent. 30.3 cm reactor (1 mm glass spheres, surface shear stress of 0.17 gm cm^{-1} sec^2 - exp 3).

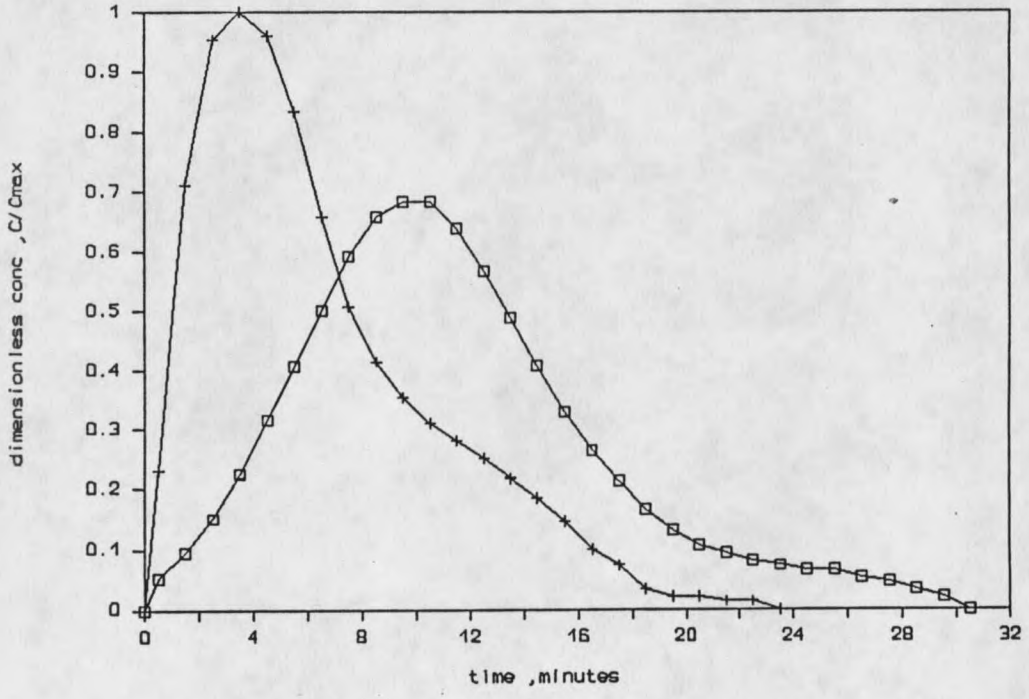

Figure 14 Effluent tracer curves with steady-state biomass growth after 364 hours for above reactor - exp 3. Higher peaks correspond to influent.

Initial Adsorption Processes

Experiment 5 determined that the axial biofilm pattern remained unbiased by the inoculation technique. The 36 cm reactor contained 10 sections, each 3 to 4 cm long, connected together with silicone tubing. The internal cross sectional area was 0.9 x 0.3 cm^2 and the total void reactor volume was 5.6 cm^3. It was inoculated with 25 ml of a suspension of *Pseudomonas aeruginosa* with a viable cell concentration of 7.3 x 10^9 CFU ml^{-1}. The reactor system was then left undisturbed for about four hours. Later, sterile substrate proceeded through the reactor for 45 minutes (12 residence times) at a constant flow rate (0.0217 ml/sec). The substrate flow was then halted and the reactor cut apart into segments. Variation of TOC and viable cell concentration (Figure 15) with respect to axial distance confirms that the adsorption processes, under the conditions of

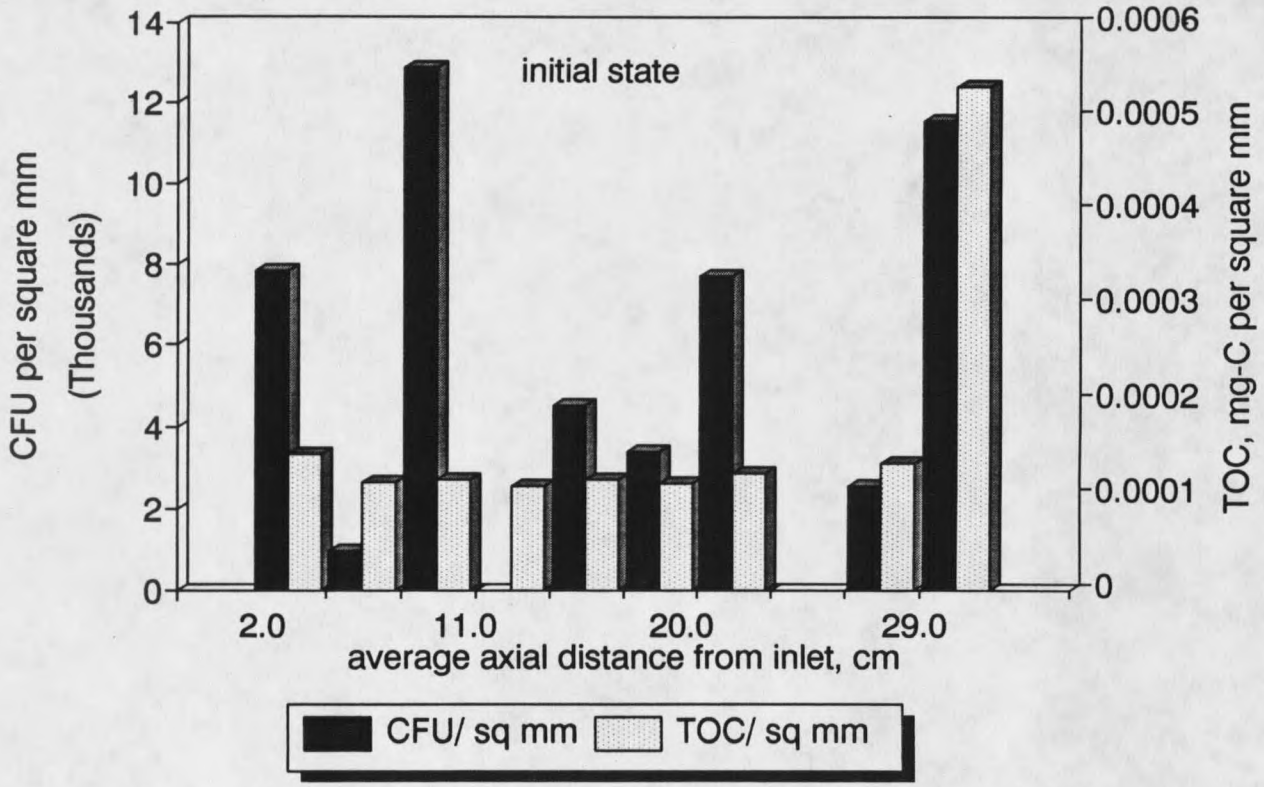

Figure 15 Distribution of total organic carbon and total viable heterotrophic plate count in a 36 cm reactor (1 mm glass spheres) immediately upon inoculation with *Pseudomonas aeruginosa*. (Coeff. of var for CFU/mm^2 was 70 % and for TOC mg-carbon/mm^2 was 91 %)

this experiment, are random and hence should not be responsible for biofilm accumulation patterns observed elsewhere.

The pore space for 1 mm spherical glass spheres is about 300 microns while the average length of bacteria is about 1.5 microns. The inoculum used for the larger reactors had a cell concentration of 10^4 to 10^5 CFU ml^{-1}. Under these circumstances, no significant filtration would be expected for non-biological materials, but might not be so for organisms that are capable of producing EPS, which, among other functions adheres cells to surfaces for better nutrient supply in a flowing environment.

Biotransformation Processes

Though pure culture conditions were attempted, a contaminant was detected in the segmented reactor after 200 hours of reactor operation. The "contaminant" was identified by the Rapid NFT technique to constitute a coliform, an aerobic fermentative bacteria.

Biofilm accumulation rates, substrate utilization rates and hydrodynamic parameters are intimately related through mass and energy balances. Other than glucose-carbon (electron donor) and oxygen (terminal electron acceptor), nutrients were provided in excess. Two reactors each 56 cm long and of identical cross sectional area were packed with 1 mm glass spheres. One reactor was constructed with 12 connected reactor segments and the other one was constructed from a single piece. The second reactor acted as a control to evaluate the bias of segmentation. Head loss of 4.5 cm across the reactors was kept constant.

Substrate Concentrations

The Sigma test for glucose demanded a minimum filtered sample volume of 0.5 ml (about 1.5 ml unfiltered) when the expected concentration of glucose in the sample was 20 - 25 mg L^{-1}. Since the void reactor volume was about 7 ml, no more than 0.5 ml of substrate could be extracted at a time (to maintain a sample to reactor volume ratio less than 10 % or an

extraction rate less than 10 % of reactor flow rate). In order to overcome this low sample volume limitation, dilution of extracted sample was attempted. However, large analytical errors were created. Only influent and effluent streams were therefore analyzed in replicate. Results (Table 11) indicate that glucose is almost completely depleted in the effluent stream.

Table 11 Glucose concentration in influent and effluent streams

Axial distance from entrance (cm)		Sample 1	Sample 2	Sample 3	Sample 4	Mean
		concentration (mg L^{-1})				
Influent	0.0	22.7	15.9	14.2	17.5	17.57
Effluent	56.0	5.8	0.06	0.3	0.85	1.75

Dissolved oxygen was not completely depleted in the effluent stream but (Figure 16) attained a steady minimum concentration of 3.5 mg L^{-1} at steady-state. As the carbon to oxygen ratio from stoichiometry is 0.9 gm/gm, and the average carbon concentration in the effluent was 1.75 mg L^{-1}, it follows that glucose-carbon was the growth limiting nutrient. Also, from stoichiometry, the oxygen concentration in the effluent stream would be expected to be about 1.5 mg L^{-1}. Re-aeration during analysis may be responsible for the 2 mg L^{-1} difference. The stoichiometry experimentally obtained is 1.2 gm glucose-C (gm oxygen)$^{-1}$.

The dissolved organic carbon (SOC) measurement had a high standard deviation for replicate samples taken along the reactor length (Figure 17). This error in analysis was created by the dilutions that were performed to overcome the extracted sample volume limitation, as described earlier.

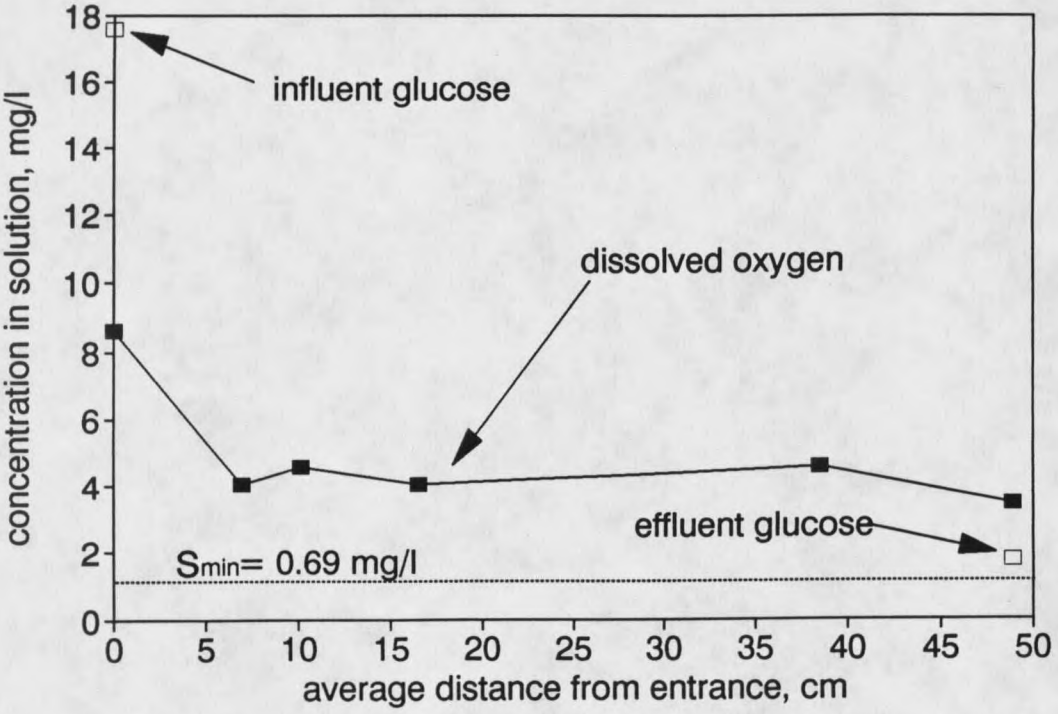

Figure 16 Observed dissolved oxygen and glucose concentration axial profile. S_{min} is the calculated minimum glucose concentration for a biofilm (Rittman and McCarty, 1980).

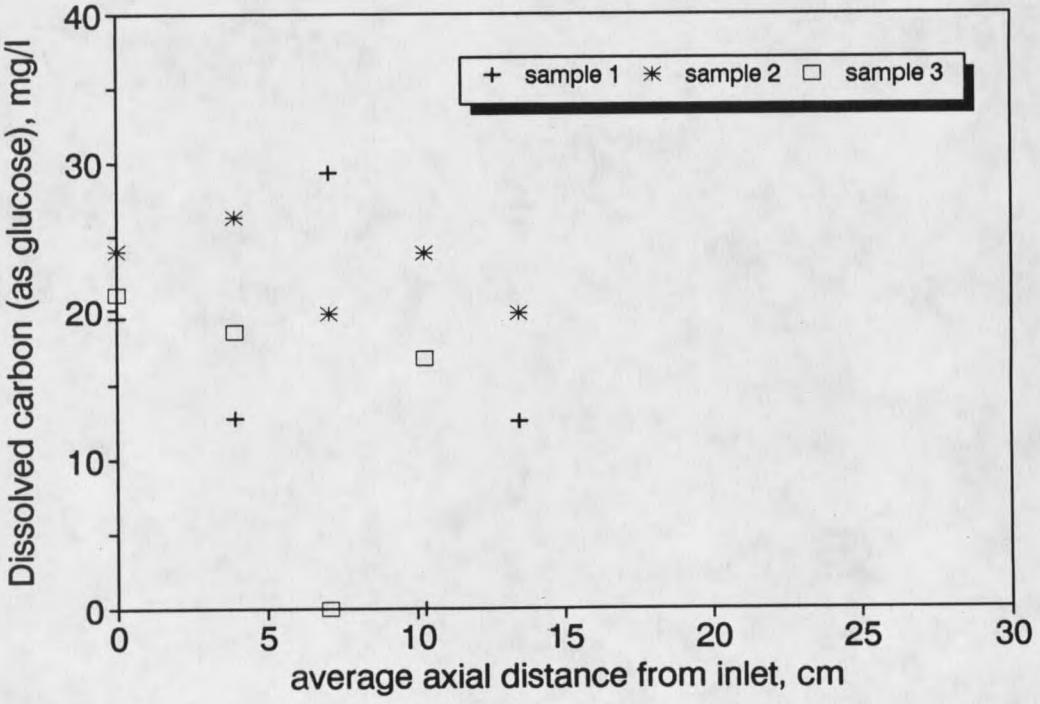

Figure 17 Axial variation of dissolved organic carbon (SOC) for 55 cm reactors - experiment 6.

Biomass Measurements

Biofilm thickness was determined post steady-state, when the relative changes in film thickness and permeability (Figure 18 and 19) reached their minimum. The biofilm is highly dynamic, with the recurrent processes of attachment, detachment, growth, death and sloughing being active, but net growth rate is constant.

Samples of suspended cells were extracted from the effluent and influent streams at intervals of time from both reactors in experiment 6. The net (effluent - influent) suspended cell number increased with time (Figure 20). A similar observation was made in another experiment using a 10 cm reactor (1mm glass spheres) at a head loss of 12 cm (Figure 40).

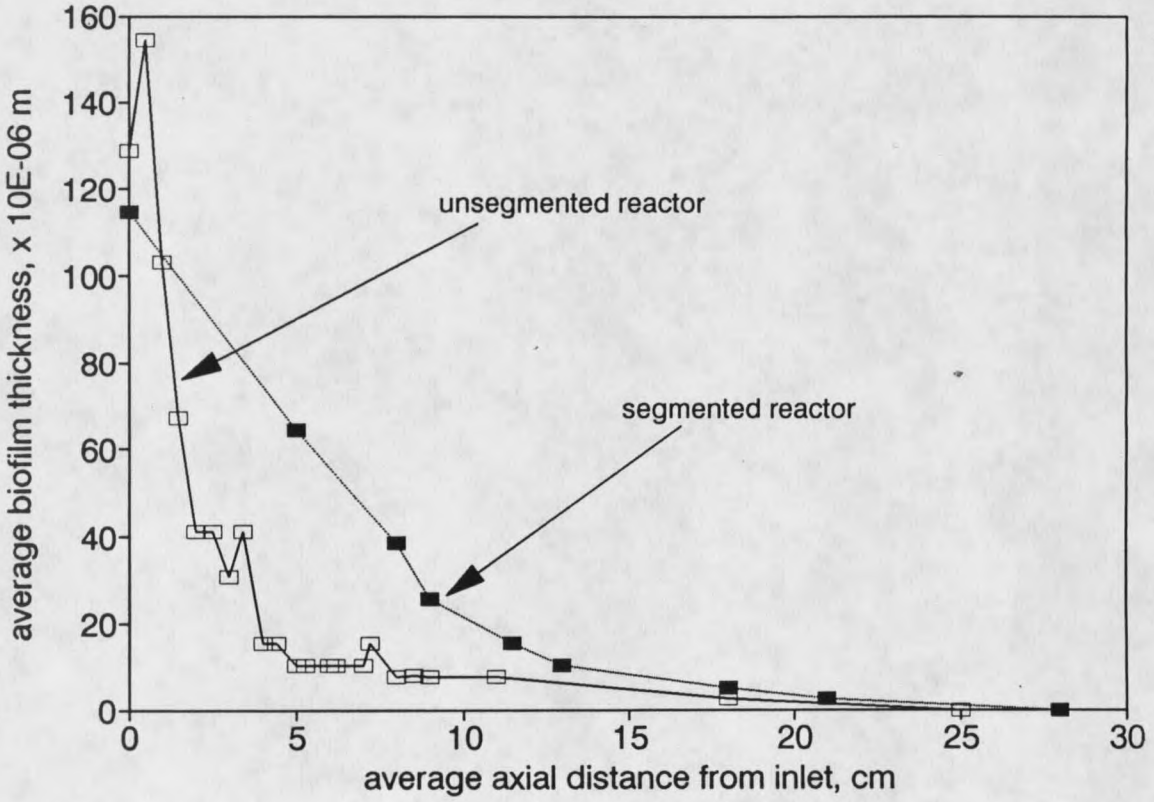

Figure 18 Axial variation of biofilm thickness time for the 55 cm reactors post steady-state. Glucose loading rate was 51 gm m-2 hr^{-1} and shear stress at the surface was 0.22 gm cm^{-1} sec^{-2}.

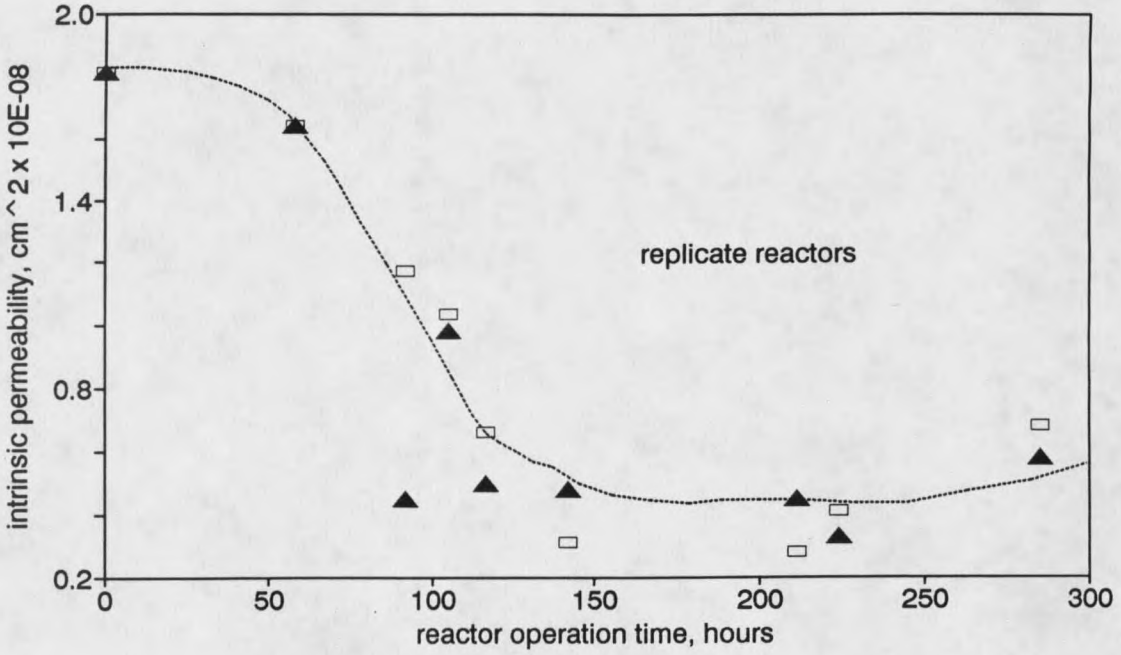

Figure 19 Variation of intrinsic permeability with time for the above reactor. Curve has been hand drawn.

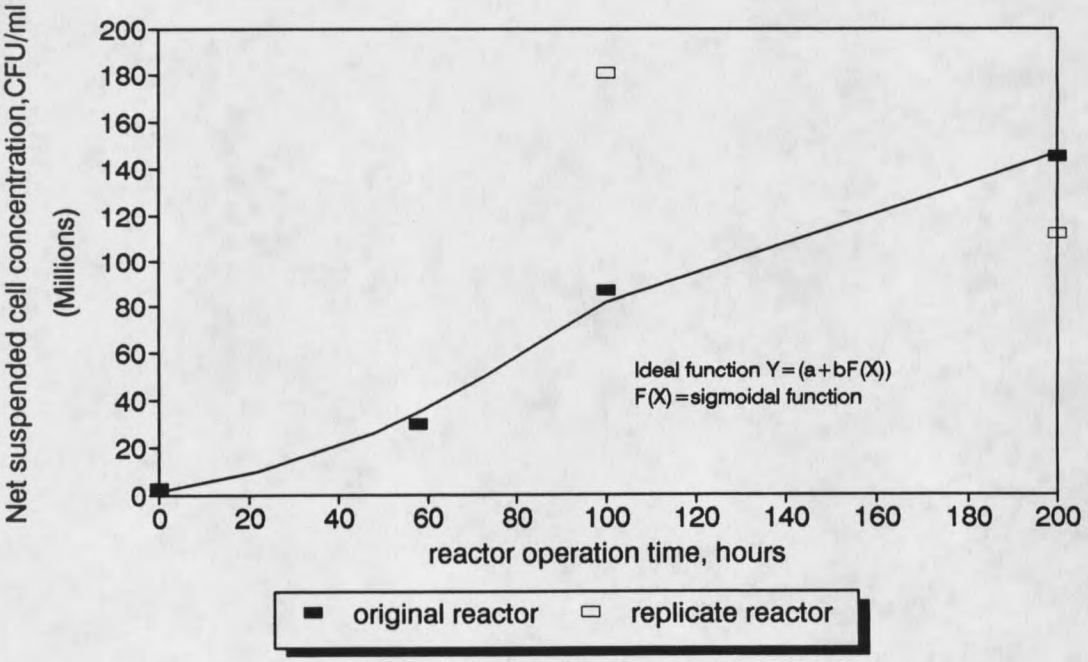

Figure 20 Net (effluent - influent) suspended cell concentration as a function of reactor operation time for 55 cm reactors.

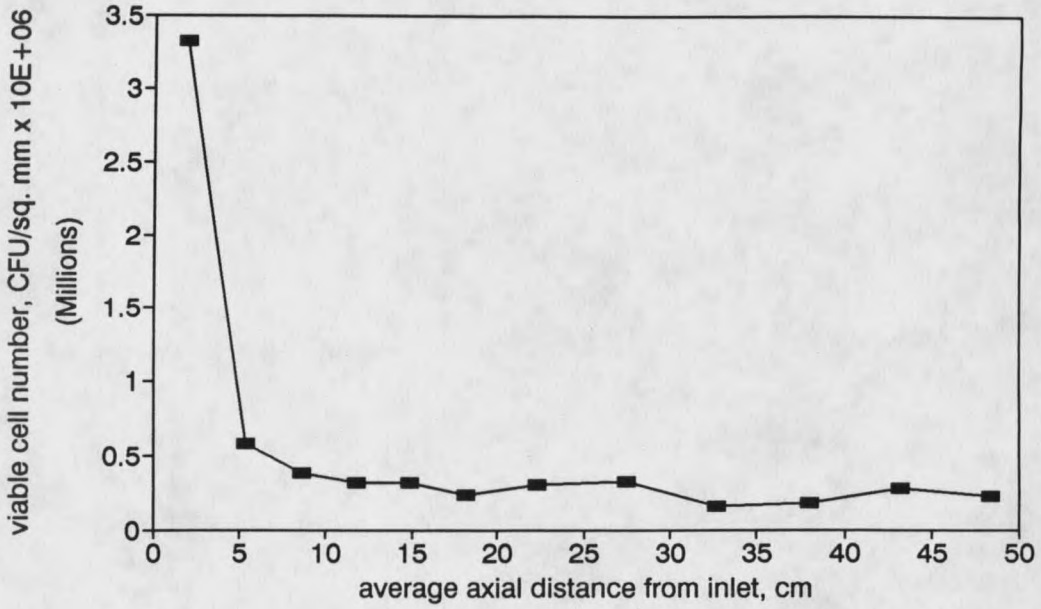

Figure 21 Axial variation of total cell concentration (suspended + attached + adsorbed) for 55 cm segmented reactor analyzed post steady-state.

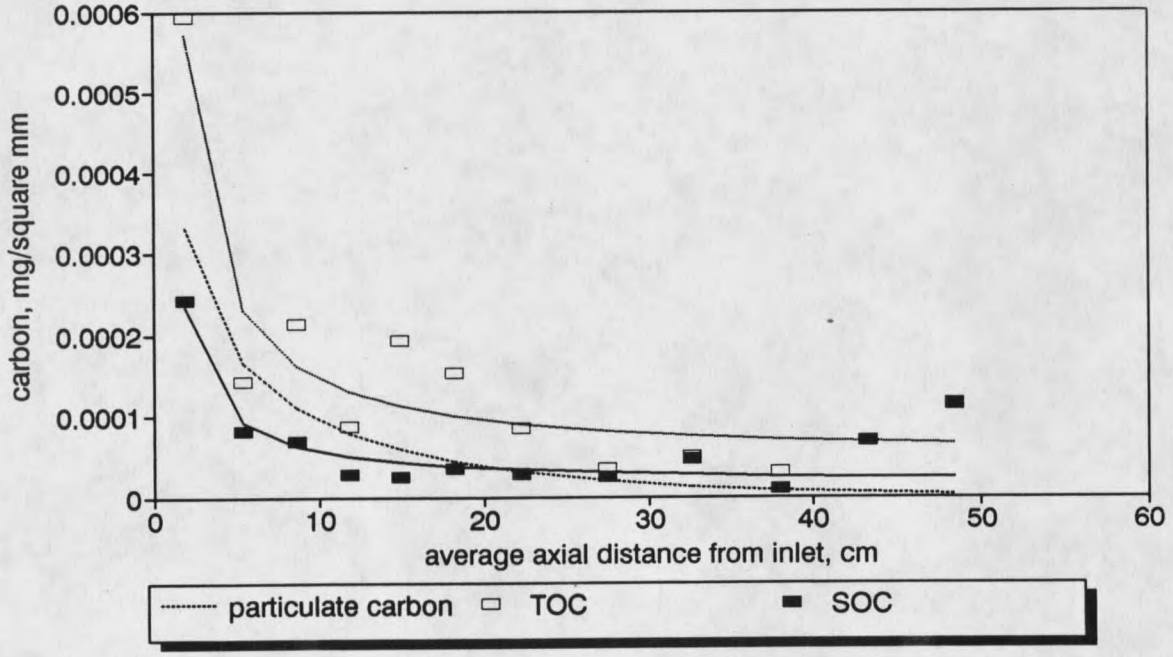

Figure 22 Post steady-state analysis of segmented reactor yielded the curves for soluble organic carbon and total organic carbon as a function of axial distance.

Upon reaching steady-state, the segmented reactor was taken apart and analyzed for total viable cell number (suspended cells + biofilm cells) (Figure 21) using the methods previously described. In order to compare different segments of the reactor, the cell counts were calculated on the basis of surface area of substratum.

Each of these segments was analyzed for TOC and filtered carbon (SOC), both of which were expressed in units of carbon per unit substratum surface area (Figure 22). The general shape of the curve follows that for cell number. The difference between TOC and SOC yields particulate carbon (or total cellular carbon), as illustrated by the carbon balance.

TOTAL ORGANIC CARBON = GLUCOSE CARBON + PARTICULATE CARBON + PRODUCT CARBON

PARTICULATE CARBON = CELLULAR CARBON + EPS CARBON

DISCUSSION

Inter-relationships between Physical Parameters

Biofilm accumulation on porous media has been found to be proportional to particle size (and tortuosity) of pore channel. Biofilm accumulation also reduces effective pore space, thereby reducing porosity, permeability and pore velocity. Jinreney, et al. (1988) found from dye tracer studies, that the mean residence time was 10 % higher than when calculated from flow rate. This discrepancy was attributed to the "tailing" phenomena seen even in dye studies of sterile porous media. The usefulness of a tracer is dependent on the diffusion characteristics of the dye. Dyes with higher molecular weight take longer to diffuse into biofilm. Diffusion rate from bulk liquid into biofilm is faster and of greater significance than diffusion from biofilm into the bulk liquid. According to this study, diffusion was the critical phenomena and not adsorption.

Table 12 Summary of change in reactor behavior with biofilm growth

Condition	Dispersion no (dimensionless)	Dispersivity (cm^2/sec)	N_{re}	N_{pe}	Permeability (cm^2) x 10^{-6}
Sterile	0.86	1.16	0.62	1634.4	2.82
With biofilm	0.56	0.16	0.124	362.6	0.58

The table (Table 12) summarizes the tracer study for dispersion in a 23 cm section of a 30 cm long reactor packed with 1 mm glass spheres (Experiment 3). The dispersion number gives an estimate of axial dispersion. The closer it is to zero, the better the plug flow. From this it may be deduced that axial dispersion is high in this reactor system and decreases slightly with biofilm growth. Keeping in mind that the measurement was made over 23 cm, while the biofilm thickness reached zero at 15 cm, the above are space average values. The observations of decreasing dispersion number and dispersivity are consistent with

decreasing Reynolds number. The Schimdt number, a ratio of viscous forces to diffusive forces, was 1268.6 for this reactor system and by definition would remain constant. The Peclet number (N_{pe}), a ratio of inertial forces to diffusive forces, decreases by 78 % during the experiment.

Table 13 Axial dispersion to molecular diffusion ratio

Relation used	D_H/D_M ratio		Percent change
	Initial	Final	
Tracer study, 1990	173000	30000	82.7
Hiby, 1959	911.3	174.4	81.7
Bear, 1972	800	120	85.0
Blackwell, 1966	50595	8690	82.7
Harleman, 1963	492.5	80.5	83.7

Table 14 Change of measured (tracer study) and calculated (flow data) MRT and mass transfer parameters with biofilm growth.

	MRT (mins)		Percent difference	Mass transfer coeff. ($cm\ sec^{-1}$)	diffusive layer (E-06 m)
	Dye study	Flow data			
Initial	3.5	3.66	2.8	1.4 E-03	47.8
Final	15.9	12.4 - 14.5	22 - 8.8*	8.9 E-04	75.6

* - assuming a porosity of 0.35 to 0.30 at steady-state.

Using the relation derived by Wilson and Geankoplis, 1966 the mass transfer resistance and diffusive boundary layer thickness was calculated assuming sterile media. As indicated (Table 14), the diffusive boundary layer is comparable to the biofilm thickness. Substrate removal is therefore limited by diffusion in the bulk liquid phases and the rate of increase of biofilm thickness is limited primarily by this condition. This is also substantiated by the observation that the biofilm was rarely greater than 60 to 70 microns thick.

Results of tracer studies in the shorter reactors were used to relate measured porosity with biofilm thickness *in situ*. It was assumed

that reactor operation time was the only independent variable, this condition being experimentally sustained by using a high substrate loading rate. Permeability, mean media porosity from tracer study and mean biofilm thickness were plotted dimensionless (Figure 23). In order to quantify biofilm accumulation on porous media, mean media porosity has been evaluated as a viable alternative measurement to biofilm thickness. However, the relationship between them is complex with the occurrence of biofilm growth. Conventional techniques for porosity measurement are destructive in nature, time consuming and inaccurate for hydrated

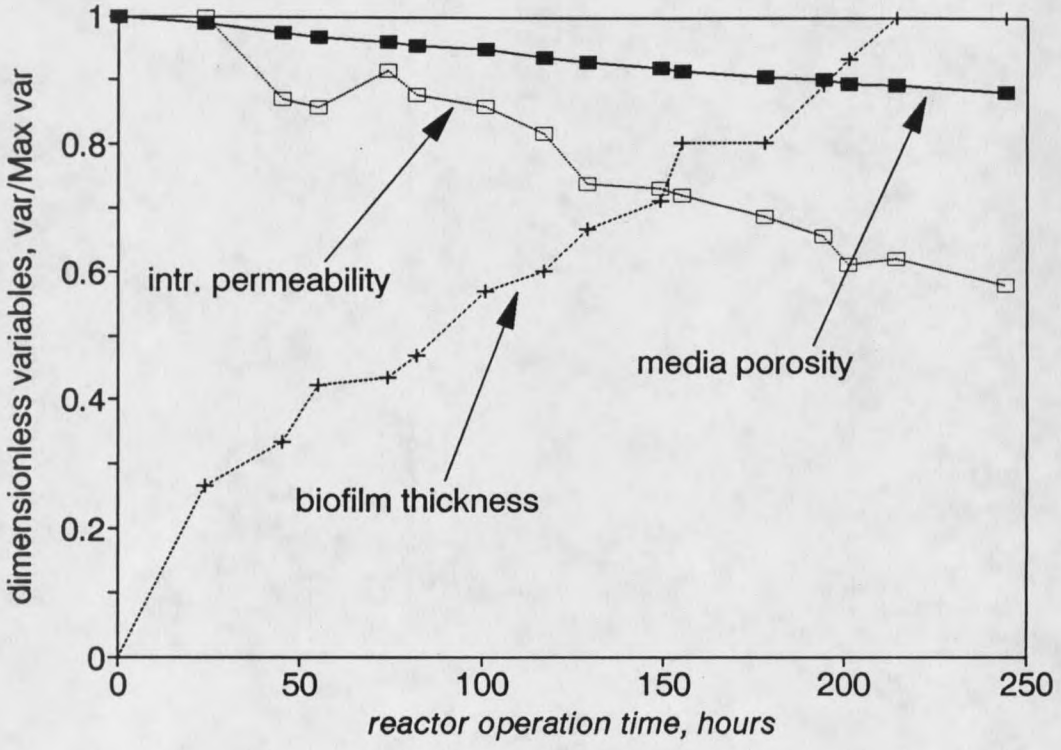

Figure 23 Relationship between media porosity (as calculated from dye study), biofilm thickness and intrinsic permeability as a function of experimental time for 5 cm reactor packed with 1 mm glass spheres and a cross sectional area 0.27 cm^2. The dimensionless variables were calculated by dividing by the maximum value.

materials such as biofilm. Pore velocity was measured *in situ* and the specific discharge was known, and porosity was calculated with insignificant error by means of the simplistic relation described earlier. In this experiment, measured porosity from tracer study was compared to that calculated from mean biofilm thickness (Figure 24). A linear relationship was observed for both methods as shown below, where L_f is in meters.

E25.. $E = -1500\ L_f + 0.44$ - tracer study

E26.. $E = -5100\ L_f + 0.43$ - film thickness

Assumption: Assuming that volume of biofilm is approximately equal to the product of the biofilm thickness and surface area of the glass sphere (E27), the following general relation may be derived:

E27.. $V_b = L_f \times A_s$

E28.. $$L_f = \frac{2\ E_i}{(k + A_s/V_r)}$$

where E_i is the initial or sterile media porosity, k is a constant for the media size and reactor characteristics, A_s the total surface area of the spheres in the reactor and V_r the total empty volume of reactor.

In reality, the above assumption is not valid because the biofilm thickness surrounding a glass sphere is not uniform and the volume of biofilm must include a factor (E29).

E29.. $V_b = S_{AF} \times L_f \times A_s$

where S_{AF} is the Surface Accumulation factor varying from 0.3 to 0.4. It was determined that if the effective surface area occupied by biofilm is taken into consideration, then the porosity from the two methods is similar. This factor, hereby called the Surface Accumulation Factor, S_{AF}, was calculated to be as low as 30 to 40 percent of the total surface area of the spheres. It may be noted that S_{AF} is a constant at steady-state but varies with time during the initial growth phases of the biofilm. Careful observation of biofilm growth showed that the biofilm started out as a very patchy one, then became more uniform but turned patchy again in the final phase preceding steady-state. These three phases correlated with the

three phase s-shaped curves of permeability and suspended cell concentration with time.

Equation E28 implies that A_s/V_r is a constant, the numerical value of which is equal to the slope of the relation between media porosity and biofilm thickness. The slope ranges between 1500 m^{-1} (tracer study) and 5100 m^{-1} (calculated using the 70 % area assumption). The analytical value from an earlier experiment was found to be 3435 m^{-1}. If the area assumed to be covered by the biofilm is decreased to 40 %, the analytical and calculated values of A_s/V_r are similar (Figure 24).

The standard deviation of the measured biofilm thickness supports this biofilm accumulation property (Figure 25 and 26). The standard deviation for a 30 - 40 micron biofilm on 1 mm glass spheres is about 30 %. Roughness of biofilm is a direct function of standard deviation and

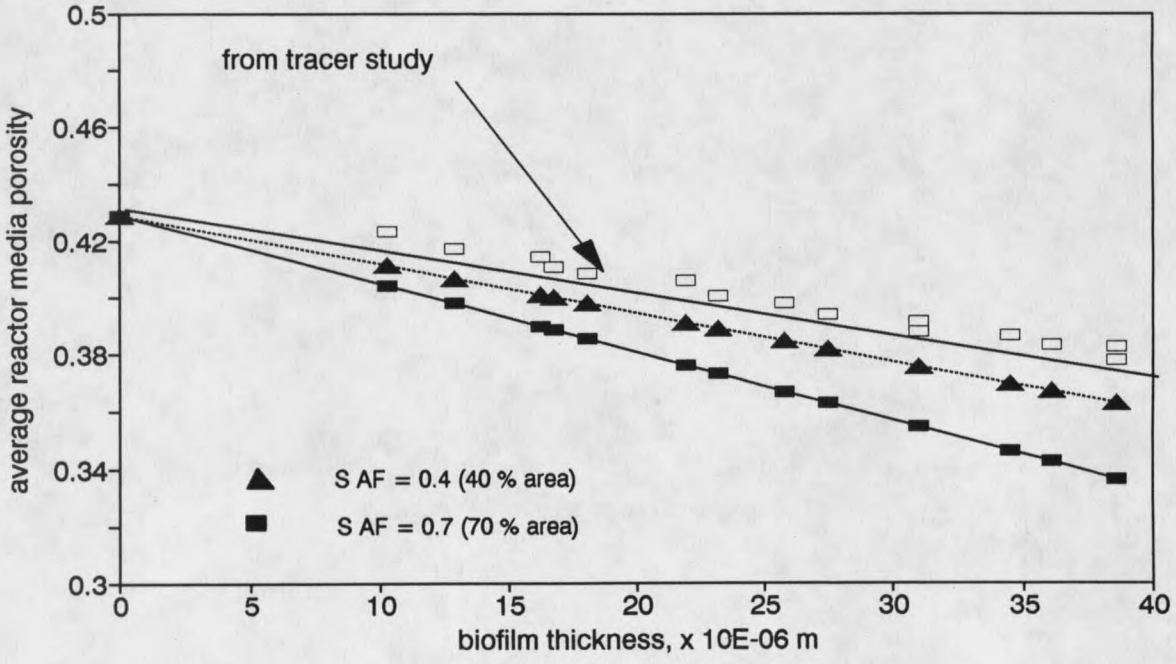

Figure 24 Linear relationship between media porosity and biofilm thickness for the same reactor. S_{AF}, the Surface Acc. factor of 0.7 and 0.4 are used in the calculation of porosity and compared to porosity determined from tracer study.

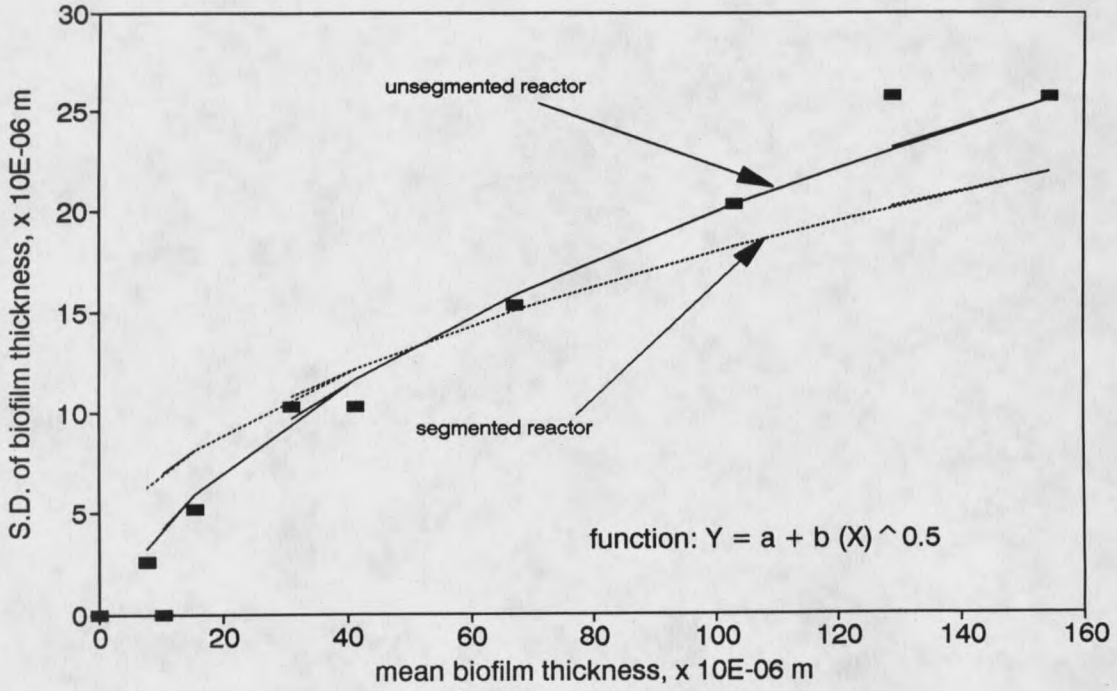

Figure 25 Standard deviation of optically measured biofilm thickness as a function of mean biofilm thickness. Replicate reactors (experiment 6).

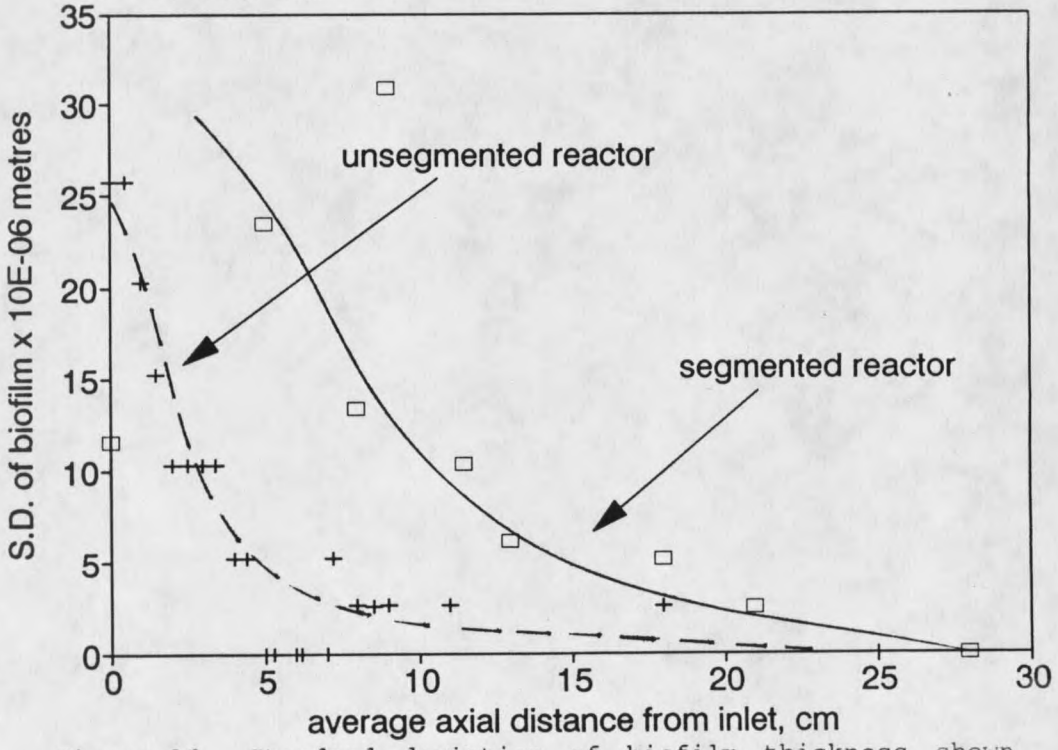

Figure 26 Standard deviation of biofilm thickness shown plotted as a function of average axial distance from entrance for the previous reactor.

biofilm accumulation is a direct function of time. Therefore, in the longer reactor, the surface area of biofilm accumulation may be considered to be a function of time. In the shorter reactors, where biofilm thickness never exceeds 40 micron, the axial change in net surface area of biofilm accumulation may be assumed to be relatively constant.

The percent standard deviation of the biofilm decreases with increasing biofilm thickness and the Surface Accumulation factor cannot be assumed to be constant through an experiment, until steady-state conditions prevail.

As mentioned earlier, flow rate (or intrinsic permeability) decreased significantly initially and then gradually tapered off to a relatively constant minimum value. A log-linear relation existed between permeability and biofilm thickness (Figure 27). In all experiments, the

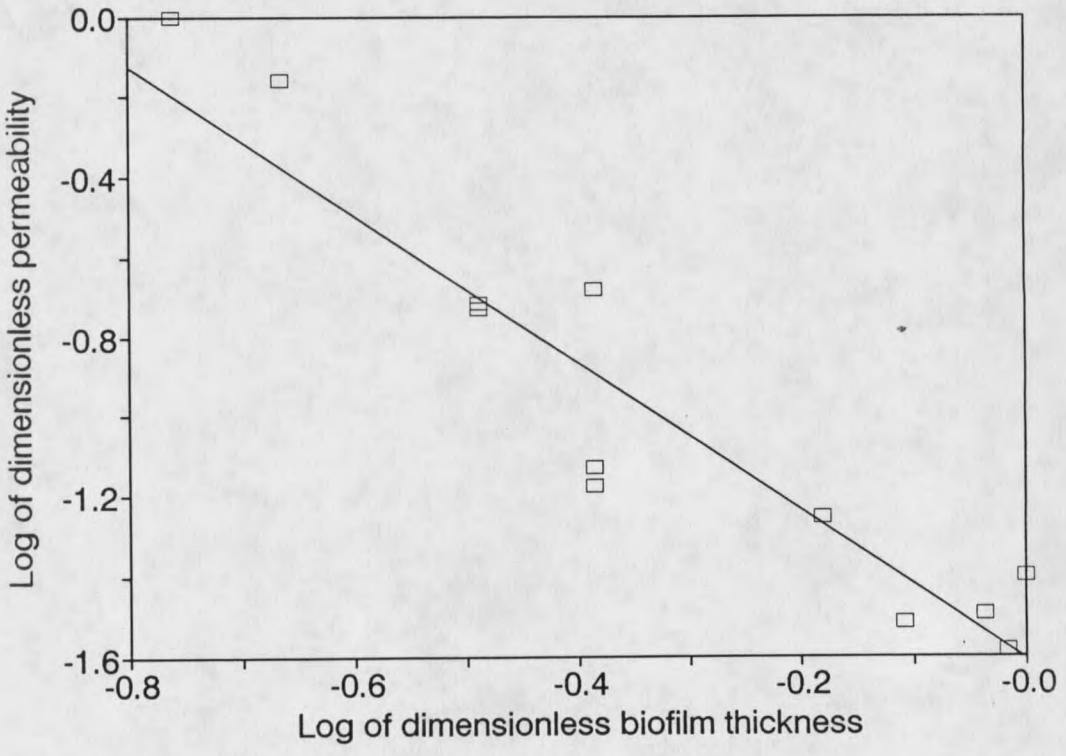

Figure 27 Relationship between intrinsic permeability and biofilm thickness, for a 110 micron sand packed reactor of dimensions 5 cm x 0.12 cm^2. Initial conditions: Glucose loading rate 0.018 gm $cm^{-2}hr^{-1}$ and shear stress at biofilm-fluid interface 2.64 gm cm^2 sec^{-1}.

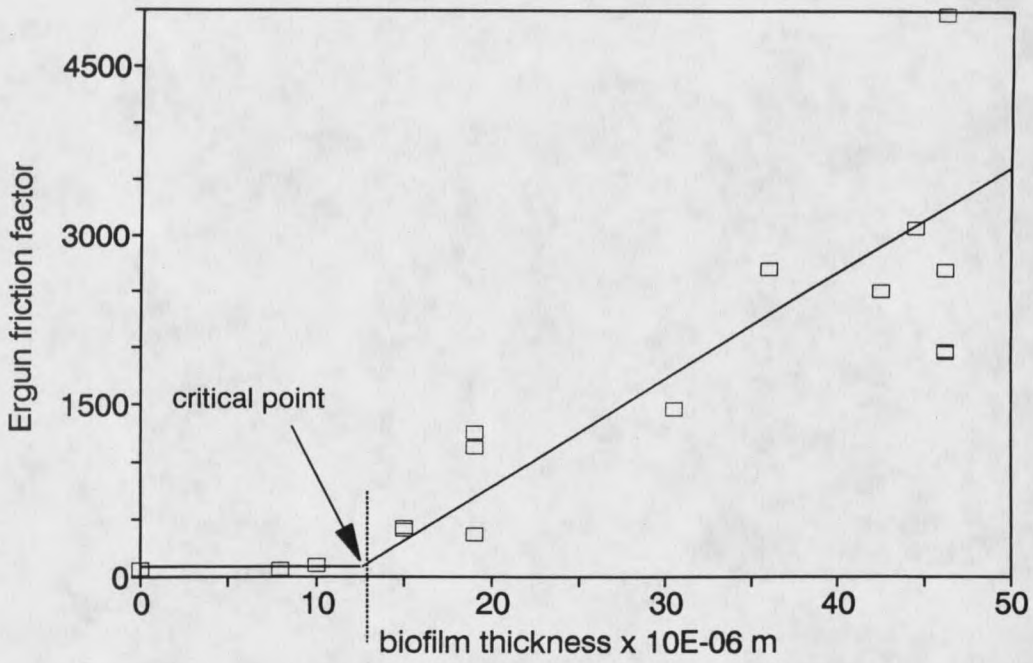

Figure 28 "Critical biofilm thickness" of 13 micron for the previous reactor observed by plotting friction factor as a function of mean biofilm thickness.

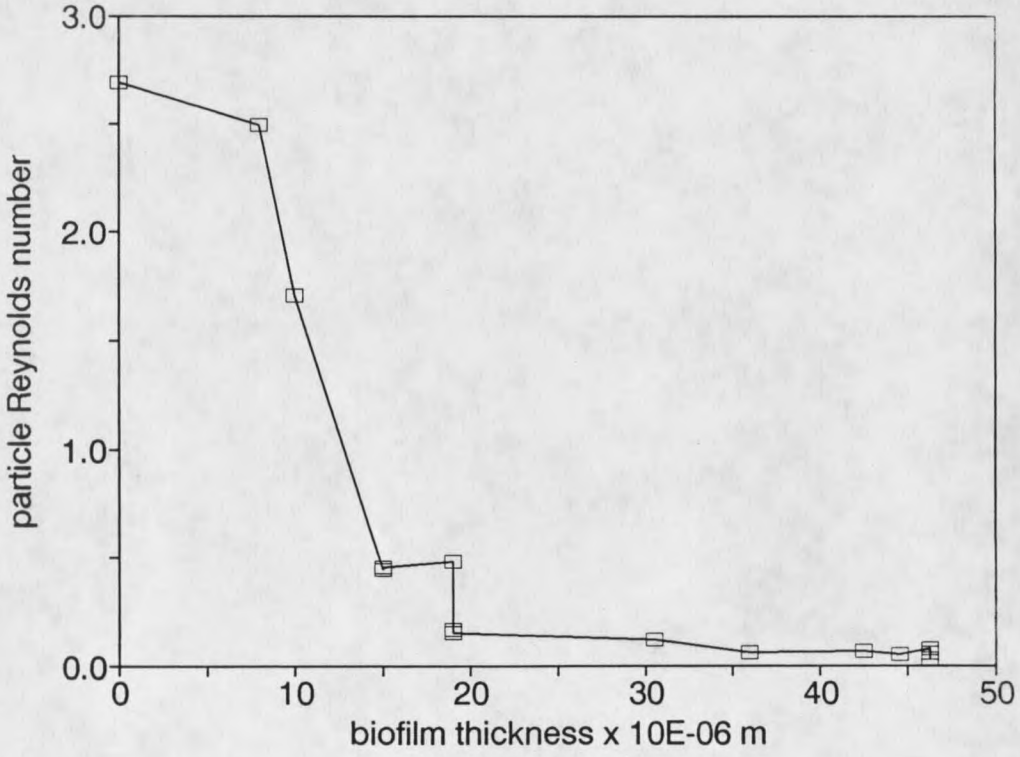

Figure 29 The relationship between Reynolds number and mean biofilm thickness for the previous reactor.

reactors achieved the lowest possible permeability, which may be called 'minimum permeability' for convenience. Keeping all other factors constant, an increase in media size elevated Reynolds number and depressed the value of friction factor. When compared to sand of similar hydraulic radii, uniform glass spheres exhibited a smaller steady-state biofilm thickness, initial permeability and Reynolds number but a higher friction factor.

As biofilm growth occurs on the media surface, the resulting biomass begins to block the free passage of substrate. Initially the fluid flow is dominated by viscous forces created by laminar flow conditions at the spherical surfaces and biomass. For a pipe flow system, the film thickness beyond which the friction factor increases spontaneously is termed the "critical film thickness". Alternatively, stated in terms of the viscous sublayer - it is the biofilm thickness equal in thickness to that of the viscous sublayer. This may be re-defined on the basis of hydraulic losses for porous media - it is the film thickness at which true laminar flow gives way to transitional or turbulent flow, at the spherical surface (biofilm-fluid interface). When the biofilm reaches a sufficient thickness (the critical point), biofilm porosity itself may critically influence fluid flow.

The "critical biofilm thickness" was determined to be about 13 microns (Figure 28) corresponding to 33.5 % of the steady-state film thickness. As Reynolds number and Ergun friction factor share a log-linear relationship even in presence of biofilm, Reynolds number would similarly predict the critical point (Figure 29). This transition from laminar flow at the biofilm-bulk liquid interface may explain the 1.5 day lag between achievement of steady-state biofilm thickness and permeability.

Biochemical Process Analysis

Chang and Rittman (1987) found that enhanced irregularity of the substratum caused better biofilm accumulation and lowered the loss rate. Simultaneously, the shear loss coefficient increased with increased biofilm accumulation on an irregular surface. In the study, four phases of biofilm accumulation were observed in a biofilm system (Figure 30). Phase I is the initial adsorption phase where there is little change in substrate concentration. Phase II is that of rapid biofilm growth when the substrate concentration begins to fall. Phase III is the bio-regeneration phase. The substrate concentration at the biofilm-substratum interface becomes diffusion limited, the biofilm loss is greatest and product formation is also is the highest. The last one, Phase IV is steady-state where there is no net biofilm accumulation. It is also steady-state for substrate concentration, -products formation, suspended biomass concentration and cell loss rates respectively.

The equations (E30 - 32) relate the biomass production of *Pseudomonas aeruginosa* with the carbon and oxygen requirement for metabolism. From theoretical stoichiometry, the carbon/oxygen ratio $Y_{c/o}$ is 0.9 gm glucose carbon (gm oxygen)$^{-1}$. In experiment 6, the effluent oxygen concentration was 3.5 mg L^{-1} and the average glucose concentration was 1.75 mg L^{-1} (or 0.7 mg L^{-1} substrate carbon) giving an experimental mass yield $Y_{c/o}$ of 1.2. Glucose measurements were however made only in the effluent and influent ports and the exact location of complete carbon depletion was unknown. Oxygen was being continuously refurbished at the reactor entrance by diffusion through the silicone tubing. Since the influent concentrations of oxygen and carbon were similar (about 8.0 mg L^{-1}), glucose was the growth limiting nutrient.

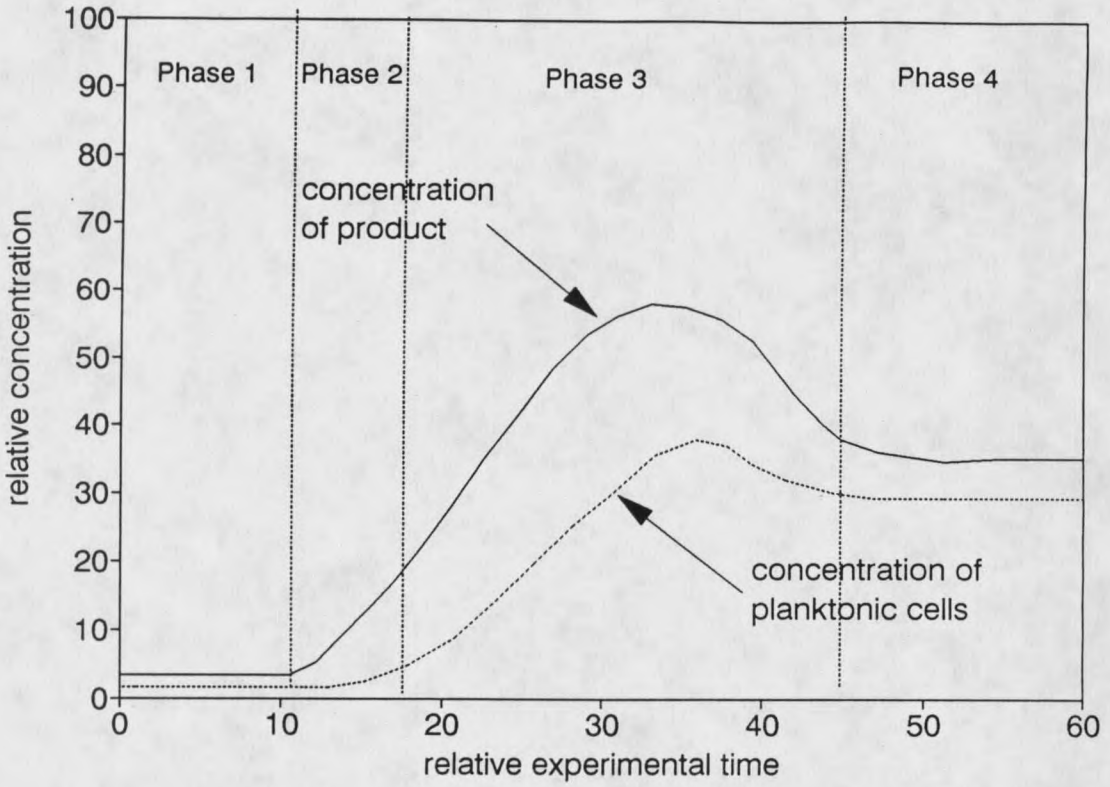

Figure 30 General stages of suspended cell concentration seen during the 'life' of a biofilm system, Chang and Rittman, 1988.

E30.. $C_6H_{12}O_6$ + 6 O_2 -----> 6 CO_2 + 6 H_2O (energy)

E31.. $C_6H_{12}O_6$ + 1.2 NH_3 -----> 6 $CH_{1.4}O_{0.4}N_{0.2}$ + 3.6 H_2O (synthesis)

E32.. $C_6H_{12}O_6$ + 2.5 O_2 + 0.7 NH_3 -----> 3.5 $CH_{1.4}O_{0.4}N_{0.2}$ + 2.5 CO_2 + 4.6 H_2O (overall stoichiometry)

Rittman and McCarty (1980) suggest the existence of a minimum substrate concentration, below which bacterial cells cannot provide sufficient maintenance energy to sustain growth and perform cellular functions. A low organic nutrient concentration has often been measured in natural waters and waste waters and the authors use this concept as a plausible explanation. At steady-state, the net available energy per unit time per unit area is assumed to be equal to the net maintenance energy

per time per unit area. Hence, the total mass of biofilm is just equal to that which can be supported by the flux of substrate into it. S_{min}, the minimum substrate concentration, is assumed to be approximately equal to the minimum substrate concentration in the bulk liquid at the biofilm-fluid interface. For a monolayer biofilm, substrate concentration within the biofilm, is approximately equal to the substrate concentration at the surface, as there is no diffusion limitation. A minimum substrate concentration and a deep film substrate concentration for a steady-state biofilm are calculated using the energy balance condition. Using their model, the minimum glucose concentration for a carbon limited system with an influent of 17.5 mg L^{-1} is 0.7 mg L^{-1} (Figure 16). The minimum concentration necessary to maintain a deep biofilm is 3.24 mg L^{-1}.

E33.. $J \times Y = X_f \times L_f \times b$

where J is the substrate flux into biofilm $area^{-1}$ $time^{-1}$, Y the true growth yield gm biomass gm $glucose^{-1}$, X_f the steady-state biofilm density in gm cm^3, L_f the steady-state biofilm thickness, b the maintenance respiration or specific decay coefficient, J x Y the net available energy/area/time, and, $X_f \times L_f \times b$ is the net maintenance energy $area^{-1}$ $time^{-1}$.

At the later stage of experiment 6, contamination was observed in the segmented reactor. The significance of this contamination is difficult to quantify, however, the conversion of glucose to simpler organic compounds through fermentation would lead to an accumulation of SOC at the effluent end of the reactor. This phenomena may explain the intermediate peak in SOC (Figure 31).

Even though particulate (cell and extracellular products combined) carbon shows some fluctuation, biofilm thickness, particulate carbon and viable cell number reach their minimum 30 cm from the influent end of the reactor. There is negligible cell carbon beyond 45 cm though total viable cell concentration stabilizes. Since observed biofilm beyond 30 cm is practically zero, most of the viable cells are in suspension. Noting that the total viable plate count levels out at 10 % of maximum, that is then

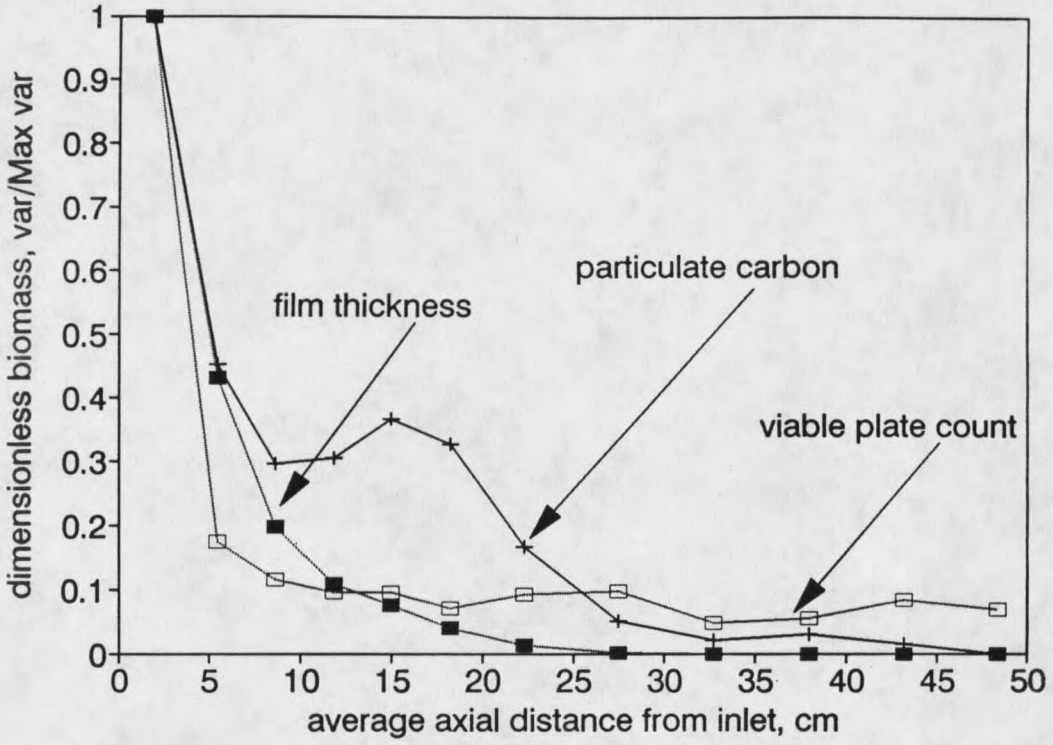

Figure 31 Axial variation of biomass variables, shown dimensionless (55 cm, 1 mm glass spheres) Viable plate count includes planktonic and sessile cells. Scales: 1:120 E-06 m - biofilm thickness, 1:4.02 E+05 CFU mm^{-2} - viable planktonic cell count and 1:3 E-06 mg-C mm^{-2} - particulate carbon.

the ratio of planktonic cells to total cells. Presuming this is the same ratio throughout the reactor, most of the particulate carbon is accounted for by the biofilm. Planktonic and sessile cellular material was not analytically separated in this experiment. Using another calculation, the planktonic cell concentration (Figure 20) is about 9.5 % of the initial total cell concentration (Figure 31), agreeing well with the 10 % figure above.

There was a dramatic change in the CFU and TOC pattern on reaching steady. The initial adsorption processes (Figure 15) did not seem to influence the accumulation pattern seen at steady-state (Figure 34).

During the initial adsorption phase, the CFU/TOC ratio is random, (Figure 32) and similar to that at steady-state (Figure 33). The cell number to particulate carbon ratio however could not be determined at the initial state. CFU/cell-C ratio at steady-state increased with axial distance, consistent with the observation of an increasing biofilm density and mass of EPS per cell.

Cell number, TOC and CFU/TOC ratio increase and decrease in a wave function pattern (with the appearance of crests and troughs). This phenomena seems to be more pronounced during the initial adsorption experiment rather than at steady-state.

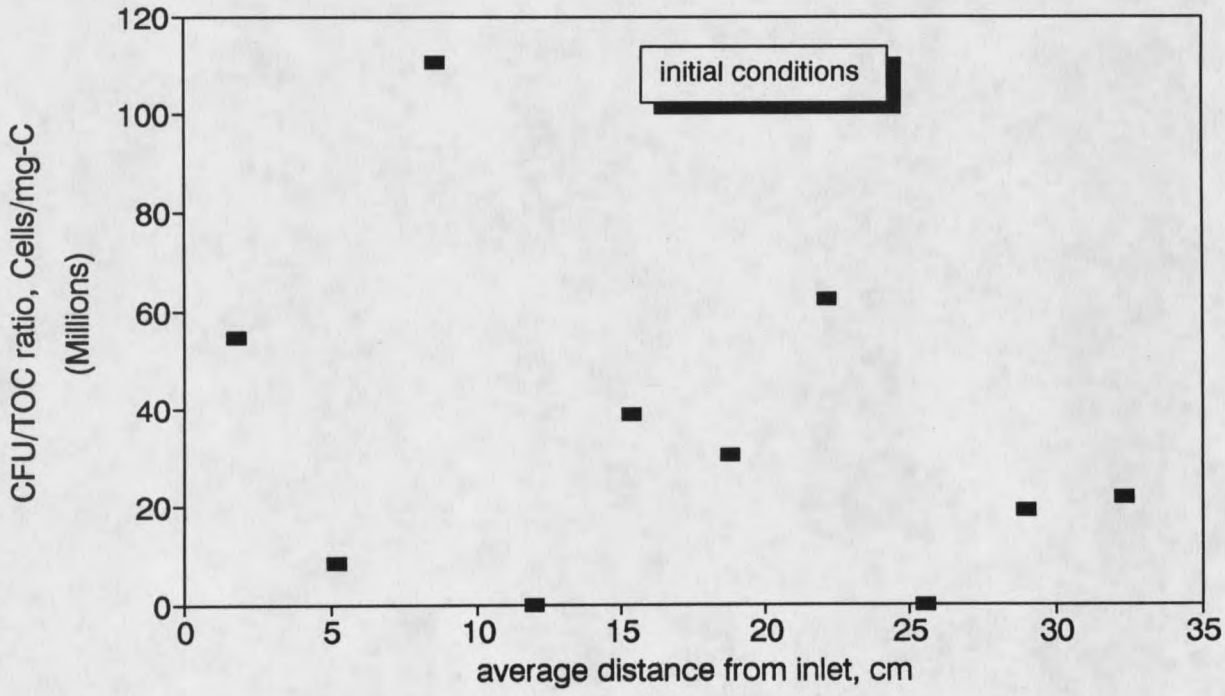

Figure 32 Axial variation of the CFU to TOC ratio during the initial phase of adsorption, immediately upon inoculation with *Pseudomonas aeruginosa* for the reactor in Figure 15. (glucose carbon is 7 x E-07 mg mm^{-2})

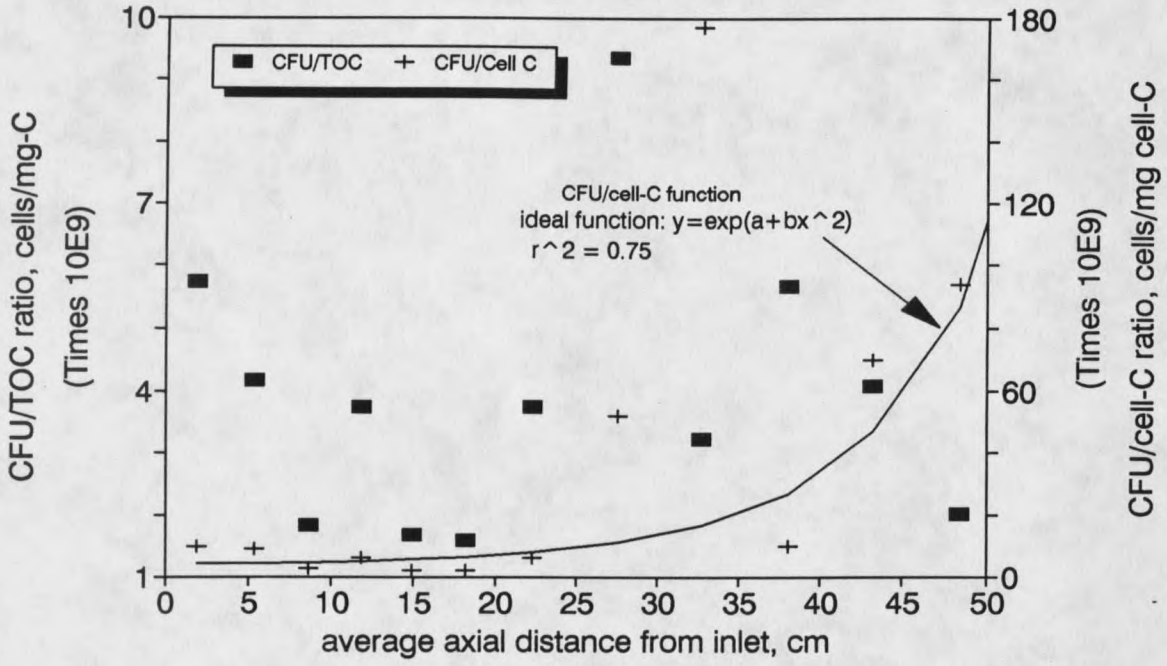

Figure 33 CFU/TOC ratio (random) and CFU/Cell-C ratio (an exponential function) at steady-state (55 cm reactors experiment 6, glucose carbon was 7 E-07 mg mm^{-2}).

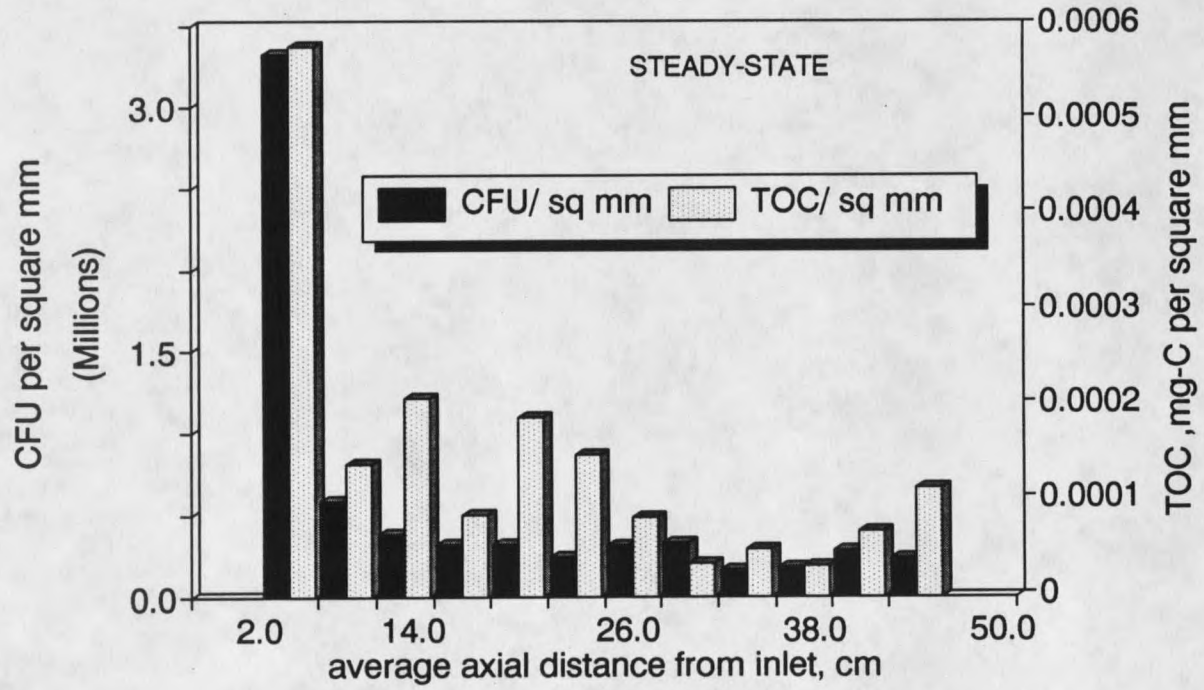

Figure 34 The distribution of viable cells and TOC axially at steady-state.

While this may appear to be an incidental occurrence, the effects of filtration may be involved. The TOC in the initial phase experiment was far greater than what the cell count indicates, due to the high content of EPS in the batch inoculum. This would provide ideal conditions for filtration of EPS and cells. In order to visualize this filtration theory, imagine packing together a hundred filter paper sheets face to face. Assume that the pore size of the filter paper is 200 times that of particles. If an aqueous suspension of these particles is passed through the filter-pack, a wave pattern of filtration (similar to Figure 15) may result. As shown in the illustration (Figure 35), filtration would probably involve three stages. In the inoculation stage, cells, EPS fibers and nutrient media are transported into the sterile reactor. After about 5 residence times, the flow is shut off, the 'acclimatization' phase begins.

This constitutes the adsorption stage, when EPS and cells would have the opportunity to form a monolayer on the glass substrata. Finally, sterile media is allowed to flow at a constant rate for about 15 residence times, causing the non-adsorbed cells and EPS to exit the reactor, hence called the 'flushing' stage. If the shear stress at the fluid-substratum interface is low enough, the fluid would tend to follow the path of least resistance. In effect, this channel may be highly tortuous, with crests and troughs in the cell concentration along the axial length. EPS would be likely to play a fundamental role in the general mechanism for filtration in porous media (Figure 36). EPS would hypothetically initiate filtration and the cellular material would accelerate it by attachment, growth and further cellular and EPS production. This would continue until steady-state was reached.

At steady-state, biofilm density was found to increase axially (Figure 37) with a decreasing biofilm thickness (Figure 38). Biofilm mass density is a function of the areal biofilm concentration (mass of cells per unit substratum area) and biofilm thickness. The mass was calculated

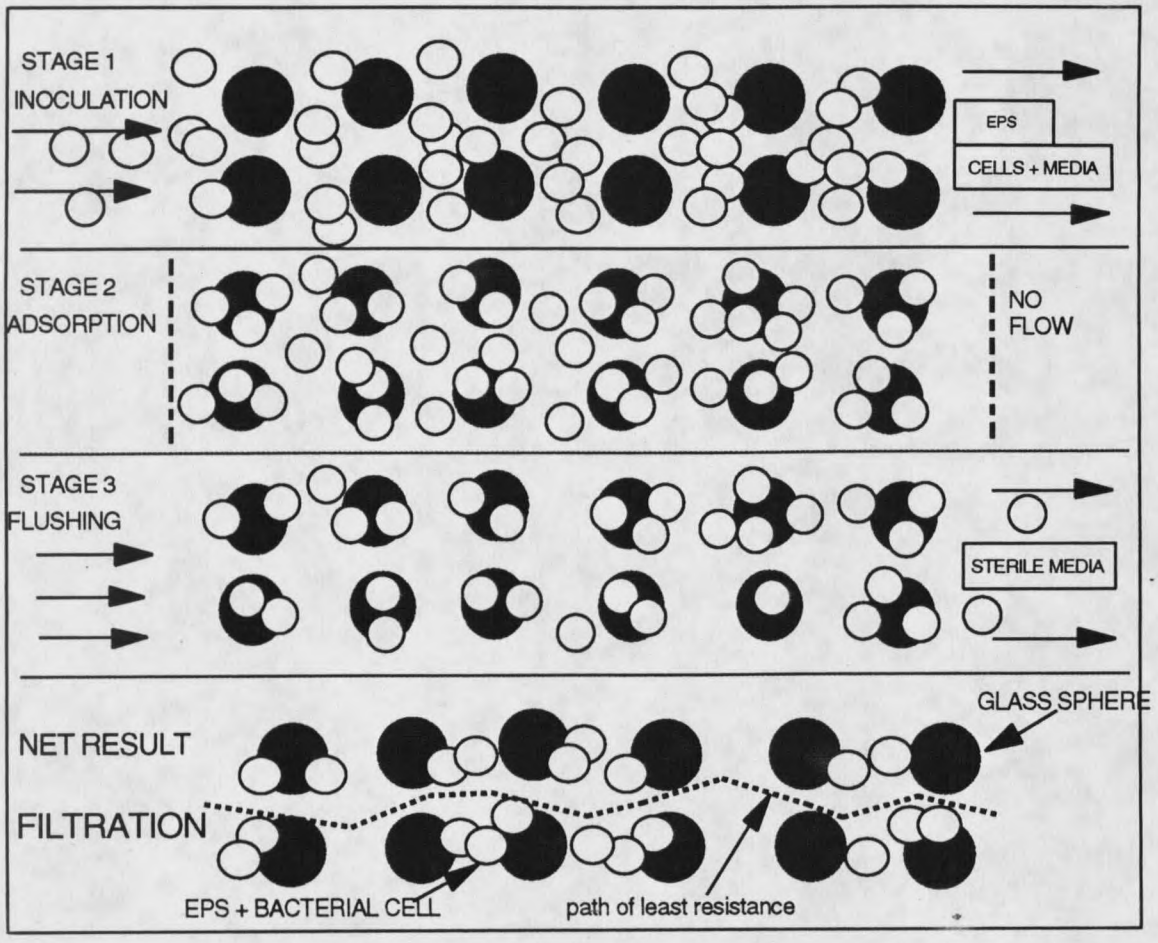

Figure 35 Illustration of the mechanism of filtration that may have occurred in Experiment 5 due to the high concentration of cells and EPS in the initial inoculum. This periodic carbon filtration may have caused the crests and troughs observed in Figure 15.

both from a carbon analysis and from a viable plate count, assuming a constant dry cell density (1.0 x 10E-12 gm CFU^{-1}). An assumption was made that the biofilm mass constituted 90 % or more of the total measured mass (based on preceding discussion). Comparable biofilm density numbers were obtained from both analyses and the average compared well to those previously calculated (Table 15).

Two critical factors determine biofilm density - substrate flux into biofilm and shear stress at the biofilm-fluid interface (Characklis, 1980). An increase in either will increase the biofilm density. In previous studies, biofilm density has also been shown to increase with time (Trulear, 1983 and Hoehn 1973) due to the accumulation of EPS. Being

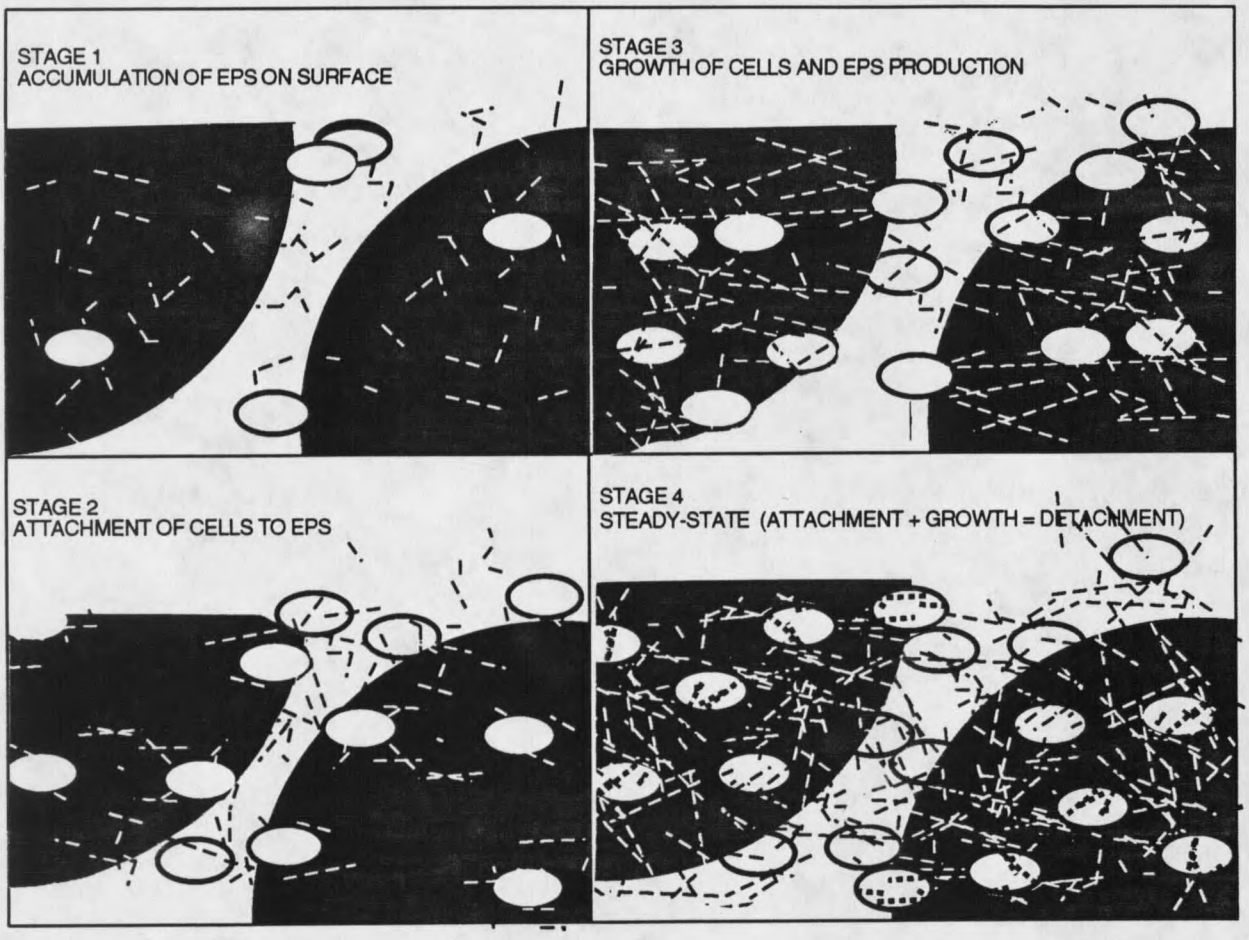

Figure 36 Schematic illustration of the suggested hypothetical stages involved in filtration of cells and EPS in porous media, based on experimental results.

Table 15 Comparison of reported biofilm density as dry mass per unit biofilm volume from literature.

Biofilm type (steady-state)	Biofilm thickness L_f x 10E-06 m	Biofilm density kg m^{-3}	Literature cited
Mixed culture (heterotrophic)	160 - 210	66 - 130	Kornegay & Andrews, 1967
	100	50	Rittman & McCarty, 1978
Pure culture (*Pseudomonas aeruginosa*)	36 - 47	17 - 47	Trulear, 1983
	0 - 60	27	Rune Bakke, 1986
	0 - 100	2 - 65	This study, 1990

a constant head loss experiment, substrate flux and shear stress both decrease with axial distance (while the mass of EPS increases). The mass of EPS per unit cell was found to be approximately equal to the mass of the cell itself. EPS content was calculated from the difference between

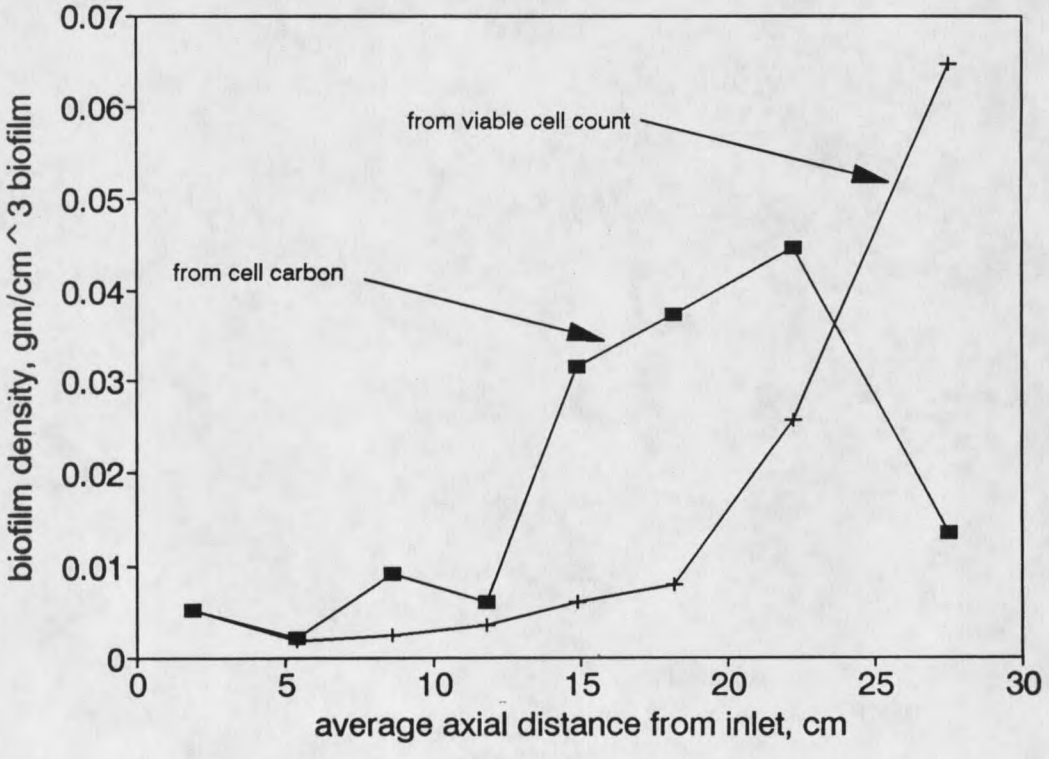

Figure 37 Biofilm density calculated from two independent but related variables versus axial distance. (Segmented reactor in experiment 6).

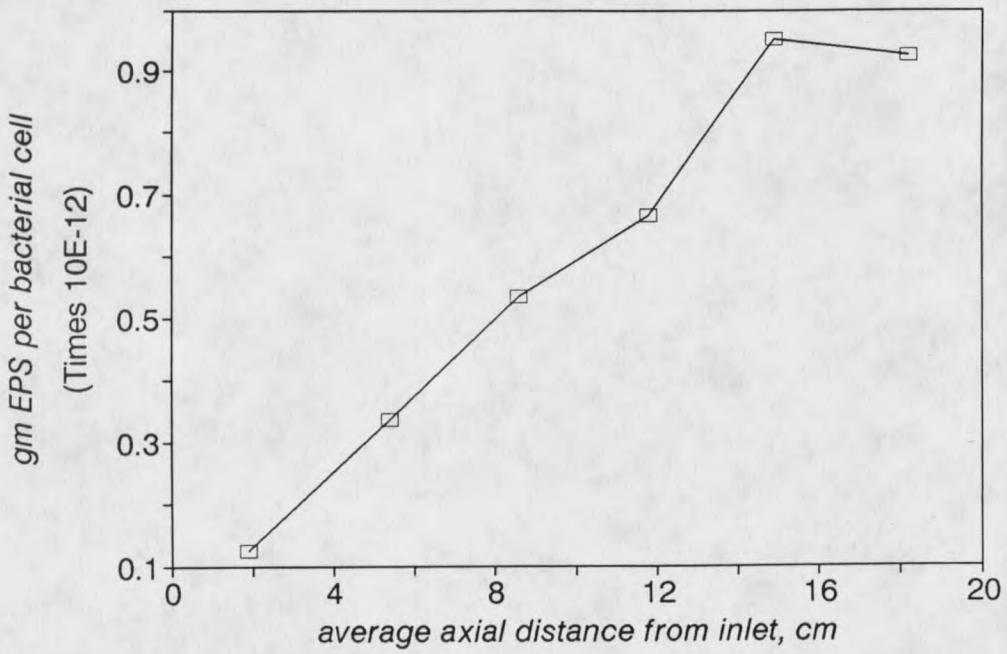

Figure 38 Mass of extracellular polymeric substances (EPS) per CFU versus axial distance. (Experiment 6)

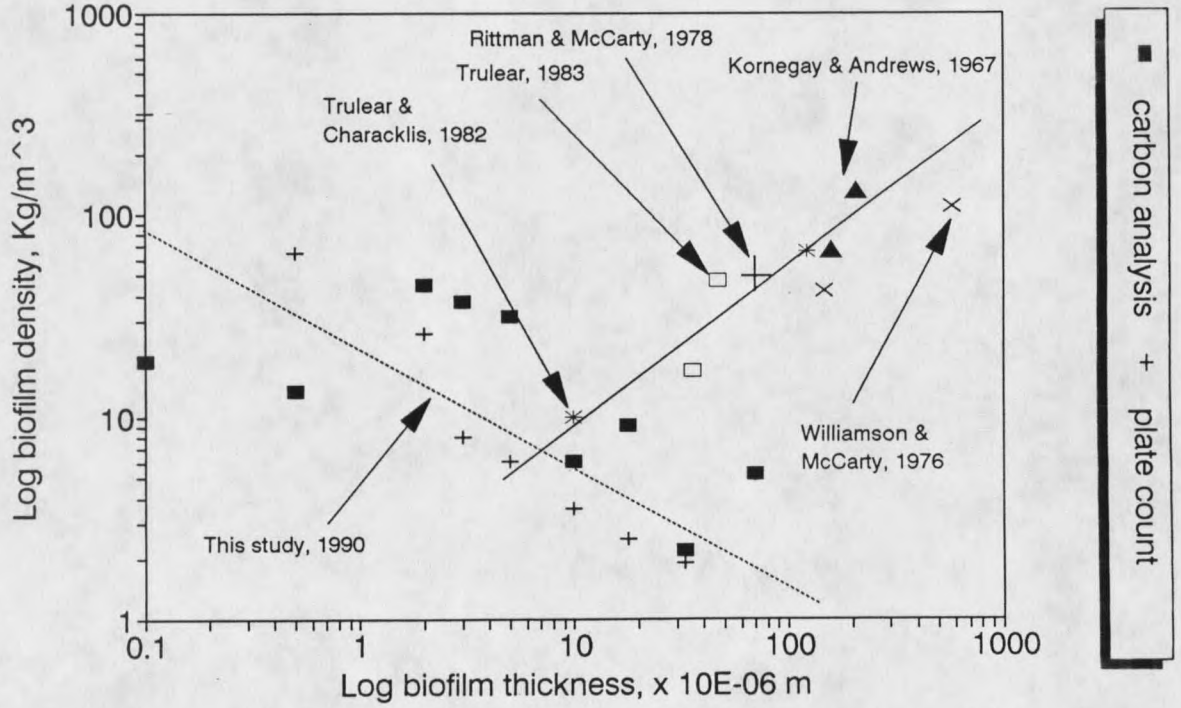

Figure 39 Variation of biofilm density with mean biofilm thickness on a logarithmic scale.

total cellular mass (cellular + non-cellular) from a carbon analysis, and cellular mass from total viable heterotrophic plate count. This was then divided by the total number of cells to give EPS mass per cell.

Detachment is an important phenomena in any biofilm system. It is of even greater significance for porous media systems due to its association with filtration. Filtration has been studied but is not easy to quantify as there are too many effecting variables. In order to quantify and derive a relationship for filtration rate, the following relationships were defined based on the study of all the porous media reactors.

1. Biofilm density = f(mass of EPS/mass of cell)

2. Mass of EPS = f(substrate concentration)
   = f(age of biofilm)

3. Extent of filtration = f(mass of EPS)
   = f(pore size)
   = f(shear stress)

4. Biomass concentration = f(growth rate)
   = f(substrate loading rate)
   = f(biofilm thickness)
   = f(Erosion rate)
   = f(diffusive boundary layer thickness)

The net relationship may be written as a function of the following variables:

Extent of filtration, M_F = f(biofilm density, X_f)
= f(pore size, r_H)
= f(shear stress, τ)
= f(substrate loading rate, q_s)
= f(growth rate, μ)
= f(Erosion rate, r_E)
= f(density of bulk liquid, σ)
= f(diffusive boundary layer thickness, L)

$$E34.. \quad M_F = K^a (X_f)^b (r_H)^c (\tau)^d (q_s)^e (\mu)^f (r_E)^g (\sigma)^h (L)^i$$

The equation (E34) illustrates why filtration is such a complex phenomena and difficult to quantify. In an experiment not previously described, using a 10 cm x 0.27 cm^2 reactor (1 mm glass spheres), the biofilm thickness and suspended cell concentration were simultaneously measured at periodic time intervals until steady-state was achieved. Net suspended cell concentration varied sigmoidally as a function of time (Figure 40). The suspended cell concentration was converted to erosion

rate by means of the flow rate and reactor substratum surface area and the order of detachment was determined.

Assuming that cells detached uniformly from the reactor surfaces over the axial distance (the suspended cell concentration was representative of the entire reactor), the relationship may be thus written:

$$E35..\ r_E = k_1 \times L_f = k_2 \times (L_f)^2 = K_n \times (L_f)^n$$

where r_E is the Net Erosion rate CFU sec^{-1} cm^{-2}, L_f the average biofilm thickness in cm and K_n is a constant for the system, its units depending on the order of the system. Taking logarithms on both sides

$$E36..\ Log[r_E] = Log[K_n] + n\ Log[L_f]$$

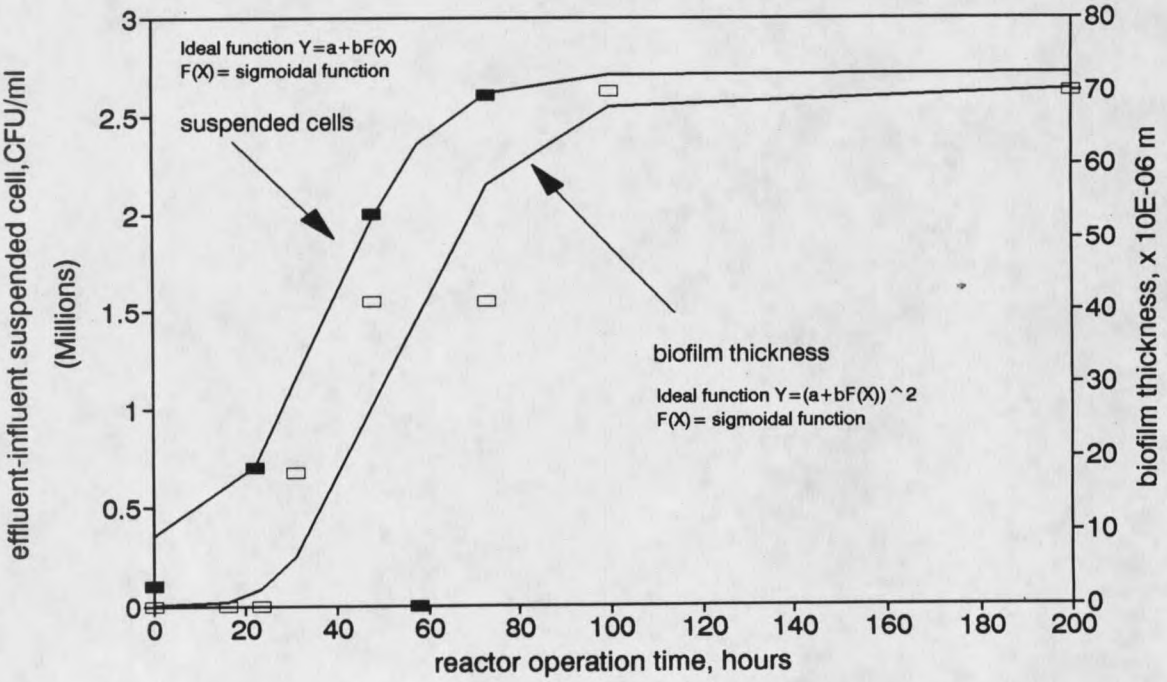

Figure 40 Relationship between biofilm thickness and suspended cell concentration as a function of time in a 10 cm reactor (1 mm glass spheres, other characteristics of experiment 2).

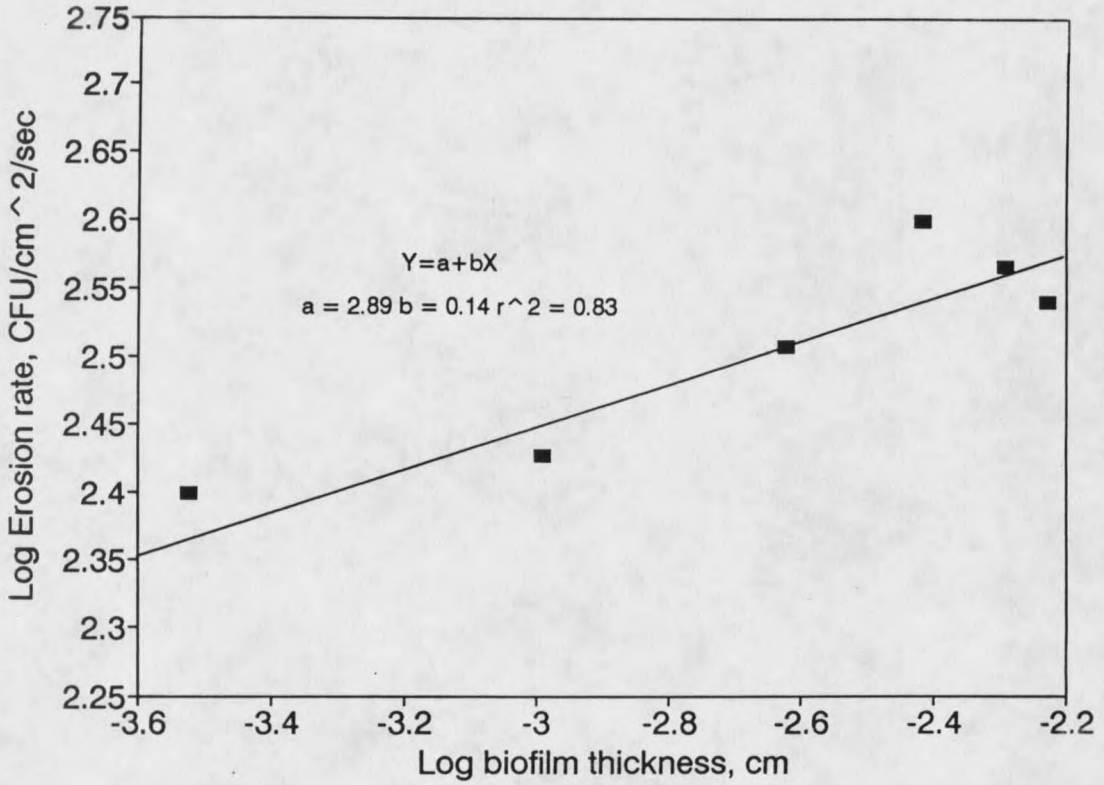

Figure 41 Relation between erosion rate and biofilm thickness for the reactor in the previous figure. (a is the y-intercept and b the slope of the curve, also the order w.r.t. biofilm thickness).

When plotted on a logarithmic scale, the slope of the line is the order of the relation between erosion rate and biofilm thickness (Figure 41). The relationship derived graphically is,

E37.. $\text{Log}[r_E] = 2.89 + 0.14\ \text{Log}[L_f]$

E38.. or $r_E = K_n \times (L_f)^{0.14}$

This is less than first order and lower than previously determined for other systems. Biofilm density increased with axial distance and there is evidence in the literature that it will also increase with time, thus the likely relationship for porous media systems is,

E39.. $r_E = K_n \times (X_f)^N \times (L_f)^{0.14}$

where N is the order with respect to biofilm density X_f, different from n.

Bio-remediation Strategy for Field Applications

The schematic (Figure 42) is a demonstration of the use of laboratory studies for utilizing biochemically enhanced strategies for bioremediation, petroleum reservoir/product souring, selective plugging and petroleum formation plugging. Four stages of data processing are needed. In each, data is screened and processed to make the end stage a working data base for predictive modelling of field situations. This would eliminate trial-and-error decisions and thereby greatly reduce environmental risks. Unfortunately, field data relating to the successful implementation of microbially influenced techniques is rare, unreliable or incomplete.

List of tasks needed to fulfill field data needs (Stage 2 of schematic):

1. Prevention strategies to avoid disasters or system failures.
2. Risk assessment studies in case (1) is imminent.
3. Identification of important monitoring variables.
4. Pre-treatment strategies for microbially enhanced operations.
5. Laboratory studies to plan out effective scale-up techniques.
6. Post-treatment effectiveness evaluation studies.

Given above are the specific tasks that must be accomplished in order to complete the "Field Data" study (Stage 2 of schematic model). Notice the overlap between laboratory and field experiments. It is important to keep in mind the direct relationship between macroscale projects (like this thesis) and 'real' industrial application.

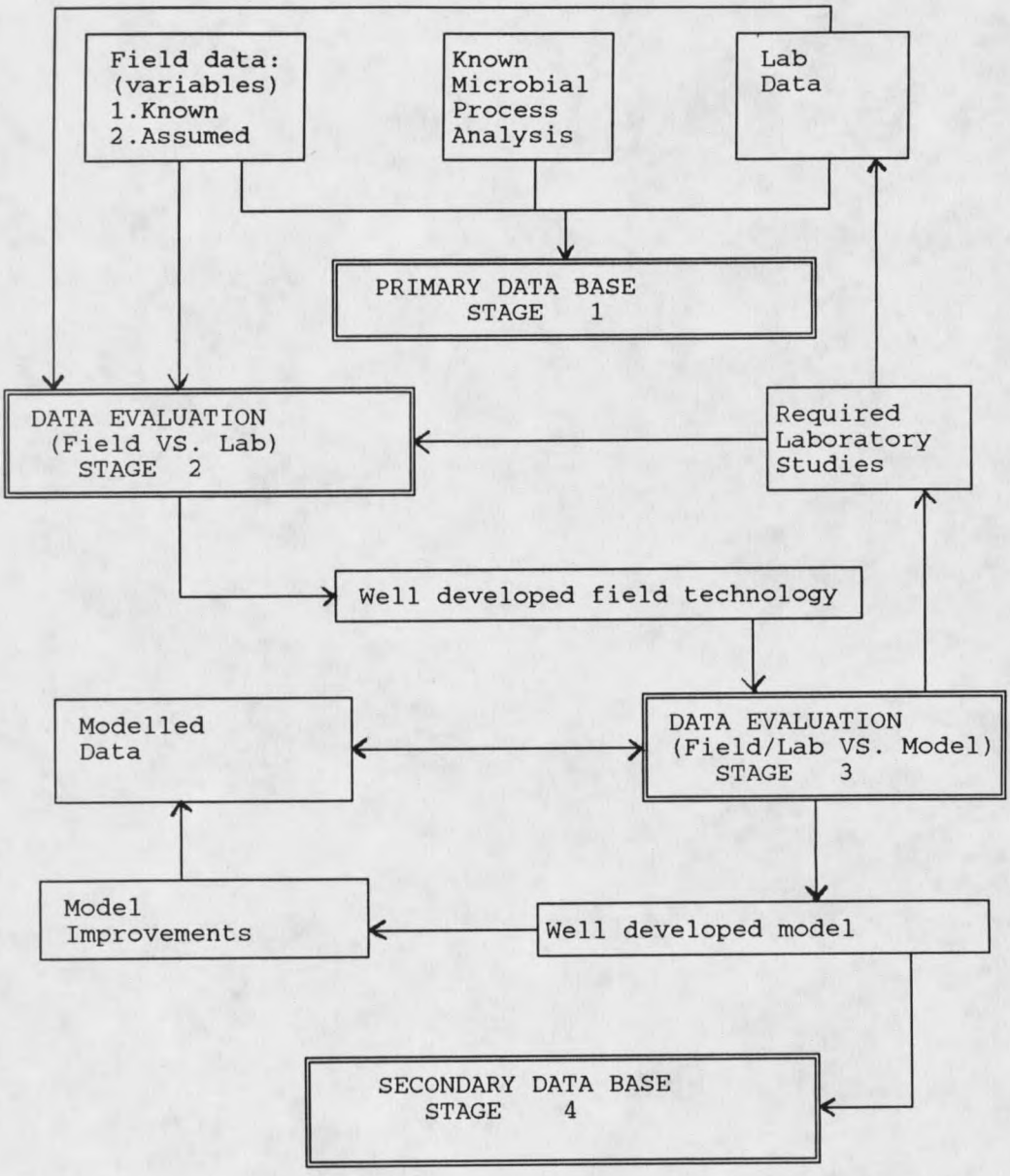

Figure 42 Schematic of suggested model for industrial application of porous media research.

Project Summary

Given below are the overall list of observations made from the experiments, and thereby summarizing this project:

1. The extent (thickness) of accumulation of biofilm on media was found to be proportional to the particle size at the same nutrient and flow conditions.

2. The calculated particle friction factor increased steeply after a 'critical biofilm thickness', (measured to be 15 microns) was obtained.

3. Theoretically calculated porosity (from an assumption of uniform biofilm thickness) and that from dye tracer study were identical only when the media surface area coverage of biofilm was taken into consideration.

4. The initial inoculation with a bacterial suspension of *Pseudomonas aeruginosa* did not appear to cause the gradients in viable cells, biofilm thickness or total organic carbon observed at steady-state.

5. Total viable cell concentration and total organic carbon, per unit surface area, was highly random during the initial stages. At steady-state an axially decreasing pattern was noticed.

6. The initial inoculation with a batch of chemostat grown cells, whose EPS content was high, may have caused filtration to occur throughout the length of the reactor in "cycles" (with corresponding cycles in the EPS content).

7. Substrate depletion and biomass quantities were predominant at the influent end of the reactor (first 15 cm, conditions of exp 6).

8. Suspended cell concentration (a function of biofilm cellular detachment), calculated as the difference of influent and effluent concentrations, varied sigmoidally with experimental time.

9. The mass of EPS per cell and the biofilm density increased with axial distance.

10. The steady-state biofilm was rougher at the influent end based on the higher standard deviation of the biofilm thickness measurements.

11. Hydrodynamic dispersion, or effective dispersivity, was found to decrease with biofilm growth and correlated with a similar decrease in Reynolds number.

12. The concentration of viable planktonic (suspended) cells was determined to be about 10 % of the total viable cell concentration in the reactor.

13. The order of the relationship between erosion rate and biofilm thickness was determined to be less than first order (= 0.14).

14. The reduction in permeability at steady-state was consistently observed to be 90 - 95 % for the short reactors and 70 - 80 % for the longer reactors.

Further Studies

Dye tracer studies were performed in the absence and presence of biofilm growth. The hydrodynamic dispersion was found to decrease with biomass growth while the diffusive mass transfer layer thickness increased. Residence time distribution studies were also used to compute the mean media porosity and related to mean biofilm thickness. However,

effect of tortuosity is neglected and the accurate experimental determination of pore velocity and effective pore volume with the growth of biofilm becomes a challenging task. An accurate measurement of porosity would be a viable alternative for *in situ* quantification of biomass.

In all experiments, the packing was presumed to be the closest possible. Mean pore size is dependent on the type of packing and would affect the substrate flux through the reactor. It also changes the tortuosity of flow paths. The effect of biomass filtration and biofilm growth on different types of media packing will in itself be an interesting experiment.

Analysis shows at steady-state, biofilm and total biomass show a decrease with axial distance while there is an increase in EPS content and biofilm density. This trend conflicts with the usual observation in pipe systems or rototorques and may be theorized on the basis of filtration. Unfortunately, the data is insufficient (no SEM/TEM analysis was made) to conclusively prove this was caused by filtration of EPS. A microscale study is needed here and the mechanism of filtration also needs to be determined. Another point of interest would be the measurement of EPS content with time for the reactor conditions of experiment 6.

The rate of cellular detachment from biofilm to bulk liquid was found to be less than first order with respect to biofilm thickness. However, the complete equation for a consistent detachment relation remains incompletely developed.

The pipe flow model has been used to simulate flow through a packed bed filled with spheres. In the "conduit approximation" of porous media the pore spaces are assumed to be a bundle of fine capillaries which may be integrated together to simulate a pipe. This idea was utilized in trying to simulate flow through the short reactors using experimental data. However, the results obtained were vastly different from the experimental. (The pipe flow model differs from a porous media model in two important respects. In a packed bed, A) Dispersion is more complex and

mass transfer is higher, and B) the presence of filtration affects biomass accumulation and attachment/detachment processes. For the 1 mm beads (0.27 cm^2 cross sectional area) reactor, the specific (per unit length) surface area for a packed bed is 4.8 times that for an equivalent pipe, also the ratio for the specific biofilm volume.) The experimental results need to be modelled and compared with a porous media model.

The concept of three phase biofilm growth needs to be investigated using data from short reactors. This may explain the S- shaped growth curve experimentally observed and approximated by Monod kinetics. There was some correlation in the phases seen during the development of biofilm thickness, effluent suspended cell concentration and permeability.

The experiments were determined to be glucose limited and suggest the existence of a "minimum substrate" concentration. The Rittman and McCarty model was used to calculate the minimum glucose concentration required for supporting a biofilm (0.69 mg L^{-1}). Also observed was a "minimum permeability" for a given porous media at steady-state. These concepts need to be further evaluated and modelled in order to prove their validity.

One of the drawbacks of the experimental system was the absence of sterile conditions immediately before the entrance of the reactor. Biomass growth occurred virtually unhindered towards the constant head reservoir. A system of sterilization that allows the maintenance of a constant pressure drop, for instance by employing ultra violet light or ultra sonic sound, is suggested.

Conclusions

1. The extent of biofilm accumulation is proportional to the particle size at similar nutrient and flow conditions. The biofilm accumulation on media is not uniform or complete over the surface area but occupies only a small fraction of it.

2. Presence of greater amount of EPS is necessary for filtration to occur in porous media provided there is sufficient cellular material to restrict flow in the pores. The axial biofilm gradient commonly observed is influenced by this phenomena, though its extent is as yet unknown.

3. Cellular erosion rate in a short reactor (10 cm) from the biofilm into bulk liquid is less than first order with respect to biofilm thickness (0.14), and may also be dependent on biofilm content (such as biofilm density or biofilm cellular concentration).

4. Media porosity, when measured with a passive dye over reasonably short distances, is a viable *in situ* alternative to microscopically measured biofilm thickness.

REFERENCES CITED

Bakke R.
"Biofilm detachment."
Unpublished doctoral thesis, Montana State University, Bozeman, (1986)

Bear J.
"Dynamics of fluids in porous media."
American Elsevier, Inc., New York (1972)

Blackwell R. J.
"Experiments on mixing by fluid flow in porous media."
32nd annual meeting of AIChE and SPE, San Francisco, preprint 29 (1959)

Bower E.J. and Cobb G. D.
"Modelling of biological processes in the subsurface."
Dept. of Geography and Env. Eng., Johns Hopkins University
Water Science and Technology Vol 19 (1987)

Bower E. J.
"Transformation of xenobiotics in biofilms."
Dept. of Geography and Env. Eng., Johns Hopkins University,
Dahlem Konferenzen Workshop on "Structure and function of biofilms."
Berlin (1988)

Brock T. D. and Madigan M. T.
"Biology of microorganisms."
Prentice Hall, New Jersey (1988)

Bryers J. D.
"Biologically active surfaces: Processes governing the formation and persistence of biofilms."
Biotech. Progress Vol 3 (2) (1987)

Bryers J. D. and Characklis W. G.
"Processes governing primary biofilm formation."
Biotech and Bioeng. Vol 24 pp. 2451-76 (1982)

Bubela B.
"Effect of biological activity on the movement of fluids through porous rocks and sediments and its application to enhanced oil recovery."
Geomicrobiology Journal Vol 4 (3) (1985)

Chang H. T. and Rittman B. E.
"Comparative study of biofilm shear loss on different adsorptive media."
Journal of Water Poll Control Federation Vol 60 pp.362-68 (1988)

Characklis W. G.
"Biofilm development and destruction."
Final report, EPRI CS-1554, Project RP902-1
Electric Power Research Institute, Palo Alto, CA (1980)

Characklis W. G.
"Microbial adhesion and aggregation."
Dahlem Konferenzen, K.C. Marshall Editor
Springer-Verlag, Berlin Number 137 (1984)

Characklis W. G. and Marshall K. C.
"Biofilms."
John Wiley and Sons, Inc. (1990)

Conn H. J.
"Biological stains."
Biotech Publications, New York (1953)

Crawford D. J.
"Hydraulic effects of biofilm accumulation in simulated porous media flow systems."
Unpublished Masters Thesis, Montana State University, (1987)

Ergun S.
Chem. Eng. Progress Vol 48 (89) (1952)

Fahien R. W. and Schriver C. B.
"Effect of porosity and transition flow on pressure drop in packed beds."
Presented at AIChE Conference, Denver (1961)

Harleman D. R. F., Melhorn P. F. and Rumer R. R.
"Dispersion - permeability correlation in porous media."
Journal of Hydraulics Div., ASCE number HY2
Proceedings paper 3459 (1963)

Hiby J. W.
Paper presented at conference on displacement in porous media.
Imperial College, London (1959)

Hoehn R. C. and Ray A. D.
J Wat. Poll. Control Fed. Vol 46 pp. 2302 (1973)

Jiminez B., Noyola A., Capdeville B., Roustan M. and Faup G.
"Dextran blue colorant as a reliable tracer in submerged filters."
Water Research Vol 22 (10) pp.1253-57 (1988)

Kolbel-Boelke J. and Hirsh P.
"Comparative physiology of biofilm and suspended organisms in the groundwater environment."
Presented at Dahlem Konferenzen Workshop on "Structure and function of biofilms." Berlin (1988)

Kornegay B. H. and Andrews J. F.
"Characteristics and kinetics of fixed film biological reactors."
Final report Grant WP 01181, Federal Water Pollution Control Administration, U.S.G.P.O. Washington (1967)

Lappin-Scott, H. M., Cusack F. and Costerton J. W.
"Nutrient resuscitation and growth of starved cells in sandstone cores: a novel approach to enhanced oil recovery."
Applied and Env. Microbiology Vol 54 (6) pp.1373-82 (1988)

Leva
"Fluidization."
Mc-Graw Hill, New York (1959)

Loosedrecht M. C. M., Lyklema J., Norde W., Schraa G. and Zehnder A. J. B.
"The role of bacterial cell wall hydrophobicity in adhesion."
Applied and Env. Microbiology Vol 53 (8) pp.1893-98 (1987)

Loosedrecht M. C. M., Lyklema J., Norde W., Schraa G. and Zehnder A. J. B.
"Electrophoretic mobility and hydrophobicity as a measure to predict the initial steps of bacterial adhesion."
Applied and Env. Microbiology Vol 53 (8) pp.1898-1901 (1987)

MacLeod. F. A. Lappin-Scott H. M. and Costerton J. W.
"Plugging of a model rock system by using starved bacteria."
Applied and Env. Microbiology Vol 54 (6) pp.1365-72 (1988)

Octave and Levenspiel
"The chemical reactor omnibook."
Oregon State University Bookstores, Inc., Corvallis (1984)

Peyton B. M.
"Literature review of hydrodynamic dispersivity correlations."
Report prepared for Graham Andrews, E. G. and G., Inc.
INEL, Biotechnology Division (1988)

Raymond R. L., Hudson J. O. and Jamison V. W.
"Oil degradation in soil."
Applied and Env. Microbiology Vol 31 (4) pp.522-35 (1976)

Rittman B. E. and McCarty P. L.
"Model of steady-state biofilm kinetics."
Biotech and Bioeng. Vol 22 pp.2343-57 (1980)

Rittman and MacCarty
"Evaluation of steady-state biofilm kinetics."
Biotech and Bioeng. Vol 22 pp.2359-73 (1980)

Robinson J. A., Trulear M. G. and Characklis W. G.
"Cellular reproduction and extracellular polymer formation by *Pseudomonas aeruginosa* in continuous culture."
Biotech. and Bioengineering Vol 26 pp. 1409-1417 (1984)

Shaw J. C., Bramhill B., Wardlaw N. C. and Costerton J. W.
"Bacterial fouling in a model core system."
Applied and Env. Microbiology Vol 149 (3) pp.693-701 (1985)

Siebel M. A.
"Binary population biofilms."
Unpublished doctoral thesis, Montana State University, Bozeman (1987)

Superfund Innovative Technology Evaluation (SITE) Program
USEPA - Superfund 89 Conference, Nov 27 - 29 (1989)

Trulear M. G.
"Cellular reproduction and extracellular polymer formation in the development of biofilms."
Unpublished Doctoral thesis, Montana State University, Bozeman (1983)

Turakhia M. H.
"The influence of calcium on biofilm processes."
Unpublished doctoral thesis, Montana State University, Bozeman, (1986)

Wilson E. J. and Geankoplis C. J.
Ind. Eng. Chem. Fundamentals (1966)

APPENDICES

APPENDIX A

NOMENCLATURE

Greek characters

α	Sticking efficiency [-]
δt_1	Constant time interval between concentration measurements [T]
σ	Absolute bulk liquid density [ML^{-3}]
τ	Shear stress at the bulk liquid-substrata interface [$ML^{-1}T^{-2}$]
Ω	Dynamic bulk liquid viscosity [$ML^{-1}T^{-1}$]
μ	Specific growth rate [$M_X M_X^{-1} T^{-1}$]
μ_{max}	Maximum specific growth rate of species for growth limiting nutrient [T^{-1}]

English characters

a	Viscous resistance coeff. (inverse hydraulic permeability) [L^{-2}]
A	Cross sectional area of channel or reactor [L^2]
A_s	Surface area [L^2]
b	Inertial resistance coefficient [L^{-1}]
c	Bulk liquid particle concentration [ML^{-3}]
C	Constant characteristic of porous media [-]
C_i	Concentration at time t_i [ML^{-3}]
D/UL	Dispersion number [-]
D	Effective dispersivity of dye [L^2T^{-1}]
DDMR	Dimensionless delta mean residence time [T]
dh/dL	Hydraulic gradient across reactor [-]
D_H	Hydrodynamic dispersion of solute in bulk liquid [L^2T^{-1}]
D_M	Molecular diffusion of solute in bulk liquid [L^2T^{-1}]
DMRT	Delta mean residence time [T]
D_{pe}	Equivalent initial diameter of particle [L]
D_{pi}	Average diameter of sterile particle [L]
D_s	Effective dispersivity of reactor [L^2T^{-1}]
DVAR	Delta mean variance [T^2]
E	Mean reactor media porosity [-]
E'	Mean effective reactor media porosity [-]
E_i	Mean sterile media porosity [-]

g_c	Newtons proportionality constant [-]
h	Head loss of water across reactor [L]
k	Intrinsic permeability of porous media [L^2]
K	Hydraulic conductivity of porous media [LT^{-1}]
K_d	Constant for erosion rate equation [depends on order]
K_g	EPS growth associated coefficient [$M_X M_P^{-1}$]
K_n	Overall particle transfer coefficient [LT^{-1}]
K_s	Monod Half-saturation constant for growth limiting nutrient [ML^{-3}]
L	Length [L]
L_f	Mean biofilm thickness [L]
MRT	Mean residence time [T]
N_p	Number of particles per reactor [-]
NRe	Reynolds number for particle [-]
P	Hydraulic pressure at a point [$ML^{-1}T^{-2}$]
Q	Volumetric flow rate of bulk fluid [L^3T^{-1}]
q_s	Substrate loading rate [$ML^{-2}T^{-1}$]
Q_s	Sphericity or shape factor for particle [-]
R	Net rate of substrate consumption [$ML^{-3}T^{-1}$]
R_{ad}	Net rate of cell adsorption from bulk fluid to substrata [$M_X L^{-3}T^{-1}$]
R_d	Net rate of cell detachment from biofilm to bulk fluid [$M_X L^{-3}T^{-1}$]
r_E	Net cell erosion rate [$M_X L^{-2}T^{-1}$]
r_H	Hydraulic radius of pore or average pore size [L]
R_p	Rate of particle capture [$ML^{-2}T^{-1}$]
S	Mean bulk substrate concentration [ML^{-3}]
S_{AF}	Surface accumulation factor [-]
S_b	Mean substrate concentration in biofilm [ML^{-3}]
t	Time [T]
t_i	Time of measurement of dye concentration [T]
v	Mean superficial velocity or specific discharge [LT^{-1}]
VAR	Mean variance [T^2]
v_p	Mean pore velocity or Darcy velocity [LT^{-1}]

V_p	Particle volume [L^3]
V_r	Reactor void volume [L^3]
V_t	Total volume of particles per reactor [L^3]
W	Weight [M]
X_b	Biofilm cellular concentration [$M_{Xb}L^{-3}$]
X_f	Biofilm density [M_XL^{-3}]
X_s	Suspended cell concentration [M_XL^{-3}]
$Y_{X/S}$	Growth or biomass yield of substrate for species [M_XM^{-1}]

APPENDIX B

RAW DATA

Experiment 1: Effect of media geometry

Table 16. Biofilm thickness as a function of time.

S.No.	Time (Hours)	Biofilm thickness (micrometers) REACTOR # 1 s,500	2 g,500	3 s,750	4 g,85	5 s,130	6 s,500	7 g,130	8 g,500
1	0	0	0	0	0	0	0	0	0
2	12	0	0	0.9	0	0	8	0	5.6
3	24	0	0	2.5	0	0	10	0	10
4	36	4.3			0.4	15	17.5		
5	40.8	19.3	19.3	4.3	0.4	0.4	15	7.7	17.5
6	45.6	19.3	19.3	5.9	0.4	0.4	19	7.7	25
7	57.6	19.3	19.3	5.9	0.4	19	7.7	25	
8	62.4	5.9			0.6	19	7.7	25	
9	69.6	9.3			0.6	30.5	42.5		
10	84	11			0.8	36	48.5		
11	108	13.5			0.8	7.7	42.5	52	
12	117.6	38.5	38.5	14.3	0.8	7.7	44.5	15.4	55
13	141.6	38.5	38.5	15.2	0.8	7.7	46.2	15.4	55
14	156	38.5	38.5	15.4	0.8	7.7	46.2	15.4	55
15	180	38.5	38.5	15.4	0.8	7.7	46.2	15.4	55
16	192	38.5	38.5	15.4	0.8	7.7	46.2	15.4	55

Size of reactors are in micrometers.
g = glass, s = sand, corresponds to type of media in reactor.

Table 17. Flow rate versus time for short reactors.

Time (Hours)	REACTOR # 1	2	3	4	5	6	7	8
	Flow rate (cm^3 sec^{-1})							
0	0.0717	0.0667	0.1	0.0385	0.0208	0.04	0.0222	0.0477
12	0.0714	0.0667	0.1	0.0385	0.0208	0.04	0.0222	0.0477
24	0.037	0.04	0.0667	0.0143	0.0083	0.0278	0.0082	0.0323
36	0.0076	0.0062	0.0143	0.0052	0.0019	0.0075	0.0024	0.0086
40.8	0.0036	0.007	0.0286	0.0052	0.0032	0.0077	0.0056	0.0101
45.6	0.0022	0.0053	0.0182	0.0182	0.0021	0.0083	0.0034	0.0133
57.6	0.0033	0.0052	0.0042	0.0094	0.0014	0.003	0.0026	0.0037
62.4	0.0022	0.0028	0.0035	0.0083	0.0011	0.0027	0.0031	0.0034
69.6	0.0027	0.0024	0.0035	0.003	0.0009	0.0022	0.0031	0.0027
84	0.0017	0.0031	0.0016	0.0033	0.0004	0.0012	0.0024	0.0013
108	0.0017	0.0013	0.0011	0.0017		0.0013	0.0014	
117.6	0.0011	0.0013	0.0011	0.0016	0.0004	0.001	0.0013	0.0011
141.6	0.0017	0.0015	0.002	0.0017	0.0003	0.0016	0.0013	0.0013
156	0.0014	0.0018	0.0016	0.0017	0.0004	0.0016	0.0014	0.0014
180	0.0016	0.0017	0.003	0.0019	0.0003	0.0007	0.0009	0.002
192	0.0016	0.001	0.0007	0.0017	0.0004	0.0012	0.0019	0.0032

Experiment 2: Frictional losses

Table 18. Mesh, media and tubing frictional losses.

S.No.	Mesh only 10 cm reactor Fl rate	Head loss	Mesh + media 10 cm reactor Fl rate	Head loss	15.4 cm reactor Fl rate	Head loss
1	1.667	0.3	0.01	0.1	0.222	5.2
2	5.556	0.9	0.154	0.9	0.962	31.1
3	8.772	1.6	0.357	7	1.786	52.7
4	12.195	2.4	2.222	31.5	2.326	66.6
5	14.706	3.3	3.333	47.7	3.03	95.4
6	15.625	4	4.348	70.3	0.021	0.4
7	5.556	95.8			0.862	17.7

Flow rate in cm^3sec^{-1} and head loss in cm of Hg.

Experiment 3: Hydrodynamic dispersion

Table 19. Tracer concentration-time data for 23 cm length.

Sterile (0 hours) Influent		Effluent		With biofilm growth (364 hours) Influent		Effluent	
Time (mins)	Conc. **	Time (mins)	Conc. **	Time (mins)	Conc. **	Time (mins)	Conc. **
0	0	0	0	0	0	0	0
0.1	0.2	0.2	0.1	1	1.75	1	0.4
0.2	1.5	0.4	0.25	2	5.4	2	0.72
0.3	2.5	0.6	0.4	3	7.25	3	1.15
0.4	3.3	0.8	0.5	4	7.6	4	1.7
0.5	3.7	1	0.6	5	7.3	5	2.4
0.6	4.1	1.2	0.75	6	6.35	6	3.1
0.7	4.2	1.4	0.85	7	5	7	3.8
0.8	4.2	1.6	1.1	8	3.85	8	4.5
0.9	4.1	1.8	1.3	9	3.15	9	5
1	3.7	2	1.6	10	2.7	10	5.2
1.1	3.2	2.2	2	11	2.35	11	5.2
1.2	2.6	2.4	2.5	12	2.12	12	4.85
1.3	2	2.6	2.6	13	1.9	13	4.3
1.4	1.5	2.8	2.6	14	1.65	14	3.7
1.5	1.1	3	2.15	15	1.4	15	3.1
1.6	0.7	3.2	1.5	16	1.1	16	2.5
1.7	0.45	3.4	0.9	17	0.75	17	2
1.8	0.2	3.6	0.55	18	0.55	18	1.6
1.9	0.05	3.8	0.35	19	0.25	19	1.25
2	0	4	0.25	20	0.15	20	1
		4.2	0.2	21	0.15	21	0.8
		4.4	0.15	22	0.1	22	0.7
		4.6	0.1	23	0.1	23	0.6
		4.8	0.1	24	0	24	0.55
						25	0.5
						26	0.5
						27	0.4
						28	0.35
						29	0.25
						30	0.15

** - absorbance units as recorded by the photosensitive cell.

Experiment 4: Porosity and pore velocity

Table 20. Data for pore velocity and porosity from tracer study as compared to theoretical computation from biofilm thickness.

5 cm length, 0.27 cm^2 area, 1 mm dia spheres reactors					
	time	film thickness (microns)		flow rate (cm^3/sec)	
S. no.	(days)	react 1	react 2	react 1	react 2
1.	0.000E+00	0.000E+00	0.000E+00	1.852E-02	1.587E-02
2.	1.000E+00	1.030E+01	1.030E+01	1.852E-02	1.587E-02
3.	1.875E+00	1.550E+01	1.030E+01	1.639E-02	1.351E-02
4.	2.292E+00	2.060E+01	1.200E+01	1.613E-02	1.333E-02
5.	3.083E+00	1.810E+01	1.550E+01	1.695E-02	1.449E-02
6.	3.417E+00	1.810E+01	1.810E+01	1.667E-02	1.351E-02
7.	4.208E+00	2.580E+01	1.810E+01	1.639E-02	1.316E-02
8.	4.875E+00	2.580E+01	2.060E+01	1.563E-02	1.250E-02
9.	5.375E+00	3.100E+01	2.060E+01	1.408E-02	1.136E-02
10.	6.208E+00	3.100E+01	2.400E+01	1.408E-02	1.111E-02
11.	6.458E+00	3.600E+01	2.600E+01	1.351E-02	1.130E-02
12.	7.417E+00	3.600E+01	2.600E+01	1.299E-02	1.064E-02
13.	8.083E+00	3.800E+01	3.100E+01	1.250E-02	1.010E-02
14.	8.375E+00	4.120E+01	3.100E+01	1.149E-02	9.524E-03
15.	8.917E+00	4.120E+01	3.600E+01	1.176E-02	9.615E-03
16	1.017E+01	4.120E+01	3.600E+01	1.087E-02	9.091E-03

Table 21. Data for calculation of pore velocity.

500 micron glass spheres, 9 cm length, 0.12 cm^2 area			
	Time (days)	Flow rate (cm^3/sec)	film thickness (microns)
1.	0.000E+00	4.750E-02	0.000E+00
2.	5.000E-01	4.580E-02	4.000E+00
3.	1.000E+00	3.170E-02	1.000E+01
4.	1.500E+00	1.420E-02	1.700E+01
5.	2.000E+00	6.700E-03	2.400E+01
6.	2.500E+00	4.200E-03	3.400E+01
7.	3.000E+00	3.000E-03	4.100E+01
8.	3.500E+00	2.200E-03	4.650E+01
9.	4.000E+00	1.700E-03	4.900E+01
10.	4.500E+00	1.700E-03	5.200E+01
11.	5.000E+00	1.300E-03	5.400E+01
12.	5.500E+00	1.300E-03	5.400E+01
13.	6.000E+00	1.300E-03	5.400E+01

Table 21 (continued)

	1000 micron glass spheres, 0.06 cm^2 area, 5 cm length time (days)	flow rate (cm^3/sec)	film thickness (microns)
1.	0.000E+00	7.500E-02	0.000E+00
2.	1.000E+00	7.500E-02	0.000E+00
3.	2.000E+00	7.200E-02	0.000E+00
4.	3.000E+00	6.800E-02	8.000E+00
5.	4.000E+00	3.600E-02	3.200E+01
6.	5.000E+00	3.000E-02	4.800E+01
7.	6.000E+00	1.600E-02	5.600E+01
8.	7.000E+00	1.100E-02	6.100E+01
9.	8.000E+00	6.000E-03	6.500E+01
10.	9.000E+00	4.000E-03	6.600E+01
11.	1.000E+01	3.000E-03	6.700E+01

Experiment 5: Initial adsorption

Table 22. Initial adsorption experiment.

Segment	distance from entrance (cm)	TOC (mg L^{-1})	Cells (CFU/cm^3)	total surface area (mm^2)
1.	2.8500E+01	9.2050E+01	3.7000E+07	3.1836E+03
2.	2.5500E+01	2.4700E+01	8.7000E+06	3.3996E+03
3.	2.2500E+01	-	1.5000E+07	-
4.	1.9500E+01	2.4200E+01	2.8000E+07	3.6156E+03
5.	1.6500E+01	2.3170E+01	1.3000E+07	3.7836E+03
6.	1.3500E+01	2.2250E+01	1.6000E+07	3.5196E+03
7.	1.0500E+01	2.3510E+01	-	3.9516E+03
8.	7.5000E+00	2.1520E+01	4.4000E+07	3.3996E+03
9.	4.5000E+00	2.2180E+01	3.5000E+06	3.5916E+03
10.	1.5000E+00	2.2740E+01	2.3000E+07	2.9196E+03

Volume of sample analyzed is 20 cm^3.

Regression output for TOC versus axial distance:

Constant	6.0578E+00
Std Err of Y Est	1.9039E-01
R Squared	3.3350E-01
No. of Observations	9.0000E+00
Degrees of Freedom	7.0000E+00
X Coefficient(s)	1.3664E-02
Std Err of Coef.	7.3013E-03

Experiment 6: Biotransformation processes

Table 23. Change of permeability with time for replicate reactors.

time in (hours)	original (cm^2 x 10^{-8})	replicate
0.0000E+00	1.8100E+00	1.8100E+00
5.8000E+01	1.6400E+00	1.6400E+00
9.2000E+01	4.5000E-01	1.1700E+00
1.0500E+02	9.8000E-01	1.0300E+00
1.1650E+02	5.0000E-01	6.6000E-01
1.4200E+02	4.8000E-01	3.1000E-01
2.1150E+02	4.5000E-01	2.8000E-01
2.2400E+02	3.3000E-01	4.1000E-01
2.8500E+02	5.8000E-01	6.8000E-01

Table 24. Change of suspended cell concentration with time.

Time (Hrs)	Influent Original	Effluent (CFU/cm^3)	Influent Replicate	Effluent
0.0000E+00	7.3000E+05	3.5000E+06	2.6000E+06	4.6000E+06
5.8000E+01	4.3000E+07	7.3000E+07		
1.0000E+02	5.7000E+06	9.3000E+07	9.1000E+06	1.9000E+08
2.0000E+02	1.5000E+07	1.6000E+08	1.8000E+08	1.3000E+08

Table 25. Variation of cell carbon and cell number with axial distance at steady-state.

Segment #	Cell-C (mg)	ax. dist (cm)	volume (cm^3 x E+06)	CFU/mm^2	total S A (mm^2)
1	1.448	1.9	0.3483	3.3228	4296
2	0.31051	5.4	0.406	0.58058	4608
3	0.50096	8.6	0.372	0.383	3600
4	0.19784	11.8	0.372	0.31806	3624
5	0.5989	14.9	0.36	0.31572	3648
6	0.39771	18.2	0.383	0.23708	3552
7	0.30561	22.3	0.476	0.30845	5712
8	0.040187	27.5	0.604	0.32314	5976
9	0.005685	32.7	0.604	0.16006	6048
10	0.11577	38	0.615	0.17958	6168
11	0.002436	43.2	0.604	0.27844	5856
12	0	48.4	0.604	0.22952	6048

total vol= 5.748 ml

Table 26. Substrate concentration profile.

S.No.	axial distance (cm)	Dissolved oxygen (mg L^{-1})
1.	-3.0000E+00	8.6200E+00
2.	3.9000E+00	4.0400E+00
3.	7.1000E+00	4.5600E+00
4.	1.3500E+01	4.0400E+00
5.	3.5500E+01	4.5600E+00
6.	4.5900E+01	3.4400E+00

Table 27. Axial variation of biofilm thickness for original reactor.

		Sample #				
S.No.	Axial dis (cm)	1	2	3	4	mean
		Biofilm thickness (micrometers)				
1	0	103	124	103	128	114.5
2	2	41.2	61.8	51.5	103	64.375
3	5	20.6	30.9	51.5	51.5	38.625
4	6	10.3	10.3	41.2	41.2	25.75
5	8.5	5	5	25.8	25.8	15.4
6	10	5	5	20	10.3	10.075
7	15	0	0	10.3	10.3	5.15
8	18	0	0	5	5	2.5
9	25	0	0	0	0	0

Table 28. Axial variation of biofilm thickness for replicate (control) reactor.

		Sample #				
S.No.	axial dis (cm)	1	2	3	4	mean
		Biofilm thickness (micrometers)				
1	0	103	154.5			128.75
2	0.5			154.5		154.5
3	1	82.4	123.6			103
4	1.5			51.8	82.4	67.1
5	2	30.9	51.5			41.2
6	2.5			30.9	51.5	41.2
7	3	20.6	41.2			30.9
8	3.4			30.9	51.5	41.2
9	4	10.3	20.6			15.45
10	4.4			10.3	20.6	15.45
11	5	10.3	10.3			10.3
12	5.3			10.3	10.3	10.3
13	6	10.3	10.3			10.3
14	6.2			10.3	10.3	10.3
15	7	10.3	10.3			10.3
16	7.2			10.3	20.6	15.45
17	8	10.3	5.1			7.7
18	8.5			5.2	10.3	7.75
19	9	10.3	5.1			7.7
20	11			10.3	5.1	7.7
21	18	0	5.15			2.575
22	25	0	0	0	0	0

Table 29. Soluble organic carbon as a function of axial distance.

S. No.	axial dis (cm)	Sample # 1	2	3
		(mg L^{-1} Carbon)		
1	0	7.8	9.59	8.4
2	6.9	5.1	10.5	7.4
3	10.1	11.7	7.9	
4	16.5	9.5	6.7	
5	38.5	5.01	7.9	
6	48.9	3.3		